Master's thesis

NTNU
Norwegian University of Science and Technology
Faculty of Information Technology and Electrical Engineering
Department of Engineering Cybernetics

Audun Gullikstad Hem

Maritime multi-target tracking with radar and asynchronous transponder measurements

Master's thesis in Cybernetics and Robotics
Supervisor: Edmund Førland Brekke
Co-supervisor: Thor Inge Fossen
January 2021

NTNU
Norwegian University of Science and Technology

Audun Gullikstad Hem

Maritime multi-target tracking with radar and asynchronous transponder measurements

Master's thesis in Cybernetics and Robotics
Supervisor: Edmund Førland Brekke
Co-supervisor: Thor Inge Fossen
January 2021

Norwegian University of Science and Technology
Faculty of Information Technology and Electrical Engineering
Department of Engineering Cybernetics

NTNU
Norwegian University of
Science and Technology

Abstract

This thesis presents a novel method of including a type of measurements with unique IDs, transmitted from surrounding vessels, in a radar target tracker. The application of the method is based in maritime target tracking, and Automatic Identification System (AIS) messages are used in combination with radar measurements. The AIS measurements are processed by the tracker as they arrive, which can be at any time, independently of when the radar delivers measurements to the tracker. The possibility of using AIS measurements is added to an already developed maneuvering multi target tracker. To accommodate the AIS measurements, the tracker is derived from a general set of modeling assumptions. When no AIS measurements are present, the tracker behaves exactly as the previously developed maneuvering target tracker. The purely sequential way of handling the AIS measurements differs from previously created radar-AIS target trackers.

Furthermore, the performance of the tracker is evaluated through a comparison between when using the AIS measurements, and when only using radar. The tracker was tested on both simulated data and real data. The analysis showed consistently better results when AIS measurements were present, with no obvious drawbacks except for an increased computational load.

Sammendrag

Denne avhandlingen presenterer en ny metode for å bruke en type målinger med unike IDer, sendt ut av omkringliggense fartøy, i en radar-basert målfølgingsalgoritme. Det tiltenkte bruksområdet er i maritim målfølging, og målinger fra systemet for automatisk identifikasjon av skip (AIS) brukes for å representere den ovennevnte typen målinger. AIS-målingene blir prosessert av målfølgingsalgoritmen med en gang de ankommer, som kan være på et hvilket som helst tidspunkt. De er uavhengige av når radaren returnerer et nytt sett med målinger. Muligheten for å bruke AIS-målinger tillegges en allerede utviklet radar-målfølgingsalgoritme. Målfølginsalgortmen har blitt avledet fra et generelt sett med antakelser for å muliggjøre bruken av AIS-målingene. I fraværet av AIS-målinger oppfører målfølgingsalgoritmen seg akkurat slik som den tidligere utviklede algoritmen. Den rent sekvensielle behandlingen av AIS-målingene skiller seg fra tidligere utviklede metoder for radar-AIS-fusjon.

Videre er målfølgingsalgoritmen evaluert gjennom en sammenligning av ytelsen med og uten bruk av AIS-målinger. Sammenlingingen ble gjort både på simulert data og ekte data. Analysen viste konsekvent bedre resultater ved bruk av AIS-målinger, med ingen åpenbare ulemper bortsett at målfølgingsalgoritmen blir mer regnekrevende.

Preface

When starting the work on this master's thesis, I had already started working on a PhD project regarding the fusion of radar with exteroceptive sensors, mainly AIS measurements. As such, some work had already been done by me on the topic, and I had several thoughts regarding different methods for how to make it work. This thesis considers one of the possible methods. It can be considered an extension of the work done for a previous article, *The VIMMJIPDA: Hybrid state formulation and verification on maritime radar benchmark data,* [1], where my pre-master project considered the implementation of the tracker in question.

The thesis is written as part of the Autosit (Autonomous ships, intentions and situational awareness) project, which is an associated project of the NTNU Centre for Autonomous Marine Operations and Systems. Autosit is a continuation of the Autosea project, from which the collected data, and some of the code, originated.

I want to thank my main supervisor Associate Professor Edmund F. Brekke for good help, and insight in the complicated world of target tracking. I also want to thank my co-supervisor Professor Thor I. Fossen for valuable insight and tips. Furthermore i want to acknowledge the work done by the Autosea project. Lastly, the radar data were recorded by Erik Wilthil, Andreas Flåten, Bjørn-Olav Eriksen and Giorgio D. K. M. Kufoalor, with assistance from Maritime Robotics and Kongsberg.

Audun Gullikstad Hem
Trondheim, January 2021

Table of Contents

List of Tables

List of Figures

Nomenclature

The field of target tracking contains a lot of abbreviations, and a lot of symbols. This thesis does the same, and to make it more manageable for the reader the most relevant abbreviations and symbols are summarized here. The remaining symbols are explained where they appear.

Abbreviations

Several abbreviations are used throughout this thesis, and they are summarized here.

AIS	Automatic identification system
ANEES	Average normalized estimation error squared
ANIS	Average normalized innovation squared
CSTDMA	Carrier sense time-division multiple access
CT	Coordinated turn
CV	Constant velocity
EKF	Extended Kalman filter
FISST	Finite set statistics
GLMB	Generalized labeled multi-Bernoulli
HO-MHT	Hypothesis oriented multiple hypothesis tracker
IMM	Interacting multiple models
IPDA	Integrated probabilistic data association
JIPDA	Joint integrated probabilistic data association
JPDA	Joint probabilistic data association
MBM	Multi-Bernoulli mixture
MC	Markov chain
MHT	Multiple hypothesis tracker

MMSI	Maritime mobile service identity
NEES	Normalized estimation error squared
NIS	Normalized innovation squared
OSPA	Optimal subpattern assignment
p.g.fl	Probability generating functional
PDA	Probabilistic data association
PDAF	Probabilistic data association filter
pdf	Probability density function
PHD	Probability hypothesis density
PMBM	Poisson multi-Bernoulli mixture
PPP	Poisson point process
RFS	Random finite set
RIB	Rigid inflatable boat
RMSE	Root mean squared error
SOTDMA	Self-organizing time division multiple access
TFAR	Track false alarm rate
TFR	Track fragmentation rate
TLE	Track localization error
TO-MHT	Track oriented multiple hypothesis tracker
TPD	Track probability of detection
TTP	Total track probability
VIMMJIPDA	Visibility interacting multiple models joint integrated probabilistic data association

Symbols

The hybrid state

The symbols used to describe the different elements of the hybrid state, the probabilities of the different states and the set of possible states.

$\mathbf{x}$	kinematic state
v	visibility state
τ	MMSI number
s	kinematic model (mode)
$\mathbf{y}$	hybrid state
o	visibility state probability
η	probability of a target being visible
$\mathcal{V}$	the set of all MMSI numbers
ξ	MMSI number probability
μ	mode probability
M	number of modes in the hybrid state
$\mathbf{P}$	state covariance matrix

Subscripts and superscripts

Sub- and superscripts are used quite heavily throuout the thesis, take for example $\mu_{k|k-1}^{t\tau\tilde{s}}$. *Here,* τ *and* s *are described above, and the indicate that the variable is the mode probability of mode* s*, when the target has MMSI number tau. The other symbols are described below.*

$\hat{}$	estimate	t	track index
$\tilde{}$	marginalized variable	$k\|k-1$	conditional on the previous time
$\dot{}$	time derivative	R	considers radar measurements
k	time step	A	considers AIS measurements

Modeling symbols

These symbols are used to describe different aspects of the model.

b	target birth rate	P_{S_c}	constant probability of survival
P_C	probability of the MMSI numbers not being corrupted	t_k	time at time step k
		$\mathbf{f}$	state transition function
w	visibility transition matrix	$\mathbf{Q}$	process noise covariance matrix
q	MMSI number transition matrix	P_D	detection probability
π	transition probability matrix	λ	clutter intensity
$\Delta\mathrm{t}$	time between the current and previous time step	$\mathbf{z}$	measurement
		$\mathbf{p}$	positional part of an AIS measurement
$\mathbf{H}$	measurement matrix	a	association hypothesis
$\mathbf{H}^*$	velocity matrix	$\mathbf{R}$	measurement noise covariance matrix

Implementation specific symbols

Some of the symbols are used to describe the implementation of the tracker. These are summarized here.

$\mathbf{F}$	state transition matrix	T_d	Track termination threshold
$\boldsymbol{\nu}$	innovation	T_τ	MMSI pruning threshold
$\mathbf{S}$	innovation covariance	α	track fusion hypothesis significance level
g	validation gate scaling parameter		
T_{TTP}	TTP threshold for when to initialize new track	T_c	track confirmation threshold

Data generation and result evaluation specific symbols

Symbols which have been introduced to specify different aspects of the data generation and result evaluation process are described here.

P_{AIS}	probability of a generated target using AIS	$T_{dropout}$	mean for the AIS dropout time for a generated target
P_A	probability of a generated target being of SOLAS class A	N_k	number of samples
		c	OSPA$^{(2)}$ cutoff value
$P_{dropout}$	probability of an AIS dropout for a generated target	p	OSPA$^{(2)}$ order
		N	OSPA$^{(2)}$ window length

CHAPTER 1

Introduction

1.1 Motivation

Replacing or expanding existing naval equipment with autonomous ships has the potential to be economically advantageous [3] and can remove some of the risks associated with work at sea [4]. This is reflected in the initiative the industry is showing regarding current research projects undertaking the task of making autonomous ships a reality, for example, the recently started Centre for Research and Innovation SFI Autoship at NTNU [5].

One of the many important puzzle pieces for increased degrees of autonomy in the maritime sector is the ability for a ship to observe its surroundings. And to be able to avoid collisions and safely navigate the waters, it is important to know where the surrounding ships are situated. For this to work safely and robustly, target tracking algorithms that provide good estimates of the position and direction of the surrounding ships, also known as targets, have to be developed. For this task radar-based target tracking algorithms have largely been the norm when navigating outside of close encounter harbor areas. There is, however, also a system in place to help with collision avoidance at sea: the Automatic identification system (AIS). This system provides messages with valuable information that could help give better estimates than what could be done using only radar. Concerning the use of AIS in modern target tracking algorithms, much is left to be decided, which leaves a valuable source of information unused.

1.2 Previous work

This thesis builds upon an implementation of a multi-target tracker which was done as a pre-master project in 2019. The tracker that was implemented in the pre-master project was recently published in connection with the Global OCEANS 2020 conference [1], and is currently in the review process for journal publication. The tracker is called the VIMMJIPDA. The quite long abbreviation can be broken up to describe the different characteristics of the tracker:

V stands for visibility and indicates that the tracker allows the targets to be in a state where they are not visible to the tracker, but nevertheless exists.

IMM stands for Interacting Multiple Models. This is a framework that allows for the use of several kinematic models to be used in parallel, to better account for the movement of a target.

JIPDA stands for Joint Integrated Probabilistic Data Association and is a target tracking algorithm. It accounts for the probability of existence for the individual tracks, which is the estimate the tracker returns. It is also a multi-target tracker, which means that it can consider several potential targets when assigning measurements to targets. This process is what is denoted as data association.

This multi-target tracker has shown good promise for radar tracking and is used here as a basis. The VIMMJIPDA builds upon work done in the target tracking community through the past several decades. It is an extension of the JIPDA, introduced by Darko Musicki and Rob Evans in [6]. Here, the concept of visibility, as it is explained above, is mentioned, but is not used. It has, however, been explored in relation to other trackers and the problem of estimating target detectability, through e.g. [7]. The JIPDA can be considered an extension of the Joint probabilistic data association (JPDA) method developed by Yaakov Bar-Shalom [8], which again is an extension of Bar-Shalom's own Probablistic Data Association (PDA) method [9]. These methods are well established in the target tracking community, and have been used for a range of different purposes, such as collision avoidance for marine vessels [10] and autonomous navigation [11]. The IMM method has also been in use for several decades, and was introduced by Henk A. P. Blom and Yaakov Bar-Shalom in [12]. These methods are all more thoroughly described in Chapter 2. Furthermore, a IMM-JIPDA algorithm was presented in [13] by Musicki and Suvorova. Here, similar to what is done in the VIMMJIPDA, the concept of IMM was integrated in a JIPDA. This was, however, done from a somewhat different point of view as to what is done for the VIMMJIPDA.

Some work on the fusion of radar and AIS measurements has been done previously, perhaps most notably by Gaglione et. al. [14]. This approach used a framework similar to the JIPDA framework, but was formulated using probabilistic graphical models and used loopy belief propagation. A similar algorithm was made by the author for the course TK8102 at NTNU, but without using graphical models. For this, the VIMMJIPDA was also used as a basis. Both methods processed the radar and AIS measurements simultaneously each time the radar provided new measurements.

1.3 Problem formulation

This thesis is concerned with the problem of radar and AIS fusion for target tracking. The main question posed is if it is possible to include the processing of AIS measurements in the VIMMJIPDA sequentially. Here, sequential means that the AIS measurements are processed as they arrive, as opposed to how it is done in the previously made algorithm, where all AIS measurements are collected and processed only when new radar measurements arrive. There are a couple of reasons why this way of doing it may be beneficial. Firstly,

it simply seems more intuitive to process the AIS measurements just as they arrive. Furthermore, it can simplify or improve the initialization of targets. Lastly, it can provide improved estimates for some tracks in between radar updates, which can be beneficial for a collision avoidance system relying on the tracker.

Potential drawbacks of this method will also have to be considered. It is reasonable to assume an increase in the computational complexity, and if this is of a magnitude that creates the need for approximations that degrade the performance considerably the, gain from including AIS measurements could be negligible. Furthermore, it has to be examined if the inclusion of AIS measurements has the potential to cause problems in specific situations, where the different nature of the AIS measurements, in comparison with radar measurements, could create undesired behavior.

To summarize, the thesis considers

1. The construction of a tracker that handles AIS measurements as they arrive.
2. The performance of such a method as opposed to using only radar.
3. Whether the increase in computational complexity makes such an approach infeasible.

1.4 Main contributions

This project presents a novel multi-target tracker utilizing both radar and AIS measurements, built upon the framework of the VIMMJIPDA. The main difference from previous methods is the ability to handle the AIS measurements as soon as they arrive. The mathematical formulation of the tracker is presented, and simulation studies on both simulated and real maritime data are used to evaluate the tracking performance in relation to a pure radar tracker. In addition, a method for evaluating the probability of the existence of new tracks is presented, called the Total track probability. This method is analyzed for use on AIS measurements, both mathematically and through simulations.

1.5 Outline

Chapter 2 presents some background theory regarding the two different measurement types, radar, and AIS, in addition to a walk through some of the most notable target tracking methods. These ranges from simpler methods to the most complex, state of the art methods available. Chapter 3 lays the mathematical foundation for the target tracker, describing how the problem is modeled, before the method, i.e. the tracker itself, is described in Chapter 4. Chapter 5 details the implementation details of the tracker, describing how the tracker is realized.

In Chapter 6 the experimental setup is elaborated upon, both the physical setup resulting in the real maritime data, and the program for generating simulated data. In addition, the different metrics used to evaluate the tracking performance are explained. The tracking results on both real and simulated data are presented in Chapter 7 before a discussion follows in Chapter 8. Lastly, conclusions are drawn in Chapter 9.

CHAPTER 2

Target tracking

2.1 Radar and AIS

2.1.1 Radar

The radar emerged as a useful tool for determining the position of surrounding targets in the 1930s. It had previously been shown by Herbert Hertz in the late 1800s that radio waves could be reflected off of metallic objects, and after some less successful attempts at creating maritime radars the technology was ready to be used in practice at the onset of the Second World War [15].

Basic working principle

The name radar comes from *Radio detection and ranging* and hints at the way a radar works. A radar rotates continuously, emitting radio waves that are reflected from objects within the range of the radar. The bearing of the object which reflects the radar wave is found using the direction of the radio wave detecting the object. Roughly speaking, this direction is determined by what direction the antenna is facing. There are also several other factors determining the bearing, such as beamforming, but as the field of radar technology is large with a multitude of different solutions a more in-depth analysis is omitted. The range is in turn found by using the time the reflected signal uses to return to the radar. As the speed of the radio waves is well known this is easily calculated. This is done either by transmitting a short pulse and registering when it returns, or by sending a longer pulse with increasing frequency and registering the frequency of the reflected signal. The physical properties of the radar lead to some limitations and potential problems. The radar will have a limited maximum range, and limited resolution both with regards to range and bearing. The maximum range is the largest distance of which an object can be detected. The bearing resolution is the number of times radar waves are emitted during a single radar revolution, while the range resolution is determined by the finite number of distances which can be quantified by the radar. Both the range and the resolution will depend on the setup of the radar, in addition to the properties of the radar itself.

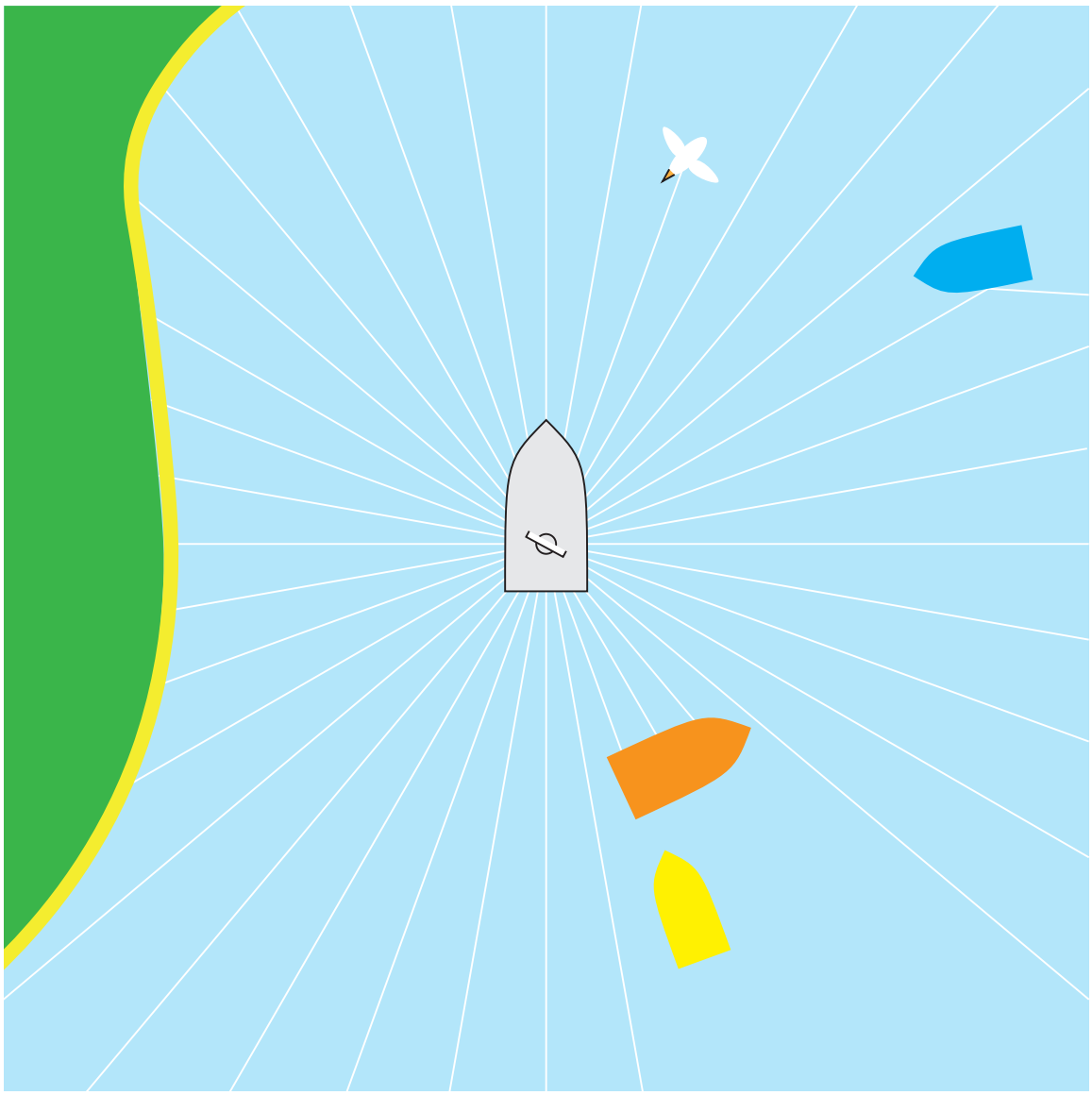

Figure 2.1: Illustration of a boat with radar.

In addition to the range and resolution limitations, the radar is far from guaranteed to detect all surrounding objects. This can be due to the angle of the reflection, waves, or a lot of other factors. In Figure 2.1, both the yellow and blue boat remain undetected. The radar is also prone to creating false alarms, or clutter as it is usually called. Clutter measurements are measurements which do not stem from an actual target, or ship in the case of maritime surveillance, but rather environmental objects such as waves, birds, and so forth [16]. This is exemplified by the bird in Figure 2.1.

Radar in a target tracking context

While the first radars used a real-time rendering of the surrounding object, the ability to collect and process the radar measurements using computers has made more advanced analysis possible. This involves a modeling framework for handling missed detections, clutter measurements, and the measurement error of the detections. The measurement

error in this context means the difference between the actual position of the target and the measured position. By using a filtering method, such as a Kalman filter, with a prediction and an update step the measurement errors are mitigated. A probabilistic framework working on the received measurements can be used to decide which measurements come from which target, whether a target has failed to be detected and whether a measurement is a clutter measurement. A missed detection is when a target has failed to create a radar measurement even though it exists, as represented by the blue boat in Figure 2.1. Furthermore, the radar can give several measurements for each target, as can be seen for the orange boat in Figure 2.1. Most trackers want only one measurement for each target, so if a target has returned several measurements these have to be clustered before the radar measurements are delivered to the tracker.

2.1.2 Automatic identification system (AIS)

The need for a ship to be able to identify surrounding ships arose as radio communication between different ships became more prominent. Without the possibility of precise identification, establishing communication could be cumbersome and in the worst-case scenario create dangerous situations as a result of this. This need for efficient communication led to the creation of the Automatic identification system (AIS), which in 2004 became a requirement for all ships covered by the Safety Of Life At Sea (SOLAS) convention [17].

Basic working principle

Ships that are using an AIS transmitter are sending AIS messages which are received by the surrounding ships. The main protocol used to send and receive messages is called self-organizing time division multiple access (SOTDMA). An AIS receiver can only receive one AIS message at a time, and this protocol ensures that the different ships organize their transmissions so they don't interfere with other AIS messages. The transmission rate for each ship varies with the speed and class of the ship. The AIS regulation differentiates between SOLAS regulated ships, which are denoted Class A ships, and other ships, which are denoted Class B ships. The transmission rates for positioning data for Class A ships can be seen in Table 2.1, and for Class B ships they can be seen in Table 2.2. While Class A ships mainly use the SOTDMA protocol, Class B ships also use the carrier sense time-division multiple access (CSTDMA) protocol, where the AIS transmitter checks if a message is being transmitted by other ships before transmitting. In crowded waters, as in harbor areas, the transmitting schedule of AIS messages can also be controlled by onshore controllers.

Each ship can transmit several different types of AIS messages. Firstly there are the dynamic messages which inform of the current movement and navigational status of the ship. These are transmitted according to Table 2.1 and Table 2.2. Furthermore static and voyage-related information regarding the ship is transmitted every six minutes, or on request from another ship. Safety-related manually entered messages can be transmitted when needed, in addition to several other, less important message types. A thorough explanation of all the different message types can be found in [18].

Ship type	Reporting interval
Ship at anchor or moored and not moving faster than 3 knots	3 min
Ship at anchor or moored and moving faster than 3 knots	10 s
Ship 0-14 knots	10 s
Ship 0-14 knots and changing course	3 1/3 s
Ship at 14-23 knots	6 s
Ship at 14-23 knots and changing course	2 s
Ship >23 knots	2 s
Ship >23 knots and changing course	2 s

Table 2.1: AIS transmitting frequency for SOLAS class A ships.

Ship type	Reporting interval
Class B "SOTDMA" not moving faster than 2 knots	3 min
Class B "SOTDMA" 2-14 knots	30 s
Class B "SOTDMA" 14-23 knots	15 s
Class B "SOTDMA" >23 knots	5 s
Class B "CSTDMA" not moving faster than 2 knots	3 min
Class B "CSTDMA" moving faster than 2 knots	30 s

Table 2.2: AIS transmitting frequency for SOLAS class B ships.

AIS in a target tracking context

Using AIS messages for target tracking requires a somewhat different mindset than when using radar measurements. Perhaps most importantly a tracker cannot rely only on AIS messages, as can be done when using radar measurements. There are no guarantees that all surrounding ships will have an AIS transmitter, and as such secure collision avoidance cannot be guaranteed. Thus, the AIS messages can be viewed as a supplement to radar-based target tracking. The technical properties of the two signal types are also completely different. AIS messages are transmitted from surrounding ships, with the consequence that there will be no clutter measurements. This means that all received AIS messages must come from a ship. In addition to this, modeling missed detections as part of a probabilistic framework becomes difficult. This will require the establishment of a timetable consisting of the expected transmission times for all surrounding ships at any given time. This also gets increasingly difficult as the protocol changes time slots randomly after some time to avoid interference issues. Because of this, it is difficult for a tracker to extract any information from the fact that an AIS message hasn't arrived at any given time. The perhaps most intriguing information to be extracted from the AIS messages is the Maritime mobile service identity (MMSI) number of the transmitting ship, which is a unique identification number. This can greatly help with the data association, i.e. connecting a measurement to a track. For radar measurements, there are naturally no such IDs to help with the data association problem. However, a limitation in tracking using AIS lies in the relatively high rate of incorrect messages. As described in [19], approximately 4.6% of all transmitted AIS messages with dynamic data have errors. If this error is in form of a bit flip, it can result in wrong positional information or a wrong MMSI number.

While the first type of error is easily handled using standard target tracking techniques the second will be harder to amend.

2.2 Single target tracking

The field of target tracking is concerned with detecting and estimating the position of potential targets. In the context of maritime target tracking, these targets are other vessels populating the waters surrounding the vessel conducting the target tracking, or the *ownship* as it is often called. The ownship is equipped with one or several exteroceptive sensors. An exteroceptive sensor gathers measurements from the surroundings, this in contrast to interoceptive sensors which measure the state of the ownship itself. The problem of finding the position of the ownship is called *navigation*, but in target tracking the position of the ownship itself is often assumed known. The field of target tracking emerged in the wake of the invention of the radar, and with the invention of the Kalman filter in 1960 by R.E. Kalman [20] a foundation for many of the later advances was created. However, target tracking is concerned with more than just filtering of incoming measurements. The fact that several measurements can arrive at each time step, that not all measurements come from a target, and that some targets are not detected creates the need for the application of statistical decision theory. The term *single target tracking* is used for methods where the data association between tracks and measurements is done one track at a time.

2.2.1 Probabilistic data association

The Probabilistic data association (PDA) method and the resulting Probabilistic data association filter (PDAF) were introduced in 1975 [9]. The PDAF provided a minimum mean square error (MMSE) approach for situations where the sources of the measurements are uncertain. The data association problem arises from the fact that targets can remain undetected and that measurements have an uncertain origin. The PDA approach solves this problem by calculating the probability that the different measurements came from the target in question, in addition to the probability of a missed detection. These probabilities are then used to calculate the innovation to use in the filter, giving several distributions which together represent the final estimate. To avoid that each of these distributions have to be considered individually when the next set of measurements arrive, and thus making the problem grow exponentially, they are merged to a final posterior estimate. This is illustrated in Figure 2.2, where three potential measurements, the gray dots, have resulted in an estimate consisting of three distributions, in blue. The track is shown in orange, while the distribution resulting from the merging is shown in red. Previously the standard method to solve the data association problem was to choose a measurement using a nearest-neighbor type of decision, such as in [21] from 1971. The PDA introduced a more robust method which is still an important part of many target tracking algorithms.

2.2.2 Integrated probabilistic data association

The PDA approach takes for granted that a target exists when it starts processing measurements, and delegates the concerns regarding a target's probability of existence to other parts of the program. With the introduction of the Integrated probabilistic data

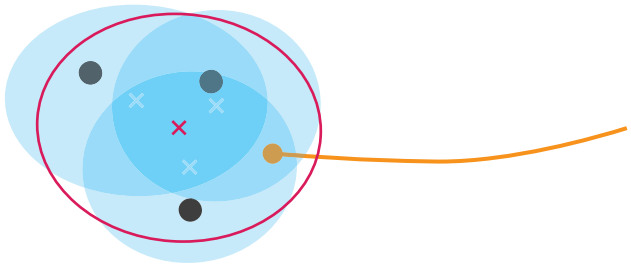

Figure 2.2: An estimate consisting of several distributions, and the merged estimate of these.

association (IPDA) [22] the concept of existence became an integrated part of the tracking method, hence the name. When combined with an initialization scheme and a termination scheme utilizing the existence probability, it provides a good basis for a target tracking framework.

2.2.3 Interacting multiple models

Even though the Interacting multiple models (IMM) method is not a tracker in it's own right, it is widely used in target tracking in combination with some other method, e.g. the PDA. The IMM was presented by Henk A. P. Blom and Yaakov Bar-Shalom in 1988 [12], and allows for use of several different kinematic models when estimating the state of a target. Predictions and updates are done in parallel for each model and the probability of each model being the correct one is calculated to merge the resulting distributions.

2.3 Multi-target tracking

The difference between single-target tracking and multi-target tracking lies in how the data association is done. If only one target is present the two approaches will behave similarly, but with several targets present using a multi-target tracker can give better results. Simply put, single-target tracking methods perform data association independently of other targets, calculating the probability of the association between target and measurements with no regard for eventual other targets nearby. Multi-target trackers on the other hand include other targets when calculating the association probabilities. This can be helpful when targets are close to each other and are "fighting" for the same measurements. Situations like this can occur when many targets are present, but single-target trackers have also shown to have good performance in many situations, for example in [23]. However, using a multi target tracker in a multi-target environment can lead to some problems, such as track coalescence [24].

Below, some of the most widely used approaches to the multi-target tracking problem are presented. These include both some older methods which has been around for decades, and some newer tracking methods which have appeared with the development of the Random finite set framework.

2.3.1 Joint probabilistic data association

The Joint probabilistic data (JPDA) tracker was first presented by Fortman et. al. in 1980 [8] before it was expanded upon in 1983 by the same authors [25]. As indicated

by its name, the method expands upon the previous PDA method but allows the data association procedure to jointly process measurements for several tracks. To make this computationally feasible only the measurements in the area around the predicted position of each track are potential measurements for said track. This is known as validation gating, and in practice, it means that measurements that have a very low probability of being associated with a target are disregarded. This is also done in the PDA and IPDA methods. Furthermore, tracks are clustered, and only the tracks and measurements in each cluster are considered when performing the data association.

Such a cluster is shown in Figure 2.3. The tracks are in orange, the measurements are the black dots and the validation gates are the blue ellipses. All tracks and measurements in the surveillance area can potentially be included in a single cluster, but as the computational complexity is exponential in the number of tracks the clustering process should ensure that the clusters are of a manageable size. The joint computation of the data association for all tracks in a cluster, which differentiates the JPDA from the PDA, creates the need for more refined association hypothesis generation. An association hypothesis is a combination of possible associations between tracks and measurements, which for example requires that only one track can be associated with a measurement in the same hypothesis. The JPDA method is a track-oriented approach, as the tracks are the focal point when creating the association hypotheses, i.e. each track has a measurement associated with it and not vice versa. Then, as in the PDA or IPDA, the probability for each association hypothesis is calculated which again decides the innovation input in the filter. An approximation method is often used to avoid calculating the probability of all association probabilities. An example of such a method is the Murty method [26], which simplifies calculations by returning only a number of the most likely association hypotheses.

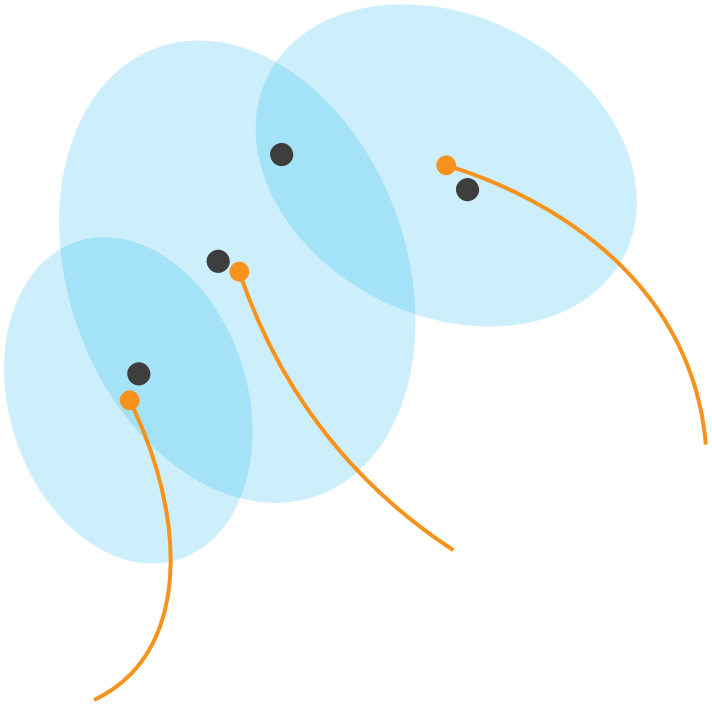

Figure 2.3: Three tracks with overlapping measurements in their validation gates.

2.3.2 Joint integrated probabilistic data association

In 2004 Musicki et. al. introduced the Joint integrated probabilistic data association (JIPDA) tracker [6]. Similar to what the IPDA did for the PDA, the JIPDA did for the JPDA by introducing track existence within the JPDA framework. The JIPDA is a derivation of the JPDA without assuming initial track existence, making the probability of existence an inherent part of the tracker. This simplifies the track management, making it easier to initialize and terminate tracks.

2.3.3 Multiple hypothesis tracker

Whereas the JPDA is a target-oriented method the Multiple hypothesis tracker (MHT) introduced by Donald B. Reid in 1979 [27], is a measurement-oriented method. This means that each measurement is associated with an existing track, a new track, or no track. Then the probability of each possible scenario is calculated. The concept of validation gates and clustering is utilized here as well, in a manner similar to what is done in the JPDA. Even with such measures to reduce the computational complexity the tracker will result in an ever-growing tree of different hypotheses as time goes on. This is amended by removing the hypotheses with negligible probability, a technique known as *pruning*.

The MHT presented by Reid is often further described as a Hypotheses Oriented MHT (HO-MHT). An aspect of this approach is that the hypotheses, which are carried over form one time step to the next, are far grater in number than the number of tracks, i.e. feasible combinations of associations. This is an argument for a track-oriented approach, called Track-Oriented MHT (TO-MHT) [28]. Here, only the tracks from the previous time steps are maintained to the next time step, and not all the hypotheses.

2.3.4 On random finite sets

Around the turn of the millennium, the need to properly model the multi-target multi-sensor problem became evident. To facilitate progress in the field of target tracking a rigorous framework was needed, which arrived with the introduction of finite set statistics (FISST) [29]. In short terms, FISST is a different formulation of point process theory which is somewhat easily understandable for those already accustomed to the Bayesian statistics used for single-target tracking. A random finite set (RFS) is a set-valued random variable, with a finite number of elements. Each individual element is defined on a space, which is the base space of the RFS. The set density describes the property of the RFS, in that it specifies the cardinality and the behavior of the individual points in the set. Cardinality is the term used for the number of elements in a set. As can be deducted from this short description this is a mathematical framework that is well suited to describe an uncertain number of targets with uncertain kinematic properties.

As this new way of modeling the multi-target tracking problem emerged it was desirable to see how it connected with the previous multi-targe trackers, most notably JIPDA and MHT. It was shown in [30] that through approximations and assumptions, variants of JIPDA could be derived by using RFSs. Early on, a connection between MHT and the RFS framework was also established, and this link was examined further in [31]. Results like this established the connection between the well-established trackers from the past several decades and the new RFS framework which is now driving much of the innovation done in the field.

2.3.5 Probability hypothesis density

Building upon the FISST framework, Ronald Mahler presented the Probability hypothesis density (PHD) filter in 2003 [32]. The motivation behind the method was to use the first-order moment of the multi-target distribution so that it can be propagated using a filter instead of using the complete distribution. This is what is done in the Kalman filter, where higher-order moments are neglected and only the first- and second-order moments are propagated. For a Gaussian distribution, these are the mean and covariance, respectively. For a Poisson point process, all information regarding the distribution can be found in its first-order moment, the PHD. The PHD is a distribution which is characterized by having its integral over a region of the state space being the expected number of targets in the region. Thus, the use of the PHD method requires the approximation of the multi-target distribution as a Poisson RFS. This is a reasonable approximation when the targets are many and evenly distributed, as the binomial distribution tends toward the Poisson distribution for a large outcome space. The approximation becomes questionable, however, when the number of targets is small. To amend some of the issues with the PHD method the cardinality PHD filter was introduced [33]. The cardinalized PHD filter propagates the cardinality distribution in addition to the PHD, resulting in better results in exchange for a more complex structure.

2.3.6 Poisson multi-bernoulli mixture

A different way of modeling the multi-target tracking problem is found in the Poisson multi-Bernoulli mixture (PMBM) filter and subsequent trackers. The PMBM filter was first introduced in [30], before two PMBM trackers were presented in [34]. In this context, tracker refers to the estimation of trajectories while filter refers to the estimation of the current states. One of the two trackers presented in [34] estimated the current track trajectories, while the other estimated both current and previously terminated track trajectories. The core of PMBM estimation lies in the PMBM density, which is the union between a Poisson distribution and a multi-Bernoulli mixture. When representing tracks as a PMBM density, the Poisson part represents unknown targets, i.e. undetected targets which are hypothesized to exist. The multi-Bernoulli mixture part represents already detected targets. By performing sufficient approximations this model is computationally tractable for a Gaussian-linear model.

2.3.7 Generalized labeled multi-Bernoulli

The Generalized labeled multi-Bernoulli (GLMB) density is an RFS density with both a state space and a label space. It was first presented in [35] and further detailed for practical applications in [36]. The concept of a labeled RFS is introduced, which as the name indicates essentially is an RFS with a distinct ID. Both the labeled Poisson RFS and the labeled multi-Bernoulli RFS are special cases of the GLMB. A class of GLMBs, the δ-GLMB is also introduced in [35], which is more easily applicable to multi-target tracking problems and can be implemented using only simple approximation techniques, such as Gaussian mixture matching. It has been shown, in [37], that the δ-GLMB filter can be seen as a special case of the PMBM filter. There it is claimed that the δ-GLMB class is a less efficient version of an MBM parametrization, regardless of whether the MBM is labeled or not.

2.3.8 Measurement-to-track and track-to-track fusion

The question of how to utilize measurements from different sensors is not new, and has been studied extensively [38]. Many methods have been developed, and, roughly speaking, they can be split into two groups: measurement-to-track and track-to-track fusion. The difference between the two methods is in large part revealed by their names; measurement-to-track fusion uses measurements from several sensors to create an estimate, while track-to-track fusion creates estimates for each sensor before these are fused. The methods have their advantages and disadvantages. When using track-to-track fusion the tracks themselves also become an association problem, as these have to be associated to the correct track from the other sensors before the estimates can be fused. This is avoided in measurement-to-track fusion. Measurement-to-track fusion is, however, reliant on some centralized processing unit. This is one of the big advantages of track-to-track fusion, the fact that it works well in a decentralized system. The individual nodes in the system perform calculations on their own measurements, and fuse this estimate with any received estimates before the resulting final estimate is transmitted. Which method is best depends on the problem at hand. For the case of fusion of radar and AIS measurements for maritime tracking, a centralized processing unit is often available as both sensors are placed on the ship. On the other hand, for a large tracking system consisting of a lot of sensors at different locations a decentralized solution might be the best.

2.3.9 On track continuity

Track continuity can be described as the ability to follow the position of a specific target across time steps. The counterpart would be a situation where estimates are presented for each time step, but there is no mechanism to say how the current estimates relate to the previous ones. For track-oriented methods such as the JIPDA, track continuity is preserved through the origin measurement of each track. For MHT, track continuity is also implicitly present as each measurement can be associated with a previous track. While the first PMBM filter didn't formally show track continuity this was nevertheless shown through PMBM trajectory filters in [39]. The PHD filter does not inherit track continuity in it's original form, but it has later been extended to do so through the inclusion of additional schemes [40]. In the GLMB filter, there is explicit track continuity through the use of labels, which connects estimates between time steps. Here, the labels occur as part of the labeled RFSs and are unknown random state variables, as opposed to the labels of the aforementioned methods [41]. For single target tracking the concept of track continuity loses its relevance, as only one track is present and any estimate must necessarily be a continuation of the previous estimate.

The tracker presented in this thesis inhabits track continuity, as it is an extension of a JIPDA tracker. The possibility of identifying targets through their MMSI numbers, does, however, provide an additional layer to this. These MMSI numbers are not labels as they are thought of in the context of most other filters, as they have an actual physical meaning and are not a tool to ensure track continuity. They can, instead, be considered as something to be estimated, and do not necessarily have a direct connection to what track continuity means with regards to target tracking.

CHAPTER 3

Model: Inclusion of asynchronous transponder measurements

3.1 The hybrid state

The track estimates, which in the tracker are propagated from one-time step to the next, contain both continuous and discrete states. This is reflected in the state space which can contain both continuous states $x \in \mathcal{X} \subset \mathbb{R}^{n_x}$ and discrete states $l \in \mathcal{L} \subset \mathbb{N}^{n_l}$. n_x and n_l are the dimensions of the continuous and discrete spaces, respectively. A hybrid state is a state where the state space contains both discrete and continuous states, or uncertainties as it is formulated in [42, p. 441]. This structure is useful in target tracking as the kinematic state will be continuous, while for example, the choice of kinematic model for the target will be discrete. A thorough analysis of the concept of the hybrid state space can be found in [43].

For the tracker detailed here, the state space consists of four elements:

$\mathbf{x}$	is the kinematic state
v	is the visibility state, indicating whether the target is visible to the sensor or not
τ	is the MMSI number of the target
s	is the kinematic model the target is following

Of these, only the kinematic state is continuous while the rest are discrete. The states are summarized in the hybrid state

$$\mathbf{y} = [\mathbf{x}, \mathrm{v}, \tau, s]^\top. \tag{3.1}$$

3.1.1 Visibility

When the IPDA was introduced in [44] two different models for target existence and observability were presented. These were called Markov Chain 1 (MC1) and Markov Chain 2 (MC2). The MC1 model assumes that a target could exist and have a certain probability

of being detected, or it could not exist. The MC2 model extended this by assuming that a target could exist but be unobservable. Thus, for the first model observability and existence were treated identically, while for the second a target could exist without being observable. The second method, MC2, is used here. This is done by introducing an observability variable, v, in the hybrid state. This is a discrete state with only two possibilities, either the target is observable or it is not. It is defined as

$$\mathrm{v} = \begin{cases} 1 & \text{if the target is visible} \\ 0 & \text{otherwise} \end{cases} \tag{3.2}$$

The probability of either state at time step k is in general denoted as $o_k^{t\mathrm{v}}$, and the probability of the target being visible, i.e. o_k^{t1} is written as η_k^t. The Markov chain transition probabilities, i.e. the probabilities of changing between the different visibility states, are represented by the matrix w. The transition probability from a previous state to the current is denoted as $w^{\mathrm{v}_{k-1}\mathrm{v}_k}$. These probabilities are user-defined parameters, and do not have to be time-dependent as they only have an impact on the radar measurements, which arrive at fixed intervals. The concept of visibility as it is used here does not impact the AIS measurements.

3.1.2 MMSI numbers

The hybrid state contains information regarding the MMSI number of the target. The MMSI numbers are denoted as τ, and the set of MMSI numbers is denoted as $\mathcal{V}$. The set contains all possible MMSI numbers, in addition to number 0, representing the absence of an MMSI number. Each MMSI number $\tau \in \mathcal{V}$ has probability $\xi_k^{t\tau}$ of being the correct MMSI number for target t at time step k, with $\xi^{0\tau}$ as the initial probability.

Whenever a new detection happens in the form of an AIS measurement, the MMSI number probabilities evolve according to the transition matrix

$$q^{\tau_{k-1}\tau_k} = \begin{cases} 0 & \text{if } \tau_{k-1} = 0 \text{ and } \tau_k = 0 \\ 1/(|\mathcal{V}| - 1) & \text{if } \tau_{k-1} = 0 \text{ and } \tau_k > 0 \\ 1 & \text{if } \tau_{k-1} = \tau_k > 0 \\ 0 & \text{otherwise} \end{cases} \tag{3.3}$$

where $|\mathcal{V}| - 1$ is the total number of possible MMSI numbers. Thus, the probability of a track having no MMSI number becomes zero conditional on association with an AIS measurement. Furthermore, all received MMSI numbers have a possibility of being corrupted, and the probability P_C denotes the confidence in the MMSI number being correct.

3.1.3 Kinematic models

The initial probability for each kinematic model s, or mode, being the correct one is denoted as μ^0, while the corresponding probability for track t at time step k, conditional on MMSI number τ, is $\mu_k^{t\tau s}$. These probabilities can also change between time steps, and the probabilities of the mode staying the same and the mode changing are considered.

The mode transition probabilities can be represented as a matrix, denoted here as π. The number of kinematic models in use is denoted M, and the π-matrix is of size $M \times M$.

$$\pi = \begin{bmatrix} \pi^{11} & \dots & \pi^{1M} \\ \vdots & \ddots & \vdots \\ \pi^{M1} & \dots & \pi^{MM} \end{bmatrix} \tag{3.4}$$

where π^{ji} is the probability that the correct mode at the current time step is i, given that the previous mode was j, or

$$\pi^{ji} = \Pr(s_k^t = i | s_{k-1}^t = j) \tag{3.5}$$

for track t. Due to the variable time intervals between time steps the π-matrix needs to be time dependent. To translate (3.4) from a scheme where all time increments are constant to one where they are not, the theory of continuous Markov Chains is used. As described in [45], a generator matrix G takes over the role of the transition matrix for discrete time Markov Chains. The generator matrix is defined as

$$G = \lim_{\Delta \mathrm{t} \to 0^+} \frac{P(h) - I}{\Delta \mathrm{t}} \tag{3.6}$$

where $P(h)$ is the transition matrix. Furthermore, we have that

$$p_{ij} \approx g_{ij} \Delta \mathrm{t} \quad \text{if } i \neq j \quad \text{and } p_{ii} \approx 1 + g_{ii} \Delta \mathrm{t}. \tag{3.7}$$

This approximation is reasonable for relatively small Δt. By translating (3.4) to a generator matrix we get

$$G = \begin{bmatrix} \pi^{11} - 1 & \dots & \pi^{1M} \\ \vdots & \ddots & \vdots \\ \pi^{M1} & \dots & \pi^{MM} - 1 \end{bmatrix} \tag{3.8}$$

which, by using (3.7) for a given time interval Δt, yields

$$\pi(\Delta \mathrm{t}) \approx \begin{bmatrix} 1 + (\pi^{11} - 1)\Delta \mathrm{t} & \dots & \pi^{1M} \Delta \mathrm{t} \\ \vdots & \ddots & \vdots \\ \pi^{M1} \Delta \mathrm{t} & \dots & 1 + (\pi^{MM} - 1)\Delta \mathrm{t} \end{bmatrix} \tag{3.9}$$

Using this the probability of switching to a different mode increases linearly as Δt increases. If no time has passed the probability of switching mode becomes zero, and π becomes the identity matrix. For large Δt the approximation breaks down, as the probabilities can become negative. The exact expressions reach a steady-state for large Δt.

3.2 Modeling assumptions

Several assumptions are made to make the algorithm tractable. A slightly modified version of the standard model for multi-target tracking [46, p. 129] is used to accommodate the sequential AIS measurements. Firstly, the model assumes that a target can only generate a single measurement, and that a measurement can only originate from a single target. Furthermore

M1 New targets are born according to a Poisson process with intensity $\mu(\mathbf{y})$.

M2 Existing targets survive from time t_{k-1} to time t_k with probability $P_S(t_{k-1}, t_k)$.

M3 The MMSI numbers only change upon detection through a measurement.

M4 The evolution of a surviving target is given by $f_{\mathbf{y}}(\mathbf{y}_k|\mathbf{y}_{k-1})$.

M5 A target with state $\mathbf{y}_k$ generates a measurement $\mathbf{z}_k$ with probability $P_D(\mathbf{y}_k)$.

M6 Radar clutter measurements occur according to a Poisson process with intensity $\lambda(\mathbf{z})$.

M7 The radar measurement of a detected target is related to the state according to $f^R_{\mathbf{z}}(\mathbf{z}_k|\mathbf{y}_k)$. The radar measurements of all detected targets are assumed to arrive at a constant frequency, and are all synchronized to have the same time stamp.

M8 The AIS measurement of a transmitting target is related to the state according to $f^A_{\mathbf{z}}(\mathbf{z}_k|\mathbf{y}_k)$, and the AIS measurement for any individual target can arrive at any time.

Independence is assumed whenever it doesn't contradict the above assumptions. An explanation of the different assumptions follows.

M1

We assume that we have the unknown target intensity

$$v(\mathbf{y}) = b1_\Omega(\mathbf{H}^{(s)}\mathbf{x})\mathcal{N}(\mathbf{H}^{*(s)}\mathbf{x}; \mathbf{0}, \mathbf{P}_v^{(s)})\mu^{0s\tau}o^{0\mathrm{v}}\xi^{0\tau} \tag{3.10}$$

where b is the overall rate of birth, $\mu^{0s\tau}$ is the initial mode probability for mode s, $o^{0\mathrm{v}}$ is the initial probability for visibility state v and $\xi^{0\tau}$ is the initial label probability for MMSI number τ. $1_\Omega(\cdot)$ is the indicator function, which is zero everywhere except in the surveillance area, where it is 1. $\mathbf{H}^{(s)}$ is the measurement matrix for mode s while $\mathbf{H}^{*(s)}$ is the matrix giving the other elements from the state for mode s. Thus,

$$\begin{bmatrix} \mathbf{H} \\ \mathbf{H}^* \end{bmatrix} \mathbf{x} = \mathbf{x} \tag{3.11}$$

Furthermore, $\mathbf{P}_v^{(s)}$ is the covariance matrix for the velocities of mode s, corresponding to the reduced state $\mathbf{H}^{*(s)}\mathbf{x}$. Before the target is detected through an AIS measurement the MMSI probabilities are defined as

$$\xi^{0\tau} = \begin{cases} 1 & \text{if } \tau = 0 \\ 0 & \text{otherwise} \end{cases} \tag{3.12}$$

Remark. This is only one of the possible ways of modeling the MMSI numbers. Conceptually, it can be explained as defining that the target has no MMSI number upon detection. The probability of the target having no MMSI number is reduced as AIS measurements are detected, while the probability of all MMSI numbers are increased. Another possibility is to initialize the MMSI number probabilities with a uniform probability for all $\tau > 0$,

with some constant as a probability for $\tau = 0$. Then, no transitions are necessary either between time steps or when new AIS measurements arrive. This may be more in touch with how the MMSI numbers are thought of in real life, as these are static IDs belonging to each target. However, when introducing a uniform prior across all MMSI numbers the independence of the unknown targets is violated, because a detected target with high probability for a given MMSI number reduces the probability of any of the unknown target having the same MMSI. This is avoided with a method such as the one used here, where transitions are used upon detection.

M2

The survival probability is modeled as a function of time since the last update. A constant parameter P_{S_c} denotes the probability of survival after one second. Thus, the survival probability of an interval between times t_{k-1} and t_k, denoted as $\Delta\mathrm{t}$, becomes

$$P_S(\mathrm{t}_{k-1}, \mathrm{t}_k) = P_{S_c}^{\Delta\mathrm{t}}. \tag{3.13}$$

M3

The MMSI numbers τ are assumed to remain unchanged between time steps, and only change when any new measurements from the target are detected. The MMSI probabilities $\xi^{t\tau}$ are assumed to change according to

$$\Pr(\tau|\text{AIS detection}) = \textstyle\sum_{\tau'} q^{\tau'\tau_k} \xi_{k-1}^{t\tau'} \tag{3.14}$$

whenever a new AIS measurement is detected. When there is no detection $\xi_{k|k-1}^{t\tau} = \xi_{k-1}^{t\tau}$.

M4

From time step $k-1$ to k the evolution of a target is given by

$$f_{\mathbf{y}}(\mathbf{y}_k|\mathbf{y}_{k-1}) = f_{\mathbf{x}}^{s\tau}(\mathbf{x}_k|\mathbf{x}_{k-1}) \pi^{s_{k-1}s_k} w^{\mathrm{v}_{k-1}\mathrm{v}_k}. \tag{3.15}$$

The π-matrix, explained in Section 3.1.3 contains the Markov chain probabilities of changing between different kinematic models. w, as explained in Section 3.1.1 contains the Markov chain probabilities of the target switching between the visible and invisible state. The MMSI numbers only change whenever a detection is made, and are therefore not included in the prediction. The kinematic transition $f_{\mathbf{x}}^{s\tau}(\mathbf{x}_k|\mathbf{x}_{k-1})$ is assumed to be on the form of a Gaussian

$$f_{\mathbf{x}}^{s\tau}(\mathbf{x}_k|\mathbf{x}_{k-1}) = \mathcal{N}(\mathbf{x}_k|\mathbf{f}^{(s)}(\mathbf{x}_{k-1}), \mathbf{Q}^{(s)}). \tag{3.16}$$

M5

For radar measurements, the detection probability $P_D(\mathbf{y}_k)$ varies based on the visibility state v and is defined as

$$P_D(\mathbf{y}) = \begin{cases} P_D & \text{if } \mathrm{v} = 1 \\ 0 & \text{if } \mathrm{v} = 0 \end{cases} \tag{3.17}$$

where P_D is a constant describing the probability of a target being detected by the radar at a given time step.

For AIS measurements, which are assumed to give no missed detections when a message is transmitted, we have that

$$P_D(\mathbf{y}) = \frac{\Pr(\tau|\text{AIS detection})\Pr(\text{AIS detection})}{\Pr(\tau)} \tag{3.18}$$

where

$$\Pr(\text{AIS detection}) = \begin{cases} 1 & \text{if an AIS measurement is received} \\ 0 & \text{otherwise} \end{cases} \tag{3.19}$$

independently of the visibility state. This, combined with (3.14), gives

$$P_D(\mathbf{y}) = \begin{cases} \dfrac{\sum_{\tau'} q^{\tau'\tau_k}\xi_{k-1}^{t\tau'}}{\xi_{k-1}^{t\tau}} & \text{if an AIS measurement is received} \\ 0 & \text{otherwise} \end{cases} \tag{3.20}$$

M6

Radar clutter measurements are assumed to be uniformly distributed, with the number of measurements following a Poisson distribution with intensity λ. The AIS measurements do not generate clutter.

M7

The radar measurements are assumed to be synchronized, and to arrive simultaneously at a fixed frequency. This means that when radar measurements arrive at time step k, the set of radar measurements contain measurements from all detected targets at time step k, in addition to clutter measurements. The radar measurement likelihood is

$$f_{\mathbf{z}}^R(\mathbf{z}_k|\mathbf{y}_k) = \mathcal{N}(\mathbf{z}_k|\mathbf{H}_R\mathbf{x}, \mathbf{R}_R). \tag{3.21}$$

M8

The AIS measurements can arrive whenever, and are not synchronized. This means that an AIS measurement can be received at any time, from any target. It is not assumed that all targets transmit AIS measurements simultaneously, in contrary to what is done for the radar measurements. The measurement likelihood for the AIS measurements is

$$f_{\mathbf{z}}^A(\mathbf{z}_k|\mathbf{y}_k) = f_{\mathbf{p}}(\mathbf{p}_k|\mathbf{y}_k)f_\tau(\tau^{\mathbf{z}_k}|\tau) \tag{3.22}$$

where $\mathbf{z}_k$ is the whole AIS measurement and $\mathbf{p}_k$ only contains the positional data of the measurement. Furthermore

$$f_\tau(\tau^{\mathbf{z}_k}|\tau) = \begin{cases} P_C & \text{if } \tau_k = \tau_k^{\mathbf{z}_k} \\ \dfrac{1-P_C}{|\mathcal{V}|-1} & \text{if } \tau_k \neq \tau_k^{\mathbf{z}_k} \text{ and } \tau > 0 \\ 0 & \text{if } \tau = 0 \end{cases} \tag{3.23}$$

where P_C is a fixed parameter describing the confidence in the MMSI number not being corrupted, denoted as the confidence probability, and $|\mathcal{V}| - 1$ is the number of MMSI numbers. The likelihood for the positional data from the AIS measurements is

$$f_{\mathbf{p}}(\mathbf{p}_k|\mathbf{y}_k) = \mathcal{N}(\mathbf{p}_k|\mathbf{H}_A\mathbf{x}, \mathbf{R}_A). \tag{3.24}$$

3.3 Modeling framework

For the purpose of deriving the tracker, the PMBM filter is used as a basis. This is the same as was done in [1], with the same perspective as in [30]. This perspective involves the use of probability generating functionals (p.g.fls) on random finite sets (RFSs). The p.g.fl of a RFS density f is

$$G[h] = \int h^X f(X)\delta X \tag{3.25}$$

where X is a RFS, and h^X is defined as

$$h^X \triangleq \prod_{x\in X} h(x). \tag{3.26}$$

The p.g.fl transforms a density to a form more suited for analytical evaluation. This is similar to the use of more familiar transformations, such as the Fourier transform.

From [30], the form of the full multi-target distribution at time step k, conditioned on the measurements up to and including time step k' is

$$f_{k|k'} = \sum_{Y\subset X} f^{ppp}_{k|k'}(Y) f^{mbm}_{k|k'}(X - Y) \tag{3.27}$$

which in its p.g.fl form is

$$G_{k|k'}[h] = G^{ppp}_{k|k'}[h] G^{mbm}_{k|k'}[h]. \tag{3.28}$$

As the time step k' can be both the current and previous time, the expression can represent both the prediction and the update. Here, PPP stands for Poisson Point Process, while MBM stands for Multi-Bernoulli Mixture. Furthermore

$$G^{ppp}_{k|k'} = \exp(v[h - 1]) \tag{3.29}$$

is the p.g.fl of a PPP representing the unknown targets. The expression $v[h - 1]$ is a functional. What differentiates a functional from a function, is that the functional has a function as argument instead of a scalar. The brackets notation is used here to signify that it is a linear functional

$$f[h] = \int h(x)f(x)dx. \tag{3.30}$$

However, as described in assumption M1 and also pointed out in [1], the predicted unknown target intensity is assumed known and stationary. This means that the PPPs posterior has no impact on the MBMs, and it can be safely ignored when calculating these.

Furthermore, $G^{mbm}_{k|k'}[h]$ represents the p.g.fl of a MBM, which is a linear combination of multi-Bernoulli distributions

$$G^{mbm}_{k|k'}[h] \propto \sum_{a \in \mathcal{A}^{k|k'}} \prod_{i=1}^{n^t_{k|k'}} w^{i,a^i}_{k|k'} G^{i,a^i}_{k|k'}[h]. \tag{3.31}$$

where $\mathcal{A}^{k|k'}$ is the set of global association history hypotheses and $n^t_{k|k'}$ is the number of tracks at time step k conditioned on the measurements up to and including time step k'. The set of global association history hypotheses are in [30] defined as

$$\begin{aligned} \mathcal{A}^{k|k'} = &\{(a^1, \dots, a^{n^t_{k|k'}}) | a^i \in \mathcal{H}^i_{k|k'}, \cup_{i=1}^{n^t_{k|k'}} \mathcal{M}^{k'}(i, a^i) = \mathcal{M}^{k'}, \\ &\mathcal{M}^{k'}(i, a^i) \ \cup \ \mathcal{M}^{k'}(j, a^j) = \emptyset \ \forall \ i \neq j\} \end{aligned} \tag{3.32}$$

where $\mathcal{H}^i_{k|k'}$ is the set of association history hypotheses for single tracks, and $\mathcal{M}^{k'}$ is the set of allowed track-to-measurement associations. An association history hypotheses for a single track, $a^t \in \mathcal{H}^i_{k|k'}$, then contains one of the possible, legal, associations for all time steps up to time k. Furthermore, this can be simplified to $\mathcal{A}^k$ for the set of global association hypotheses for only time step k.

To make the expression in (3.31) somewhat more concrete, one can consider the set density for a Bernoulli distribution:

$$f(X) = \begin{cases} 1 - p & \text{if } X = \emptyset \\ pf(x) & \text{if } X = \{x\} \\ 0 & \text{otherwise} \end{cases} \tag{3.33}$$

In a tracking context, at time step k the probability p becomes the probability of existence $r^t_{k|k'}$, and x is the hybrid state $\mathbf{y}_{k|k'}$. Taking the p.g.fl of this yields

$$G^{i,a^i}_{k|k'}[h] = 1 - r^t_{k|k'} - r^t_{k|k'} f[h] \tag{3.34}$$

This is how the targets are represented in their most general form. From this point of view there are several methods of how to calculate the different values, and how to represent the different entities. One of these methods is presented in the next chapter.

CHAPTER 4

Method: Inclusion of asynchronous transponder measurements

The VIMMJIPDA, as presented in [1], has shown good promise for multi-target radar-based tracking. In this chapter, a method for using both radar and AIS measurements in the VIMMJIPDA is presented. The fusion of the two measurement types is done on a measurement-to-measurement basis. The tracker handles radar measurements in batches, which arrive at a fixed sampling interval. The AIS measurements are handled as they arrive, which can be at any time. The overall structure of the tracker can be seen in fig. 4.1.

4.1 The prior

The prior hybrid state of track t is

$$f_{k-1}^{t}(\mathbf{y}) = f_{k-1}^{t\tau s}(\mathbf{x}) o_{k-1}^{t\mathrm{v}} \xi_{k-1}^{t\tau} \mu_{k-1}^{t\tau s}. \tag{4.1}$$

Here, $o_{k-1}^{t\mathrm{v}}$ is the prior probability for the visibility state v, $\xi_{k-1}^{t\tau}$ is the prior probability for MMSI number τ, and $\mu_{k-1}^{t\tau s}$ is the prior probability for mode s conditional on MMSI number τ. $f_{k-1}^{t\tau s}(\mathbf{x})$ is the prior kinematic density, conditional on mode s and MMSI number τ.

Remark. Some care has to be taken regarding what constitutes the previous time step $k-1$. As described in assumption M8, the AIS measurements can arrive at any time. This means that the previous time step $k-1$ can point to any time before time step k. To avoid having to introduce a complicated notation describing all time steps in detail, $k-1$ is used in general for the most recent time in the past where the track in question has been updated. For situations where the time indices point to a radar update specifically, this is denoted by the subscript R.

4.2 The prediction

Proposition 1. The existence probability is predicted using the probability of survival for each target as a function of the time between time steps Δt

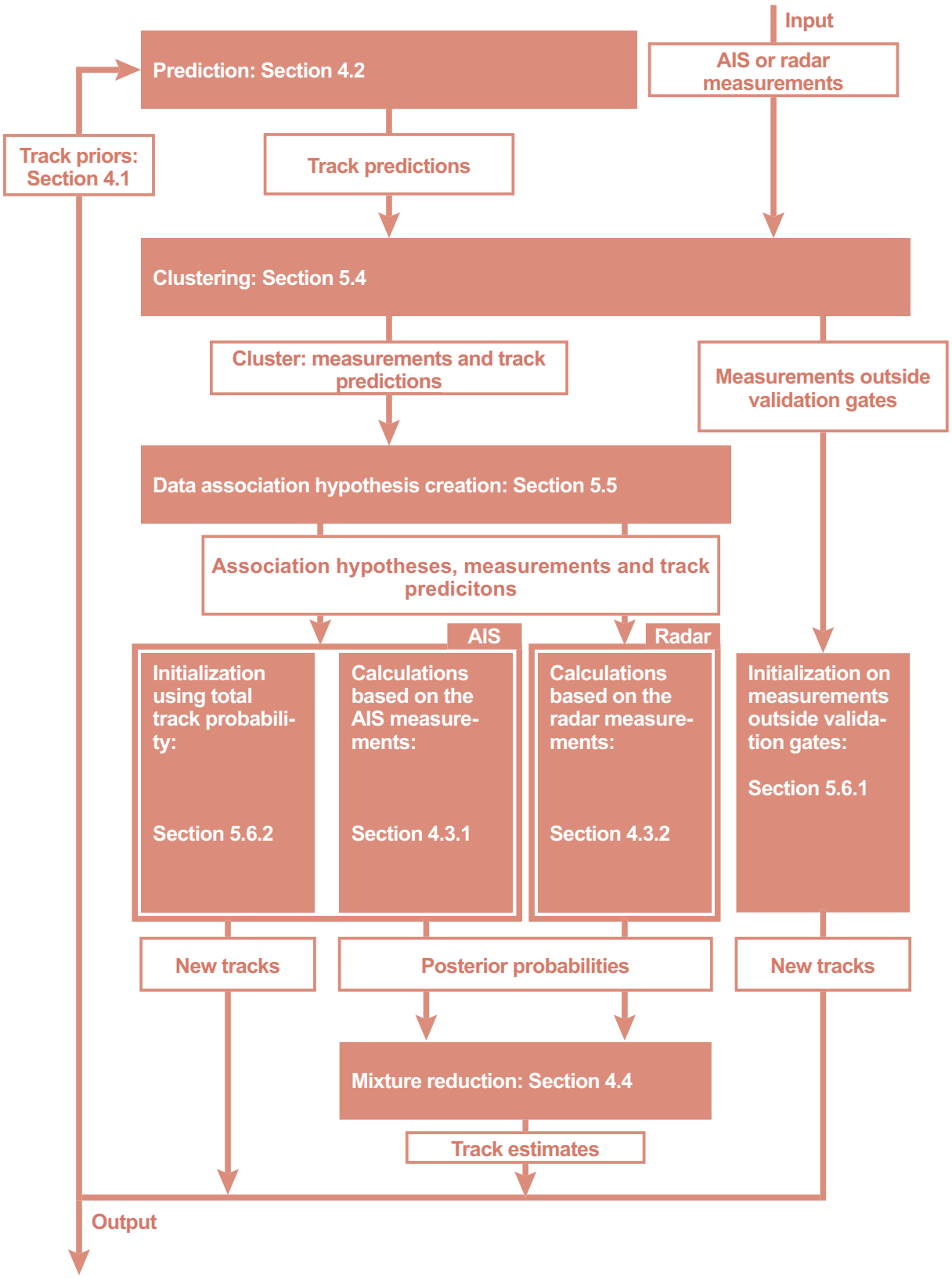

Figure 4.1: Diagram showing the work flow and structure of the tracker.

$$r_{k|k-1}^{t} = P_S(\Delta \mathrm{t}) r_{k-1}^{t}. \tag{4.2}$$

The predicted visibility probability is calculated as

$$\eta_{k_R|(k-1)_R}^{t} = (\omega^{01})(1 - \eta_{(k-1)_R}^{t}) + (\omega^{11})\eta_{(k-1)_R}^{t} \tag{4.3}$$

The prediction of the mode and kinematic state of the target is done according to

$$\mu_{k|k-1}^{t\tau s} = \textstyle\sum_{\tilde{s}} \pi^{\tilde{s}s}(\Delta \mathrm{t}) \mu_{k-1}^{t\tau\tilde{s}} \tag{4.4}$$

$$f_{k|k-1}^{t\tau s}(\mathbf{x}) = \textstyle\int f_{\mathbf{x}}(\mathbf{x}|\tilde{\mathbf{x}}) f_{k-1}^{t\tau s,0}(\tilde{\mathbf{x}}) \mathrm{d}\tilde{\mathbf{x}} \tag{4.5}$$

where the mode- and MMSI-conditional prior is

$$f_{k-1}^{t\tau s,0}(\tilde{\mathbf{x}}) = \frac{1}{\sum_{\tilde{s}} \pi^{\tilde{s}s}(\Delta \mathrm{t}) \mu_{k-1}^{t\tau\tilde{s}}} \sum_{\tilde{s}} \pi^{\tilde{s}s}(\Delta \mathrm{t}) \mu_{k-1}^{t\tau\tilde{s}} f_{k-1}^{t\tau\tilde{s}}(\tilde{\mathbf{x}}) \tag{4.6}$$

Lastly, the MMSI number probabilities remain unchanged, and

$$\xi_{k|k-1}^{t\tau} = \xi_{k-1}^{t\tau}. \tag{4.7}$$

Proof: From [30], the equations for the prediction are

$$r_{k|k-1}^{t} = r_{k-1}^{t} f_{k-1}^{t}[P_S(\tilde{\mathbf{y}})] \tag{4.8}$$

$$f_{k|k-1}^{t}(\mathbf{y}) = \frac{\int f_{\mathbf{y}}(\mathbf{y}|\tilde{\mathbf{y}}) P_S(\tilde{\mathbf{y}}) f_{k-1}^{t}(\tilde{\mathbf{y}}) \mathrm{d}\tilde{\mathbf{y}}}{f_{k-1}^{t}[P_S(\tilde{\mathbf{y}})]} \tag{4.9}$$

Firstly, $f_{k-1}^{t}[P_S(\tilde{\mathbf{y}})] = P_S(\Delta \mathrm{t}) f_{k-1}^{t}[1] = P_S(\Delta \mathrm{t})$ because $P_S(\Delta \mathrm{t})$ is only dependent on the times t_k and t_{k-1} which are not part of the state $\mathbf{y}$, and the linear functional $f_{k-1}^{t}[1]$ becomes 1. This gives (4.2). By using this for (4.9) as well results in

$$f_{k|k-1}^{t}(\mathbf{y}) = \int f_{\mathbf{y}}(\mathbf{y}|\tilde{\mathbf{y}}) f_{k-1}^{t}(\tilde{\mathbf{y}}) \mathrm{d}\tilde{\mathbf{y}} \tag{4.10}$$

which can be written as

$$f_{k|k-1}^{t}(\mathbf{y}) = \Big(\sum_{\tilde{\mathrm{v}}} w^{\tilde{\mathrm{v}}\mathrm{v}} o_{k-1}^{t\tilde{\mathrm{v}}} \Big) \xi_{k-1}^{t\tau} \sum_{\tilde{s}} \pi^{\tilde{s}s}(\Delta \mathrm{t}) \mu_{k-1}^{t\tau\tilde{s}} \int f_{\mathbf{x}}(\mathbf{x}|\tilde{\mathbf{x}}) f_{k-1}^{t\tau\tilde{s}}(\tilde{\mathbf{x}}) \mathrm{d}\tilde{\mathbf{x}} \tag{4.11}$$

This gives the predicted visibility probability $\eta_{k|k-1}^{t}$. Furthermore, the MMSI number probabilities do not change between time steps, giving $\xi_{k|k-1}^{t\tau} = \xi_{k-1}^{t\tau}$. This leaves

$$\begin{aligned} f_{k|k-1}^{t}(\mathbf{x}, s) &= \sum_{\tilde{s}} \pi^{\tilde{s}s}(\Delta \mathrm{t}) \mu_{k-1}^{t\tau\tilde{s}} \int f_{\mathbf{x}}(\mathbf{x}|\tilde{\mathbf{x}}) f_{k-1}^{t\tau\tilde{s}}(\tilde{\mathbf{x}}) \mathrm{d}\tilde{\mathbf{x}} \\ &= \sum_{\tilde{s}} \pi^{\tilde{s}s}(\Delta \mathrm{t}) \mu_{k-1}^{t\tau\tilde{s}} \int f_{\mathbf{x}}(\mathbf{x}|\tilde{\mathbf{x}}) \frac{\sum_{\tilde{s}} \pi^{\tilde{s}s}(\Delta \mathrm{t}) \mu_{k-1}^{t\tau\tilde{s}} f_{k-1}^{t\tau\tilde{s}}(\tilde{\mathbf{x}}) \mathrm{d}\tilde{\mathbf{x}}}{\sum_{\tilde{s}} \pi^{\tilde{s}s}(\Delta \mathrm{t}) \mu_{k-1}^{t\tau\tilde{s}}} \end{aligned} \tag{4.12}$$

as is also shown in [1], which provides the resulting expressions $\mu_{k|k-1}^{t\tau s}$ and $f_{k-1}^{t\tau s,0}(\tilde{\mathbf{x}})$

Remark. By assuming that both $f_{\mathbf{x}}(\mathbf{x}|\tilde{\mathbf{x}})$ and $f_{k-1}^{t\tau s,0}(\tilde{\mathbf{x}})$ are Gaussian-linear, $f_{k|k-1}^{t\tau s}(\mathbf{x})$ can be evaluated in a regular manner. However, the mode- and MMSI-conditional prior $f_{k-1}^{t\tau s,0}$ is, assuming the individual $f_{k-1}^{t\tau s}$ are Gaussian, a Gaussian mixture. This means that some approximation technique is needed, due to the exponential nature of the mode histories. This is done by using moment matching, as is described in [46] and [42]. In this way, the prediction $f_{k|k-1}^{t\tau s}(\mathbf{x})$ is approximated as a single Gaussian.

4.3 The posterior

4.3.1 AIS measurements

If the first measurement of a track is claimed by another track by being within the validation gate of the other track, the track is *empty*, i.e. $a_{k'}^t = 0 \; \forall \; k'$, and no initialization will be performed.

Proposition 2. For a *new target* initialization on an AIS measurement, that is when $a_{k'}^t = 0 \; \forall \; k' < k$ and $a_k^t > 0$, we have that

$$w_k^j \approx b \sum_{\tilde{\tau}} \sum_{\tau'} q^{\tau'\tilde{\tau}} \xi^{0\tau'} f_\tau(\tau^{\mathbf{z}_k}|\tau) \tag{4.13}$$
$$r_k^j = 1 \tag{4.14}$$
$$\mu_k^{\tau sj} = \mu^{0s} \tag{4.15}$$
$$\eta_k^j = \eta^0 \tag{4.16}$$
$$\xi_k^{t\tau j} = f_\tau(\tau^{\mathbf{z}_k}|\tau) \tag{4.17}$$
$$f_k^{\tau sj}(\mathbf{x}) \approx \mathcal{N}(\mathbf{x}, \hat{\mathbf{x}}_0^s, \mathbf{P}_0^s) \tag{4.18}$$

where $\hat{\mathbf{x}}_0^s = [\mathbf{p}_k^j; \mathbf{0}]$ and $\mathbf{P}_0^s = \text{diag}(\mathbf{R}_A^s, \mathbf{P}_v)$.

Proof: From [30], with notation changed to the one used here, the general equations for the initialization of a target on an AIS measurement are given as

$$w_k^j = \lambda + v[f_{\mathbf{z}}^A(\mathbf{z}_k^{a^t}|\tilde{\mathbf{y}}) P_D(\tilde{\mathbf{y}})] \tag{4.19}$$
$$r_k^j = \frac{v[f_{\mathbf{z}}^A(\mathbf{z}_k^{a^t}|\tilde{\mathbf{y}}) P_D(\tilde{\mathbf{y}})]}{\lambda + v[f_{\mathbf{z}}^A(\mathbf{z}_k^{a^t}|\tilde{\mathbf{y}}) P_D(\tilde{\mathbf{y}})]} \tag{4.20}$$
$$f_k^{tj}(\mathbf{y}) = \frac{f_{\mathbf{z}}^A(\mathbf{z}_k^{a^t}|\mathbf{y}) P_D(\mathbf{y}) v(\mathbf{y})}{v[f_{\mathbf{z}}^A(\mathbf{z}_k^{a^t}|\tilde{\mathbf{y}}) P_D(\tilde{\mathbf{y}})]} \tag{4.21}$$

For a new target the expression $f_{\mathbf{z}}^A(\mathbf{z}_k^{a^t}|\mathbf{y}) P_D(\mathbf{y}) v(\mathbf{y})$ is given by

$$b o^{0\mathrm{v}} \xi^{0\tau} \mu^{0s} 1_\Omega(\mathbf{H}^s \mathbf{x}) \mathcal{N}(\mathbf{z}_k^{a^t}|\mathbf{H}^s \mathbf{x}, \mathbf{R}_A^s) \mathcal{N}(\mathbf{H}^{*s}\mathbf{x}|\mathbf{0}, \mathbf{P}_v^s) P_D(\mathbf{y}) f_\tau(\tau^{\mathbf{z}_k}|\tau) \tag{4.22}$$

The Gaussian distributions are combined into $\mathcal{N}(\mathbf{x}|\hat{\mathbf{x}}_0^s, \mathbf{P}_0^s)$. If the region Ω is large

enough $1_\Omega(\mathbf{H}^s\mathbf{x})$ has no impact on the expression as a function of $\mathbf{x}$. This means that the integral over the latent variable $\mathbf{x}$ can be approximated as 1 for all s. In addition, when summing over all possible MMSI numbers the product $\xi^{0\tau}P_D(\mathbf{y})f_\tau(\tau^{\mathbf{z}_k}|\tau)$ is

$$\textstyle\sum_{\tilde{\tau}} \xi^{0\tilde{\tau}}P_D(\tilde{\mathbf{y}})f_\tau(\tau^{\mathbf{z}_k}|\tilde{\tau}) = \sum_{\tilde{\tau}}\sum_{\tau'} q^{\tau'\tilde{\tau}}\xi^{0\tau'}f_\tau(\tau^{\mathbf{z}_k}|\tilde{\tau}) \tag{4.23}$$

The sum of the mode probabilities μ^{0s} when summing over all modes becomes 1, and the same is the case for $o^{0\mathrm{v}}$ when summing over the visibility states. Thus

$$v[f_{\mathbf{z}}(\mathbf{z}_k^{at}|\tilde{\mathbf{y}})P_D(\tilde{\mathbf{y}})] \approx b\textstyle\sum_{\tilde{\tau}}\sum_{\tau'} q^{\tau'\tilde{\tau}}\xi^{0\tau'}f_\tau(\tau^{\mathbf{z}_k}|\tilde{\tau}) \tag{4.24}$$

The AIS measurements generates no clutter measurements, i.e. $\lambda = 0$, which leads to the existence probability $r_k^j = 1$. The rest of the expressions are found through marginalization of (4.21), which is (4.22) divided by (4.23). The mode probabilities and the visibility probability can be extracted directly from this expression. The MMSI probabilities $\xi_k^{t\tau j}$ are found through

$$\begin{aligned}
\xi_k^{t\tau j} &= \frac{\xi^{0\tau}P_D(\mathbf{y})f_\tau(\tau^{\mathbf{z}_k}|\tilde{\tau})}{\sum_{\tilde{\tau}}\xi^{0\tilde{\tau}}P_D(\tilde{\mathbf{y}})f_\tau(\tau^{\mathbf{z}_k}|\tilde{\tau})} \\
&= \frac{\sum_{\tau'} q^{\tau'\tau}\xi^{0\tau'}f_\tau(\tau^{\mathbf{z}_k}|\tau)}{\sum_{\tilde{\tau}}\sum_{\tau'} q^{\tau'\tilde{\tau}}\xi^{0\tau'}f_\tau(\tau^{\mathbf{z}_k}|\tilde{\tau})} \\
&= \begin{cases} \dfrac{1/(|\mathcal{V}|-1)f_\tau(\tau^{\mathbf{z}_k}|\tau)}{\sum_{\tilde{\tau}} 1/(|\mathcal{V}|-1)f_\tau(\tau^{\mathbf{z}_k}|\tilde{\tau})} & \text{if } \tau > 0 \\ 0 & \text{if } \tau = 0 \end{cases} \\
&= \begin{cases} \dfrac{f_\tau(\tau^{\mathbf{z}_k}|\tau)}{\sum_{\tilde{\tau}} f_\tau(\tau^{\mathbf{z}_k}|\tilde{\tau})} & \text{if } \tau > 0 \\ 0 & \text{if } \tau = 0 \end{cases} \\
&= f_\tau(\tau^{\mathbf{z}_k}|\tau)
\end{aligned} \tag{4.25}$$

by keeping in mind the definition of the q-matrix and $f_\tau(\tau^{\mathbf{z}_k}|\tau)$, in addition to the fact that $\sum_{\tilde{\tau}} f_\tau(\tau^{\mathbf{z}_k}|\tilde{\tau}) = 1$.

Lastly the kinematic probability distribution is approximated as $\mathcal{N}(\mathbf{x}; \hat{\mathbf{x}}_0^s, \mathbf{P}_0^s)$, assuming a large region Ω.

For an AIS *missed detection*, or more precisely a non-association, the posterior is simply the prediction.

Remark. The concept of a missed detection, when considering AIS measurements, is not readily translated from the way it is used for radar measurements. While it for radar measurements is relatively easy to model when a hypothesized target should be detected, the same is not the case for AIS measurements. This is due to how the AIS protocol works, and to predict the time of the incoming AIS measurements is difficult. This problem is avoided by assuming that no information can be gathered from the fact that a target does not transmit an AIS measurement at any given time. In line the framework described in section 3.3, it would be more precise to say that no association is made when an AIS measurement is not received. To call every time $k' \in ((k-1)_R, k_R)$ a target does not associate with an AIS measurement a missed detection would be analogous to saying

the same for radar measurements $\forall\ k' \in ((k-1)_R, k_R)$. However, due to how mixture reduction is performed in a JIPDA, association hypotheses need to be created between every track and measurement in the cluster. This creates the need for introducing the concept of a missed detection also for AIS measurements.

Proposition 3. For a *detection* in the form of an AIS measurement, when $a_k^t > 0$ and $a_{k'}^t > 0\ \exists\ k' < k$, we have that

$$w_k^{tj} = r_{k|k-1}^t \sum_{\tilde{\tau}} \sum_{\tau'} (q^{\tau'\tilde{\tau}} \xi_{k-1}^{\tau'\tilde{\tau}}) l_A^{t\tilde{\tau}j} \tag{4.26}$$

$$r_k^{tj} = 1 \tag{4.27}$$

$$\mu_k^{t\tau sj} = \mu_{k|k-1}^{t\tau sj} l_A^{t\tau sj} / \sum_{\tilde{s}} \mu_{k|k-1}^{t\tau\tilde{s}} l_A^{t\tau\tilde{s}j} \tag{4.28}$$

$$\xi_k^{t\tau j} = \big(\sum_{\tau'} q^{\tau'\tau} \xi_{k-1}^{\tau'}\big) l_A^{t\tau j} / \sum_{\tilde{\tau}} \big(\sum_{\tau'} q^{\tau'\tilde{\tau}} \xi_{k-1}^{\tau'}\big) l_A^{t\tilde{\tau}j} \tag{4.29}$$

The kinematic state becomes

$$f_k^{t\tau sj}(\mathbf{x}) = \frac{f_{\mathbf{z}}^A(\mathbf{z}_k^j|\mathbf{x}) f_{k|k-1}^{t\tau s}(\mathbf{x})}{l_A^{t\tau sj}}. \tag{4.30}$$

Furthermore, $l_A^{t\tau sj}$ and $l_A^{t\tau j}$ are defined as

$$l_A^{t\tau sj} = f_\tau(\tau^{\mathbf{z}_k}|\tilde{\tau}) \int f_{\mathbf{p}}^s(\mathbf{p}_k^j|\tilde{\mathbf{x}}) f_{k|k-1}^{t\tau s}(\tilde{\mathbf{x}}) \mathrm{d}\tilde{\mathbf{x}} \tag{4.31}$$

and

$$l_A^{t\tau j} = \sum_{\tilde{s}} \mu_{k|k-1}^{t\tau\tilde{s}j} l_A^{t\tau\tilde{s}j} \tag{4.32}$$

Proof: From [30], the PMBM expressions for an AIS measurement detection are

$$w_k^{tj} = r_{k|k-1}^t f_{k|k-1}^t [f_{\mathbf{z}}^A(\mathbf{z}_k^{a^t}|\tilde{\mathbf{y}}) P_D(\tilde{\mathbf{y}})] \tag{4.33}$$

$$r_k^{tj} = 1 \tag{4.34}$$

$$f_k^{tj}(\mathbf{y}) = \frac{f_{\mathbf{z}}^A(\mathbf{z}_k^{a^t}|\mathbf{y}) P_D(\mathbf{y}) f_{k|k-1}^t(\mathbf{y})}{f_{k|k-1}^t [f_{\mathbf{z}}^A(\mathbf{z}_k^{a^t}|\tilde{\mathbf{y}}) P_D(\tilde{\mathbf{y}})]} \tag{4.35}$$

The existence probability follows directly from the above expression. The weight w_k^{tj} is found by recognizing that

$$f_{k|k-1}^t [f_{\mathbf{z}}^A(\mathbf{z}_k^{a^t}|\tilde{\mathbf{y}}) P_D(\tilde{\mathbf{y}})] = \sum_{\tilde{\tau}} \xi_{k-1}^{t\tilde{\tau}} P_D(\tilde{\mathbf{y}}) l_A^{t\tilde{\tau}j} \tag{4.36}$$

where the product $\xi_{k-1}^{t\tilde{\tau}} P_D(\tilde{\mathbf{y}})$ can be written as

$$\xi_{k-1}^{t\tilde{\tau}} P_D(\tilde{\mathbf{y}}) = \xi_{k-1}^{t\tilde{\tau}} \frac{\sum_{\tau'} q^{\tau'\tilde{\tau}} \xi_{k-1}^{t\tau'}}{\xi_{k-1}^{\tilde{\tau}}} = \sum_{\tau'} q^{\tau'\tilde{\tau}} \xi_{k-1}^{t\tau'} \tag{4.37}$$

Furthermore, (4.35) becomes

$$
\begin{aligned}
&\frac{o_{k-1}^{\text{tv}}\xi_{k-1}^{t\tau}\mu_{k|k-1}^{t\tau s}f_{\mathbf{z}}^{A}(\mathbf{z}_k^{a^t}|\mathbf{x})P_D(\mathbf{y})f_{k|k-1}^{t\tau s}(\mathbf{x})}{\sum_{\tilde{\tau}}\xi_{k-1}^{t\tilde{\tau}}P_D(\tilde{\mathbf{y}})\sum_{\tilde{s}}\mu_{k|k-1}^{t\tilde{s}\tilde{\tau}}l_A^{t\tilde{\tau}\tilde{s}j}} \\
=&o_{k-1}^{\text{tv}}\ \frac{\left(\sum_{\tau'}q^{\tau'\tau}\xi_{k-1}^{\tau'}\right)}{\sum_{\tilde{\tau}}\left(\sum_{\tau'}q^{\tau'\tilde{\tau}}\xi_{k-1}^{t\tilde{\tau}}\right)\sum_{\tilde{s}}\mu_{k|k-1}^{t\tilde{s}\tilde{\tau}}l_A^{t\tilde{\tau}\tilde{s}j}}\ \mu_{k|k-1}^{t\tau s}\ f_{\mathbf{z}}^{A}(\mathbf{z}_k^{a^t}|\mathbf{x})f_{k|k-1}^{t\tau s}(\mathbf{x}) \\
=&o_{k-1}^{\text{tv}}\frac{\left(\sum_{\tau'}q^{\tau'\tau}\xi_{k-1}^{\tau'}\right)l_A^{t\tau j}}{\sum_{\tilde{\tau}}\left(\sum_{\tau'}q^{\tau'\tilde{\tau}}\xi_{k-1}^{\tau'}\right)l_A^{t\tilde{\tau}j}}\frac{\mu_{k|k-1}^{t\tau s}l_A^{t\tau sj}}{l_A^{t\tau j}}\frac{f_{\mathbf{z}}^{A}(\mathbf{z}_k^{a^t}|\mathbf{x})f_{k|k-1}^{t\tau s}(\mathbf{x})}{l_A^{t\tau sj}}
\end{aligned}
\tag{4.38}
$$

The visibility does not change, because the AIS measurements are independent on the visibility. The mode probabilities are found through

$$
\mu_k^{t\tau sj}=\frac{\mu_{k|k-1}^{t\tau s}l_A^{t\tau sj}}{l_A^{t\tau j}}=\frac{\mu_{k|k-1}^{t\tau s}l_A^{t\tau sj}}{\sum_{\tilde{s}}\mu_{k|k-1}^{t\tau\tilde{s}}l_A^{t\tau\tilde{s}j}} \tag{4.39}
$$

The MMSI probabilities are

$$
\xi_k^{t\tau j}=\frac{\left(\sum_{\tau'}q^{\tau'\tau}\xi_{k-1}^{\tau'}\right)l_A^{t\tau j}}{\sum_{\tilde{\tau}}\left(\sum_{\tau'}q^{\tau'\tilde{\tau}}\xi_{k-1}^{\tau'}\right)l_A^{t\tilde{\tau}j}}. \tag{4.40}
$$

Lastly the kinematic state is found from

$$
f_k^{t\tau sj}(\mathbf{x})=\frac{f_{\mathbf{z}}^{A}(\mathbf{z}_k^{a^t}|\mathbf{x})f_{k|k-1}^{t\tau s}(\mathbf{x})}{l_A^{t\tau sj}}. \tag{4.41}
$$

4.3.2 Radar measurements

The following section contains the equations needed for a radar measurement update. Apart from some modifications to accommodate the MMSI numbers it is mainly a reiteration of the equations found in [1].

Identically to how it is for the AIS measurements, when the first measurement of a track is claimed by another track the track is *empty* and no initialization will be performed.

Proposition 4. For a *new target*, that is when $a_{k'}^t=0\ \forall\ k'<k$, initialized on a radar measurement we have that

$$
w_k^j=\lambda+b\eta^0 \tag{4.42}
$$

$$
r_k^j=\frac{b\eta^0}{\lambda+b\eta^0} \tag{4.43}
$$

$$
\mu_k^{\tau sj}=\mu^{0s} \tag{4.44}
$$

$$
\eta_k^j=1 \tag{4.45}
$$

$$
\xi_k^{t\tau}=\xi^{0\tau} \tag{4.46}
$$

$$
f_{k,R}^{t\tau sj}(\mathbf{x})=\mathcal{N}(\mathbf{x},\hat{\mathbf{x}}_0^s,\mathbf{P}_0^s) \tag{4.47}
$$

where $\hat{\mathbf{x}}_0^s=[\mathbf{z}_k^j;\mathbf{0}]$ and $\mathbf{P}_0^s=\text{diag}(\mathbf{R}_R^s,\mathbf{P}_v)$.

Proof: To show this the expressions from [30] are used again.

$$w_k^j = \lambda + v[f_{\mathbf{z}}^R(\mathbf{z}_k^{a^t}|\tilde{\mathbf{y}})P_D(\tilde{\mathbf{y}})] \tag{4.48}$$

$$r_k^j = \frac{v[f_{\mathbf{z}}^R(\mathbf{z}_k^{a^t}|\tilde{\mathbf{y}})P_D(\tilde{\mathbf{y}})]}{\lambda + v[f_{\mathbf{z}}^R(\mathbf{z}_k^{a^t}|\tilde{\mathbf{y}})P_D(\tilde{\mathbf{y}})]} \tag{4.49}$$

$$f_k^{tj}(\mathbf{y}) = \frac{f_{\mathbf{z}}^R(\mathbf{z}_k^{a^t}|\mathbf{y})P_D(\mathbf{y})v(\mathbf{y})}{v[f_{\mathbf{z}}^R(\mathbf{z}_k^{a^t}|\tilde{\mathbf{y}})P_D(\tilde{\mathbf{y}})]} \tag{4.50}$$

This is nearly identical to (4.19)-(4.21), except for the measurement likelihood. The expression $f_{\mathbf{z}}(\mathbf{z}_k^{a^t}|\mathbf{y})P_D(\mathbf{y})v(\mathbf{y})$ becomes

$$b\eta^0\xi^{0\tau}\mu^{0s}q^{0\tau}1_\Omega(\mathbf{H}^s\mathbf{x})\mathcal{N}(\mathbf{z}_k^{a^t}|\mathbf{H}^s\mathbf{x},\mathbf{R}_R^s)\mathcal{N}(\mathbf{H}^{*s}\mathbf{x}|\mathbf{0},\mathbf{P}_v^{(s)})P_D \tag{4.51}$$

if v = 1, and otherwise it is 0. Furthermore, the expression $v[f_{\mathbf{z}}(\mathbf{z}_k^{a^t}|\tilde{\mathbf{y}})P_D(\tilde{\mathbf{y}})]$ is found with a similar reasoning as for the AIS measurements. The Gaussian distributions are again combined, giving $\mathcal{N}(\mathbf{x};\hat{\mathbf{x}}_0^s,\mathbf{P}_0^s)$. Also, assuming that Ω is large enough the integral over $\mathbf{x}$ can be approximated as 1. The sum over both MMSI- and mode-probabilities are also 1. This leaves

$$v[f_{\mathbf{z}}(\mathbf{z}_k^{a^t}|\tilde{\mathbf{y}})P_D(\tilde{\mathbf{y}})] \approx b\eta^0 \tag{4.52}$$

which gives w_k^j and r_k^j. Inserting the above expressions in (4.50) provides the resulting expressions. The initial mode probabilities and MMSI probabilities can be taken directly from (4.51), while the visibility probability becomes 1, as η^0 is present both in the numerator and the denominator. As b is also present both in the numerator and the denominator it has no impact, leaving the kinematic pdfs as $\mathcal{N}(\mathbf{x};\hat{\mathbf{x}}_0^s,\mathbf{P}_0^s)$.

Proposition 5. For a *missed detection*, when $a_k^t = 0$ and $a_{k'}^t > 0 \; \exists \; k' < k$, we have that

$$w_k^{t0} = 1 - r_{k|k-1}^t \eta_{k|k-1}^t P_D \tag{4.53}$$

$$r_k^{t0} = \frac{r_{k|k-1}^t(1 - \eta_{k|k-1}^t P_D)}{1 - r_{k|k-1}^t \eta_{k|k-1}^t P_D} \tag{4.54}$$

$$\mu_k^{t\tau s0} = \mu_{k|k-1}^{t\tau s} \tag{4.55}$$

$$\xi_k^{t\tau 0} = \xi_{k-1}^{t\tau} \tag{4.56}$$

$$\eta_k^{t0} = \frac{(1 - P_D)\eta_{k|k-1}^t}{1 - P_D\eta_{k|k-1}^t} \tag{4.57}$$

$$f_k^{t\tau s0}(\mathbf{x}) = f_{k|k-1}^{t\tau s}(\mathbf{x}) \tag{4.58}$$

Proof: From [30], the PMBM equations for a missed detection are

$$w_k^{a^t} = 1 - r_{k|k-1}^t + r_{k|k-1}^t f_{k|k-1}^t[1 - P_D(\tilde{\mathbf{y}})] \tag{4.59}$$

$$r_k^{tj} = \frac{r_{k|k-1}^t f_{k|k-1}^t[1 - P_D(\tilde{\mathbf{y}})]}{1 - r_{k|k-1}^t + r_{k|k-1}^t f_{k|k-1}^t[1 - P_D(\tilde{\mathbf{y}})]} \tag{4.60}$$

$$f_k^{tj}(\mathbf{y}) = \frac{(1 - P_D(\mathbf{y}))f_{k|k-1}^t(\mathbf{y})}{f_{k|k-1}^t[1 - P_D(\tilde{\mathbf{y}})]} \tag{4.61}$$

Firstly, we have that

$$f_{k|k-1}^t[1 - P_D(\tilde{\mathbf{y}})] = \sum_{\tilde{\mathrm{v}}} o_{k|k-1}^{t\tilde{\mathrm{v}}}(1 - P_D(\tilde{\mathbf{y}})) = 1 - \eta_{k|k-1}^t P_D \tag{4.62}$$

which promptly gives w_k^{t0} and r_k^{t0} when inserting in (4.59) and (4.60), respectively. Furthermore, inserting (4.62) in (4.61) yields

$$f_k^{tj}(\mathbf{y}) = \frac{(1 - P_D(\mathbf{y}))o_{k|k-1}^{t\mathrm{v}}}{1 - \eta_{k|k-1}^t P_D} \xi_{k-1}^{t\tau} \mu_{k|k-1}^{t\tau s} f_{k|k-1}^{t\tau s}(\mathbf{x}) \tag{4.63}$$

which provides the remaining expressions by marginalization. The visibility probability becomes

$$\eta_k^{t0} = \frac{(1 - P_D)\eta_{k|k-1}^t}{1 - P_D \eta_{k|k-1}^t} \tag{4.64}$$

and $\xi_k^{t\tau}$, $\mu_k^{t\tau s0}$ and $f_k^{t\tau sj}(\mathbf{y})$ follows from the remaining expression.

Proposition 6. Lastly, for a radar *detection*, which is when $a_k^t > 0$ and $a_{k'}^t > 0 \; \exists \; k' < k$, we have

$$w_k^{tj} = P_D r_{k|k-1}^t \eta_{k|k-1}^t \sum_{\tilde{\tau}} \xi_{k-1}^{t\tilde{\tau}} l_R^{t\tilde{\tau}j} \tag{4.65}$$

$$r_k^{tj} = 1 \tag{4.66}$$

$$\mu_k^{t\tau sj} = \mu_{k|k-1}^{t\tau sj} l_R^{t\tau sj} / \textstyle\sum_{\tilde{s}} \mu_{k|k-1}^{t\tau\tilde{s}} l_R^{t\tau\tilde{s}j} \tag{4.67}$$

$$\xi_k^{t\tau} = \xi_{k-1}^{t\tau} l_R^{t\tau j} / \textstyle\sum_{\tilde{\tau}} \xi_{k-1}^{\tilde{\tau}} l_R^{t\tilde{\tau}j} \tag{4.68}$$

$$\eta_k^{tj} = 1 \tag{4.69}$$

$$f_k^{t\tau sj}(\mathbf{x}) = f_{\mathbf{z}}^R(\mathbf{z}_k^j|\mathbf{x}) f_{k|k-1}^{t\tau s}(\mathbf{x}) / l_R^{t\tau sj} \tag{4.70}$$

Here, similarly as for the AIS measurements

$$l_R^{t\tau sj} = \int f_{\mathbf{p}}^s(\mathbf{x}_k^j|\tilde{\mathbf{x}}) f_{k|k-1}^{t\tau s}(\tilde{\mathbf{x}}) \mathrm{d}\tilde{\mathbf{x}} \tag{4.71}$$

and

$$l_R^{t\tau j} = \sum_{\tilde{s}} \mu_{k|k-1}^{t\tau\tilde{s}j} l_R^{t\tau\tilde{s}j} \tag{4.72}$$

Proof: The proof for this is similar to its AIS measurement counterpart. From [30] we have

$$w_k^{tj} = r_{k|k-1}^t f_{k|k-1}^t [f_{\mathbf{z}}^R(\mathbf{z}_k^{a^t}|\tilde{\mathbf{y}}) P_D(\tilde{\mathbf{y}})] \tag{4.73}$$

$$r_k^{tj} = 1 \tag{4.74}$$

$$f_k^{tj}(\mathbf{y}) = \frac{f_{\mathbf{z}}^R(\mathbf{z}_k^{a^t}|\mathbf{y}) P_D(\mathbf{y}) f_{k|k-1}^t(\mathbf{y})}{f_{k|k-1}^t [f_{\mathbf{z}}^R(\mathbf{z}_k^{a^t}|\tilde{\mathbf{y}}) P_D(\tilde{\mathbf{y}})]} \tag{4.75}$$

which is the same as (4.33)-(4.35), except for the measurement likelihood. The existence probability follows directly from (4.74). We also have that

$$f_{k|k-1}^t [f_{\mathbf{z}}^R(\mathbf{z}_k^{a^t}|\tilde{\mathbf{y}}) P_D(\tilde{\mathbf{y}})] = P_D \eta_{k|k-1}^t \textstyle\sum_{\tilde{\tau}} \xi_{k-1}^{t\tilde{\tau}} l_R^{t\tilde{\tau}j}. \tag{4.76}$$

which is used to find the weight w_k^{tj}. Furthermore, (4.35) becomes

$$\begin{aligned} &\frac{P_D \eta_{k|k-1}^t \xi_{k-1}^{t\tau} \mu_{k|k-1}^{t\tau s} f_{\mathbf{z}}^R(\mathbf{z}_k^{a^t}|\mathbf{x}) f_{k|k-1}^{t\tau s}(\mathbf{x})}{P_D \eta_{k|k-1}^t \sum_{\tilde{\tau}} \xi_{k-1}^{t\tilde{\tau}} l_R^{t\tilde{\tau}j}} \\ =&1 \frac{\xi_{k-1}^{t\tau} l_R^{t\tau j}}{\sum_{\tilde{\tau}} \xi_{k-1}^{\tilde{\tau}} l_R^{t\tilde{\tau}j}} \frac{\mu_{k|k-1}^{t\tau s} l_R^{t\tau sj}}{l_R^{t\tau j}} \frac{f_{\mathbf{z}}(\mathbf{z}_k^{a^t}|\mathbf{x}) f_{k|k-1}^{t\tau s}(\mathbf{x})}{l_R^{t\tau sj}} \end{aligned} \tag{4.77}$$

when v = 1, and 0 otherwise. This provides the resulting expressions.

4.4 Mixture reduction

After having calculated the expressions for the individual measurements, as described in Section 4.3, one ends up with an MBM on the form of

$$G_k^{mbm}[h] \propto \sum_{a_k \in \mathcal{A}^k} \prod_{t=1}^{n_k} w_k^{t,a^t} (1 - r_k^{ta^t} - r_k^{ta^t} f_k^{ta^t}[h]) \tag{4.78}$$

which has to be reduced to a multi-Bernoulli on the form of

$$G_k^{mb}[h] = \prod_{t=1}^{n_k} (1 - r_k^t - r_k^t f_k^t[h]). \tag{4.79}$$

The posterior hybrid state pdfs have to be on the same form as the priors, i.e.

$$f_k^t(\mathbf{y}) = f_k^{t\tau s}(\mathbf{x}) \mu_k^{t\tau s} o_k^{t\mathrm{v}} \xi_k^{t\tau}. \tag{4.80}$$

This is done here by performing a mixture reduction similar to the one used in a regular JIPDA. The association probabilities are calculated as

$$\begin{aligned}\Pr(a_k) &\propto \prod_t w_k^{ta^t} \prod_{j \ s.t \ a^t \neq j \ \forall \ t} \lambda \\ &\propto \prod_{t \ s.t \ a^t=0} w_k^{ta^t} \prod_{t \ s.t \ a^t>0} w_k^{ta^t}/\lambda \end{aligned} \tag{4.81}$$

where

$$\sum_{a_k} \Pr(a_k) = 1 \tag{4.82}$$

The marginal association probabilities are calculated as

$$\Pr(a^t = j) = \sum_{a_k \ s.t. \ a^t=j} \Pr(a_k) = p_k^{tj}. \tag{4.83}$$

These are then used to calculate the marginal existence probability

$$\begin{aligned} r_k^t &= \sum_{j=0}^{m_k} \Pr(E, a^t = j) = \sum_{j=0}^{m_k} \Pr(E|a^t = j) \Pr(a^t = j) \\ &= \sum_{j=0}^{m_k} r_k^{tj} p^{tj} \end{aligned} \tag{4.84}$$

where E denotes existence. The marginal visibility probability is found in a similar manner, as

$$\begin{aligned} \eta_k^t &= \sum_j^{m_k} \Pr(\mathrm{v} = 1, a^t = j|E) = \sum_j^{m_k} \frac{\Pr(\mathrm{v} = 1|a^t = j, E) \Pr(E|a^t = j) \Pr(a^t = j)}{\Pr(E)} \\ &= \frac{1}{r_k^t} \sum_{j=0}^{m_k} p_k^{tj} r_k^{tj} \eta_k^{tj}. \end{aligned} \tag{4.85}$$

For calculation of the mode- and MMSI-conditional kinematic pdfs $f_k^{t\tau s}$ the mode- and MMSI-conditional marginal association probabilities are needed. These are given by

$$\begin{aligned} \beta_k^{t\tau sj} &= \Pr(a^t = j|s^t, \tau^t, E) \\ &= \frac{\Pr(s^t|a^t = j, \tau^t, E) \Pr(\tau^t|a^t = j, E) \Pr(E|a^t = j) \Pr(a^t = j)}{\Pr(s^t|\tau^t, E) \Pr(\tau^t|E) \Pr(E)}. \end{aligned} \tag{4.86}$$

through extensive use of Bayes rule. Here, s^t and τ^t means the event that track t follows mode s and has MMSI number τ, respectively. Firstly, $\Pr(a^t = j)$ is found from (4.83), and $\Pr(E)$ from (4.84). The association-conditional MMSI probabilities $\Pr(\tau^t|a^t = j, E) = \xi_k^{t\tau j}$ follows from the previous section, and the MMSI- and association-conditional mode probabilities $\Pr(s^t|a^t = j, \tau, E) = \mu_k^{t\tau sj}$ do the same.

The posterior MMSI probabilities are found as

$$\begin{aligned}\Pr(\tau^t|E) &= \sum_{j=0}^{m_k} \Pr(\tau^t, a^t = j|E) \\ &= \sum_{j=0}^{m_k} \frac{\Pr(\tau^t|a^t = j, E)\Pr(E|a^t = j)\Pr(a^t = j)}{\Pr(E)} \\ &= \frac{1}{r_k^t} \sum_{j=0}^{m_k} \xi_k^{t\tau j} r_k^{tj} p_k^{tj} = \xi_k^{t\tau}\end{aligned} \tag{4.87}$$

and lastly, the marginal MMSI-conditional posterior mode probabilities are found as

$$\begin{aligned}\Pr(s^t|\tau^t, E) &= \sum_{j=0}^{m_k} \Pr(s^t, a^t = j|\tau^t, E) \\ &= \sum_{j=0}^{m_k} \frac{\Pr(s^t|\tau^t, a^t = j, E)\Pr(\tau^t|a^t = j, E)\Pr(E|a^t = j)\Pr(a^t = j)}{\Pr(\tau^t|E)\Pr(E)} \\ &= \frac{1}{\xi_k^{t\tau} r_k^t} \sum_{j=0}^{m_k} \mu_k^{t\tau sj} \xi_k^{t\tau j} r_k^{tj} p_k^{tj} = \mu_k^{t\tau s}.\end{aligned} \tag{4.88}$$

Using this, the posterior kinematic state is calculated as

$$f_k^{t\tau s}(\mathbf{x}) = \sum_{j=0}^{m} \beta^{t\tau sj} f_{k_i}^{t\tau sj}(\mathbf{x}) = \sum_{j=0}^{m} \frac{\mu_k^{t\tau sj} \xi_k^{t\tau j} r_k^{tj} p_k^{tj}}{\mu_k^{t\tau s} \xi_k^{t\tau} r_k^t} f_{k_i}^{t\tau sj}(\mathbf{x}) \tag{4.89}$$

which can be done by standard moment-matching techniques, assuming each $f_k^{t\tau sj}(\mathbf{x})$ is Gaussian.

Remark. It can be valuable to compare the tracker described here, to the IMM-JIPDA from [13]. The VIMMJIPDA should reduce to the IMM-JIPDA when the visibility is forced to always be in a visible state, i.e. $\mathrm{v} = 1$, when no AIS measurements are present and the target is assumed to always have MMSI number 0. Then, both the expressions calculating $\xi_k^{t\tau}$ and η_k^t can be ignored, as can all conditionals on these. The output of mixture reduction is in [13, eq. (32)] written as

$$r_k^t = \sum_{j=0}^{m_k} \Pr(a^t = j, E) = \sum_{s=1}^{M} \Pr(s^t, E) \tag{4.90}$$

$$\beta_k^{tsj} = \frac{\Pr(a^t = j, s^t, E)}{\Pr(s^t, E)} \tag{4.91}$$

$$\mu_k^{ts} = \frac{\Pr(s^t, E)}{\Pr(E)} \tag{4.92}$$

where the notation has been changed to the one used here. The existence probability is identical to the expression in (4.84), which can be seen by the term after the first equality in both (4.90) and (4.84). (4.91) can be written as

$$\beta_k^{tsj} = \frac{\Pr(s^t|a^t = j, E)\Pr(E|a^t = j)\Pr(a^t = j)}{\Pr(s^t|E)\Pr(E)}. \tag{4.93}$$

When comparing this with (4.86), and assuming only MMSI number 0 is present with unity probability, one can see that the expressions are identical. Furthermore, from [13, eq. (31)]

$$\Pr(s^t, E) = \sum_{j=0}^{m_k} \Pr(s^t, a^t = j, E) \tag{4.94}$$

$$\Pr(s^t, a^t = j > 0|E) = \frac{\mu_{k|k-1}^{ts} l^{tsj}}{\sum_{\tilde{s}} \mu_{k|k-1}^{t\tilde{s}} l^{t\tilde{s}j}} \tag{4.95}$$

$$\Pr(s^t, a^t = j = 0|E) = \mu_{k|k-1}^{ts} \tag{4.96}$$

The expression for the mode probabilities, (4.92), can be written as

$$\mu_k^{ts} = \frac{\sum_{j=0}^{m_k} \Pr(s^t, a^t = j, E)}{\Pr(E)} = \sum_{j=0}^{m_k} \Pr(s^t, a^t = j|E) \tag{4.97}$$

which is identical to (4.88), again when assuming only MMSI number 0 is present.

The joint probability of existence and the marginal association probabilities are in [13, eq. (30)] formulated as

$$\Pr(a^t = 0, E) = \frac{(1 - P_D P_G) r_{k|k-1}^t}{1 - P_D P_G r_{k|k-1}^t} \sum_{a_k \ s.t. \ a^t=0} \Pr(a_k) = r_j^{t0} p_k^{t0} \tag{4.98}$$

$$\Pr(a^t > 0, E) = \sum_{a_k \ s.t. \ a^t>0} \Pr(a_k) = p_k^{tj} \quad \text{, for } j > 0 \tag{4.99}$$

where P_G is the probability that the measurement from a target falls within its validation gate. Here, the joint probability of existence and the marginal association probability is formulated as

$$\Pr(a^t = j, E) = \Pr(E|a^t = j)\Pr(a^t = j) = r_k^{tj} \sum_{a_k \ s.t. \ a^t=j} \Pr(a_k) = r_k^{tj} p_k^{tj} \tag{4.100}$$

where $r_k^{tj} = 1 \ \forall \ j > 0$. This is equivalent to (4.98) if $\eta_{k|k'}^t = 1 \ \forall \ k'$ and P_G is assumed to be equal to 1. Lastly, in [13, e. (29)] the probability of the individual association hypotheses are written as

$$\Pr(a_k) \propto \prod_{t \ s.t \ a^t=0} (1 - P_D P_G r_{k|k-1}^t) \prod_{t \ s.t \ a^t>0} P_D P_G r_{k|k-1}^t \sum_{\tilde{s}} \mu_{k|k-1}^{t\tilde{s}} l^{t\tilde{s}j} / \lambda \tag{4.101}$$

When disregarding the visibility and MMSI numbers, this is the same as (4.81) when $\eta_{k|k'}^t = 1 \ \forall \ k'$ and $P_G = 1$. This is seen by replacing $w_k^{ta^t}$ with the expressions from (4.53) and (4.65).

CHAPTER 5

Implementation choices

To make the tracker described in Chapter 4 possible to implement, several approximations have to be made, the surrounding framework has to be specified, and measurement and kinematic models has to be chosen. These implementation-specific elements are presented here.

5.1 The extended Kalman filter

The tracker is implemented using an extended Kalman filter (EKF). An EKF, as opposed to a regular Kalman filter, is able to handle nonlinearities by use of linearization. When predicting, the EKF linearizes around the most recent update, while when updating it linearizes around the most recent prediction. To further clarify the procedure, and to contextualize the different mathematical entities of this chapter, the EKF algorithm is shown in Table 5.1. The notation and structure of the algorithm is largely borrowed from [46, p.71]. However, it is altered to more precisely represent what is done with the expressions arising from the previous chapter. τ and s denotes the MMSI number and mode, and $\tau s, 0$ denotes the mode- and MMSI-conditional prior from (4.6).

5.2 Measurement models

The general equations for the measurement likelihoods for the AIS and radar measurements are presented in Section 3.2. These likelihoods do, however, have to be further specified. The positional data of both measurement types are 2-dimensional, and can in general be written as

$$\mathbf{z}_k = \mathbf{H}\mathbf{x}_k + \mathbf{w}_k, \quad \mathbf{w}_k \sim \mathcal{N}(\mathbf{0}, \mathbf{R}) \tag{5.1}$$

In	$\hat{\mathbf{x}}_{k-1}^{\tau s,0}$ and $\mathbf{P}_{k-1}^{\tau s,0}$ from $f_{k-1}^{t\tau s,0}(\mathbf{x})$, $Z_k = \{\mathbf{z}_k^1 \dots \mathbf{z}_k^{m_k}\}$	
1	$\hat{\mathbf{x}}_{k\|k-1}^{\tau s} = \mathbf{f}^{(s)}(\hat{\mathbf{x}}_{k-1}^{\tau s,0})$	Predicted state estimate
2	$\mathbf{F}^s = \dfrac{\partial}{\partial \mathbf{x}_{k-1}} \mathbf{f}^{(s)}(\mathbf{x}_{k-1})$	Prediction Jacobian
3	$\mathbf{P}_{k\|k-1}^{\tau s} = \mathbf{F}^s \mathbf{P}_{k-1}^{\tau s} (\mathbf{F}^s)^\top + \mathbf{Q}^{(s)}$	Predicted covariance
4	$\hat{\mathbf{z}}_{k\|k-1}^{\tau s} = \mathbf{h}(\hat{\mathbf{x}}_{k\|k-1}^{\tau s})$	Predicted measurement
5	$\boldsymbol{\nu}_k^{\tau s} = \sum_{j=1}^{m_k} \beta_k^{\tau s j} (\mathbf{z}_k^j - \hat{\mathbf{z}}_{k\|k-1}^{\tau s})$	Innovation
6	$\mathbf{H} = \dfrac{\partial}{\partial \mathbf{x}_k} \mathbf{h}(\mathbf{x}_k)$	Measurement Jacobian
7	$\mathbf{S}_k^{\tau s} = \mathbf{H} \mathbf{P}_{k\|k-1}^{\tau s} \mathbf{H}^\top + \mathbf{R}$	Innovation covariance
8	$\mathbf{W}_k^{\tau s} = \mathbf{P}_{k\|k-1}^{\tau s} \mathbf{H}^\top (\mathbf{S}_k^{\tau s})^{-1}$	Kalman gain
9	$\hat{\mathbf{x}}_k^{\tau s} = \hat{\mathbf{x}}_{k\|k-1}^{\tau s} + \mathbf{W}_k^{\tau s} \boldsymbol{\nu}_k^{\tau s}$	Posterior state estimate
10	$\mathbf{P}_k^{\tau s} = (\mathbf{I} - \mathbf{W}_k^{\tau s} \mathbf{H}) \mathbf{P}_{k\|k-1}^{\tau s}$	Posterior covariance
Out	$\hat{\mathbf{x}}_k^{\tau s}$ and $\mathbf{P}_k^{\tau s}$ from $f_k^{t\tau s}(\mathbf{x})$, $\hat{\mathbf{x}}_{k\|k-1}^{\tau s}$ and $\mathbf{P}_{k\|k-1}^{\tau s}$ from $f_{k\|k-1}^{t\tau s}(\mathbf{x})$, $\mathbf{S}_k^{\tau s}$	

Table 5.1: A single run-through of the extended Kalman filter.

5.2.1 Radar measurements

The radar measurement noise matrix have both a Cartesian and polar element. This reflects the physical properties of the sensor, in that the radar measurements located further away from the ownship becomes noisier than the ones closer to it. With this in mind, the measurement noise matrix for the radar measurement becomes

$$\mathbf{R}_R = \mathbf{R}_c + \mathbf{J} \mathbf{R}_p \mathbf{J}^\top \tag{5.2}$$

Here $\mathbf{R}_c$ is the Cartesian noise component, while $\mathbf{R}_p$ is the polar noise component. $\mathbf{J}$ is the Jacobian of the mapping from polar to Cartesian coordinates.

5.2.2 AIS measurements

The AIS measurements do not inherit the same physical properties as the radar measurements, and their measurement noise is only dependent on the error in the GPS data used to find the position of the transmitting ship. Thus, the AIS measurement noise matrix $\mathbf{R}_A$ only has a Cartesian component.

5.3 Kinematic models

The kinematic modeling of the targets is relevant for the prediction of the motion of a target from one time step to the next. Two popular models for movement in the target

tracking community are the *constant velocity* (CV) model and the *coordinated turn* (CT) model, and these are the ones used in this implementation. Both are quite simple but reasonable approximations for shorter time intervals. The models are thoroughly described in [42]. For a target with MMSI number τ following model s, the target is hypothesized to evolve according to

$$\mathbf{x}_{k|k-1} = \mathbf{f}^{(s)}(\mathbf{x}_{k-1}) + \mathbf{v}_k, \;\; \mathbf{v}_k \sim \mathcal{N}(\mathbf{0}, \mathbf{Q}^{(s)}) \tag{5.3}$$

where v_k is zero-mean white noise. The covariance of v_k is Q. This is a different way of writing

$$f_{\mathbf{x}}^{s\tau}(\mathbf{x}_k|\mathbf{x}_{k-1}) = \mathcal{N}(\mathbf{x}_k|\mathbf{f}^{(s)}(\mathbf{x}_{k-1}), \mathbf{Q}^{(s)}). \tag{5.4}$$

from assumption M4.

5.3.1 Constant velocity

The *constant velocity* model, also called the *discrete white noise acceleration* model, assumes that the target moves in a nearly constant straight-line motion. As presented in [42] there are two ways to model this nearly constant straight-line motion, either through the discretization of a continuous model or through a direct discrete-time model. The first version is chosen here, as it is suited for situations where the time intervals between time steps are not constant. For a target following the CV model, $\mathbf{f}^{(s)}(\mathbf{x}_{k-1})$ and $\mathbf{Q}$ in (5.3) are

$$\mathbf{f}^{(s)}(\mathbf{x}_{k-1}) = \begin{bmatrix} 1 & T & 0 & 0 \\ 0 & 1 & 0 & 0 \\ 0 & 0 & 1 & T \\ 0 & 0 & 0 & 1 \end{bmatrix} \mathbf{x}_{k-1} \tag{5.5}$$

and

$$\mathbf{Q}^{(s)} = \begin{bmatrix} \frac{1}{3}T^3 & \frac{1}{2}T^3 & 0 & 0 \\ \frac{1}{2}T^2 & T & 0 & 0 \\ 0 & 0 & \frac{1}{3}T^3 & \frac{1}{2}T^3 \\ 0 & 0 & \frac{1}{2}T^3 & T \end{bmatrix} q_a \tag{5.6}$$

where q_a is the acceleration process noise intensity. When using multiple models it is possible to use several CV models with different q_a to account for different movement. For a CV model modeling a target with nearly constant velocity the value of q_a should be low, at a magnitude of ≈ 0.05. To model a target with more varying velocity it should be set higher, at a magnitude of ≈ 0.5 [47].

5.3.2 Coordinated turn

The coordinated turn (CT) model introduces angular velocity, ω_k, as a new state in $\mathbf{x}_k$. The CT model is, as the CV model, described in [42]. Again, a discretizisation of the continuous model is used and $\mathbf{f}^{(s)}(\mathbf{x}_{k-1})$ and $\mathbf{Q}^{(s)}$ from (5.3) become

$$\mathbf{f}^{(s)}(\mathbf{x}_{k-1}) = \begin{bmatrix} 1 & \frac{\sin(\omega_{k-1}T)}{\omega_{k-1}} & 0 & -\frac{1-\cos(\omega_{k-1}T)}{\omega_{k-1}} & 0 \\ 0 & \cos(\omega_{k-1}T) & 0 & -\sin(\omega_{k-1}T) & 0 \\ 0 & \frac{1-\cos(\omega_{k-1}T)}{\omega_{k-1}} & 1 & \frac{\sin(\omega_{k-1}T)}{\omega_{k-1}} & 0 \\ 0 & \sin(\omega_{k-1}T) & 0 & \cos(\omega_{k-1}T) & 0 \\ 0 & 0 & 0 & 0 & 1 \end{bmatrix} \mathbf{x}_{k-1} \tag{5.7}$$

and

$$\mathbf{Q}^{(s)} = \begin{bmatrix} \frac{T^3}{3}q_a & \frac{T^2}{2}q_a & 0 & 0 & 0 \\ \frac{T^2}{2}q_a & Tq_a & 0 & 0 & 0 \\ 0 & 0 & \frac{T^3}{3}q_a & \frac{T^2}{2}q_a & 0 \\ 0 & 0 & \frac{T^2}{2}q_a & Tq_a & 0 \\ 0 & 0 & 0 & 0 & Tq_\omega \end{bmatrix}. \tag{5.8}$$

where q_a again is the acceleration process noise intensity, while q_ω is the angular velocity process noise intensity. As this model is nonlinear, the Jacobian is needed for it to be used in an EKF. Using the expressions from [42, p. 469], the Jacobian of $\mathbf{f}^{(s)}(\mathbf{x}_{k-1})$ is

$$\mathbf{F} = \begin{bmatrix} 1 & \frac{\sin(\omega_{k-1}T)}{\omega_{k-1}} & 0 & -\frac{1-\cos(\omega_{k-1}T)}{\omega_{k-1}} & F_{1,5} \\ 0 & \cos(\omega_{k-1}T) & 0 & -\sin(\omega_{k-1}T) & F_{2,5} \\ 0 & \frac{1-\cos(\omega_{k-1}T)}{\omega_{k-1}} & 1 & \frac{\sin(\omega_{k-1}T)}{\omega_{k-1}} & F_{3,5} \\ 0 & \sin(\omega_{k-1}T) & 0 & \cos(\omega_{k-1}T) & F_{4,5} \\ 0 & 0 & 0 & 0 & F_{5,5} \end{bmatrix} \tag{5.9}$$

where

$$\mathbf{F}_{:,5} = \begin{bmatrix} \frac{\dot{y} - (T\omega_{k-1}\dot{y} + \dot{x})\sin(\omega_{k-1}T) + (T\omega_{k-1}\dot{x} - \dot{y})\cos(\omega_{k-1}T)}{\omega_{k-1}^2} \\ -T(\dot{x}\sin(\omega_{k-1}T + \dot{y}\cos(\omega_{k-1}T)) \\ \frac{-\dot{x} + (T\omega_{k-1}\dot{x} - \dot{y})\sin(\omega_{k-1}T) + (T\omega_{k-1}\dot{y} + \dot{x})\cos(\omega_{k-1}T)}{\omega_{k-1}^2} \\ T(\dot{x}\cos(\omega_{k-1}T - \dot{y}\sin(\omega_{k-1}T)) \\ 1 \end{bmatrix} \tag{5.10}$$

Here, $\dot{}$ and $\dot{y}$ denote the velocities in the x- and y-direction, respectively.

5.4 Clustering and validation gating

To avoid having to consider all tracks simultaneously when performing data association, tracks with shared measurements within their validation gates are clustered and data association is performed on each cluster. A measurement $\mathbf{z}_k$ falls inside the validation gate if

$$(\mathbf{z}_k - \mathbf{z}_{k|k-1}^{s\tau})^\top (\mathbf{S}_k^{s\tau})^{-1} (\mathbf{z}_k - \mathbf{z}_{k|k-1}^{s\tau}) < g^2 \tag{5.11}$$

for any of the modes and MMSI numbers in the track's state. $\mathbf{z}_{k|k-1}$ is the predicted measurement and $\mathbf{S}_k$ is the innovation covariance, both from Table 5.1. g is the number of

standard deviations from the predicted measurement a measurement must be within to be included, and defines the size of the validation gate.

When all measurements have been gated, i.e. associated to any tracks which they fall inside the validation gates of, the tracks are clustered. This is done simply by placing any tracks which share measurements after the gating procedure in the same cluster. Data association is then done only between the tracks in the cluster, and not between all tracks in the surveillance area. This clustering is mainly to avoid a sharp increase in the number of computations needed when more tracks are present.

5.5 Data association hypotheses construction

Data association has to be performed between tracks and the measurements which fall inside their validation gates. For this, association hypotheses have to be constructed. These are then used for the calculation of the association probabilities in Chapter 4. The association hypotheses are track-oriented.

When considering associating hypotheses involving radar measurements each track is either associated with a measurement or it is not, which means that a missed detection has taken place. Within a single hypothesis each track can only be assigned one measurement, and each measurement can only be assigned to one track. A single association hypothesis at time step k for n_k^t tracks is denoted as $a_k = [a_k^1, a_k^2, \ldots, a_k^{n_k^t}]$ where

$$a_k^t = \begin{cases} j & \text{if measurement } j \text{ is assigned to track } t \\ 0 & \text{if no measurement is assigned to track } t \end{cases} \tag{5.12}$$

Such an association hypothesis is only valid if it is part of the set $\mathcal{A}^k$ from (3.32).

For association hypotheses involving AIS measurements, the assumption that there are no clutter measurements has to be considered. This means that all m_k AIS measurements at time k have to be assigned to a track. If there are more tracks than measurements in a cluster there will nevertheless be missed detections. With this in mind, an AIS association hypothesis is only valid if it is part of the set $\mathcal{A}^k$, and $\forall\ j \in \{1, \ldots, m_k\}\ \exists\ a_k^t = j$.

For large clusters, the number of valid association hypotheses can become computationally intractable. While there for $n_k = 2$ and $m_k = 2$ are 7 possible association hypotheses, when $n_k = 6$ and $m_k = 6$ there are 13327 possible association hypotheses. Thus, calculating the probabilities for all association hypotheses regardless of cluster size is infeasible. To mitigate this issue an approximation can be made by use of Murty's algorithm [26]. In combination with the auction algorithm [46, p. 137], a version of the Hungarian algorithm [48], this results in a fixed number of the most likely association hypotheses. These are selected by arranging the assignments in a matrix, with the cost of assigning each measurement to each track. The auction algorithm chooses the least costly assignment, which becomes the first association hypotheses. Murty's algorithm manipulates the reward matrix so the next run of the auction algorithm returns the second least costly assignment, and so forth. The assignment matrix is of size $n_k^t \times (n_k^t + m_k)$, and is constructed as follows:

$$M_{t,j} = \begin{cases} \ln(w_k^{tj}/\lambda) & \text{for } j \leq m_k, \text{ and when measurement } j \text{ is within the validation gate of track } t \\ \ln(w_k^{t0}) & \text{for } j = t + m_k \\ -\infty & \text{otherwise} \end{cases} \tag{5.13}$$

In this implementation the algorithm returns the eight most likely association hypotheses, but this number is easily changed.

For AIS measurements the data association problem becomes a lot less computationally expensive. As an AIS receiver is unable to receive more than one AIS message at a time, as evident from the protocol used for AIS communication [17], there will usually be only one measurement present in a cluster. This will keep the number of association hypotheses at a manageable level without approximations. However, approximations may nevertheless be necessary if a lot of AIS-transmitting targets are present.

5.6 Track initiation and termination

5.6.1 Initialization based on validation gating

The unknown target intensity (3.10) hypothesizes that there are undetected targets present, and defines the way they are to be initialized. The mathematical details surrounding the initialization were described in Section 4.3. To mitigate computational complexity, tracks are only initialized on radar measurements that are not within any track's validation gate, i.e. unclaimed measurements. To avoid a large amount of false tracks, the existence probability of the newly initialized tracks have to reach above a threshold before they are confirmed. However, once initialized the tracks contest for the same measurements as the already existing tracks even though they have not been confirmed.

For the AIS measurements, the initialization is done in a slightly different manner. As for the radar measurements, new tracks are initialized on all AIS measurements which fall outside any validation gate. There is, however, a necessity to be able to initialize new tracks on measurements which fall within another track's validation gate. The phenomenon necessitating this is shown in Figure 5.1. The figure depicts a scenario with two targets, both transmitting AIS measurements. For the sake of simplicity we assume that no radar measurements are present. A track is initialized on the first AIS measurement, $\mathbf{z}_1$ in the figure, which causes the next measurement, $\mathbf{z}_2$ to fall within the validation gate of the newly initialized track. However, $\mathbf{z}_2$ is in fact a measurement from a different target, but if the tracker only initializes new tracks on unclaimed measurements this will not be discovered by the tracker. As the AIS measurements cannot be false alarms the tracker is sure that measurement $\mathbf{z}_2$ originates from the same target which transmitted $\mathbf{z}_1$, resulting in the behavior in Figure 5.1. For radar measurements this problem is somewhat mitigated by the fact that the radar measurements can be considered clutter measurements, thus giving the tracker the possibility of ignoring them to a larger degree.

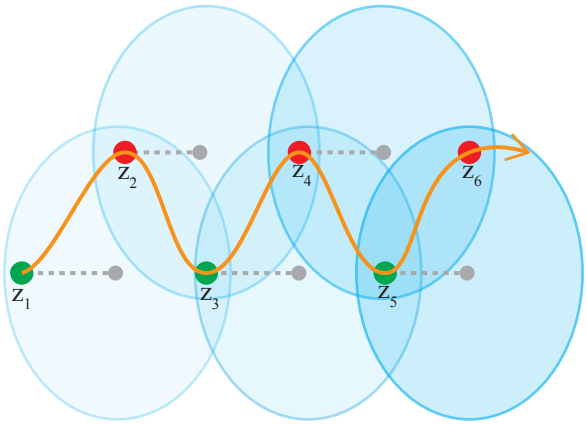

Figure 5.1: Behavior after failure to initialize track.

5.6.2 Initialization based on Total track probability

Initialization of tracks based on a concept called Total track probability (TTP) can help to solve this problem. The TTP is defined as a track's existence probability times the sum of hypotheses probabilities containing the track. For track t the TTP becomes

$$\text{TTP}^t = r_k^t \sum_{a_k \ s.t. \ a^t>0} \Pr(a_k) \tag{5.14}$$

To be able to examine this the association probabilities are calculated for the scenario where a hypothesized target is present. This is done by creating a new set of association hypotheses which include a new track, initialized as described in Section 4.3.1, before calculating the association probabilities. The TTP of the new track becomes the basis for the decision of whether to let the new track be initialized. If the TTP of the new track is larger than some threshold T_{TTP} it is initialized.

Remark. In the current implementation TTP is only used on AIS measurement with not previously encountered MMSI numbers, which arrive inside the validation gates of tracks that have already encountered an AIS measurement. It can nevertheless be used for other measurements as a tool to create more refined initialization schemes than the one described here. All measurements are, strictly speaking, potential new targets, and using TTP will conceptually be closer to this mindset than the somewhat coarse validation gate approach. However, to avoid making large structural changes to the underlying radar tracker TTP is not used on the radar measurements.

5.6.3 Track termination

Track termination is performed as it is done in [47]. Firstly, tracks are always terminated whenever their existence probability r_k^t falls below a threshold T_d. Tracks are also fused whenever they are in too close proximity of each other. This is decided by evaluating the hypothesis H_0, stating that the two tracks are the same. As described in [47], for two targets $\mathbf{x}_k^1$ and $\mathbf{x}_k^2$ the hypothesis is that $\mathbf{d} = \mathbf{x}_k^1 - \mathbf{x}_k^2 = \mathbf{0}$. The estimated distance between the two targets is

$$\hat{\mathbf{d}} = \hat{\mathbf{x}}_k^1 - \hat{\mathbf{x}_k^2} \tag{5.15}$$

while the covariance of the estimated distance is

$$\mathbf{T} = \mathbf{P}_k^1 + \mathbf{P}_k^1 - \mathbf{P}_k^{12} - \mathbf{P}_k^{21}. \tag{5.16}$$

The covariance between two tracks can be estimated with methods found in e.g. [49]. Using these values, Mahalanobis distance is used to measure the dissimilarity of the two tracks, as

$$\gamma = \hat{\mathbf{d}}^\top \mathbf{T}^{-1} \hat{\mathbf{d}} \tag{5.17}$$

This value is then used to evaluate the hypothesis, leading to the fusing of the tracks if

$$P(\gamma < \gamma_\alpha | H_0) = 1 - \alpha \tag{5.18}$$

for some γ_α. Here, α is the significance level of H_0. If the two tracks are fused, the youngest track, i.e. the one initialized most recently, is terminated.

Furthermore, tracks are terminated whenever they have gone five radar time steps without associating to a measurement, as a method of terminating tracks outside the surveillance area.

5.7 Handling of MMSI numbers

In theory, there are over a billion different MMSI numbers [18], and to calculate all the expressions in the previous chapter for all these would be infeasible. Luckily, this is not necessary. As the large majority of MMSI numbers are not going to be present in a given scenario these can be considered as a single number. The number -1 is used here to represent all the MMSI numbers not encountered by a target, as -1 is outside the range of actual MMSI numbers. All numbers which have not been observed will result in the same behavior for the tracker. They will all have the same probability of being correct, and they will give the same estimates for the modes, visibility, existence and kinematic pdfs. This also means that even though they are not calculated individually, one can always know all the relevant previous values in the case where a new MMSI number arrives. The probability for an unencountered MMSI number τ_{new} being correct at the previous time $k-1$ is

$$\xi_{k-1}^{\tau_{\text{new}}} = \frac{1 - \sum_{\tau \neq -1} \xi_{k-1}^{t\tau}}{|\mathcal{V}| - \sum_{\tau \neq -1} 1}. \tag{5.19}$$

The rest of the relevant values are found by keeping in mind that

$$f_{k-1}^{t\tau_{new}s}(\mathbf{x}) = f_{k-1}^{t\tau_{-1}s}(\mathbf{x}) \tag{5.20}$$

$$\mu_{k-1}^{t\tau_{new}s} = \mu_{k-1}^{t\tau_{-1}s} \tag{5.21}$$

while the visibility probability is independent of the MMSI number.

The influx of corrupt MMSI numbers lead to an ever-growing list of encountered MMSI numbers. As the algorithm performs calculations for each encountered MMSI number this

is unfortunate with regards to computational complexity. In addition, the probabilities of MMSI numbers can become very low, and cause numerical underflow. The problem is mitigated by removing the most unlikely MMSI numbers for each track. To do this the MMSI number probability $\xi_k^{t\tau}$ for MMSI number τ at time k, is compared with a predefined threshold T_τ. All MMSI numbers with a lower probability of being correct than T_τ are removed. This ensures that only the relevant MMSI numbers are considered for each track and that corrupted MMSI numbers that show up only once don't accumulate. MMSI number -1, however, cannot be removed, as it represents all possible MMSI numbers, also ones which could later appear to the target. To avoid numerical underflow, the probability of MMSI number -1 is denied to go beneath 1×10^{-10}.

All tracks have a dynamic list of encountered MMSI numbers, which grows as the track encounters AIS measurements with new MMSI numbers, and shrinks as low-probability numbers are pruned away. Because all possible MMSI numbers, either unencountered or previously pruned away ones, are represented by MMSI number -1, one can nevertheless argue that the state is calculated for all possible MMSI numbers at all times.

CHAPTER 6

Experimental setup

6.1 Technical implementation

The tracker was implemented in Python. The implementation was built upon an already existing target tracking library created as part of the Autosea project at NTNU[23], the code from the pre-master project and the work from TK8102. The code follows a modular structure, shown in a simplified form in Figure 6.1. In Figure 6.1, the green box represents the supporting infrastructure, while the red box represents the part of the program conducting the tracking. The supporting infrastructure, here represented by `run.py`, creates or imports measurements and provides these as input to the tracking manager. Estimates from the tracker are then returned to `run.py` and processed to evaluate the results. These are then output through a visualizing module.

6.2 Data simulation scheme

The simulated data is created in line with the assumptions in Section 3.2. The ownship is situated at the origin, and is stationary. The surveillance area is circular with a radius dependent on the preset range for the radar and AIS receiver. The simulated data consists of true target positions, radar measurements from both targets and clutter, and AIS measurements.

6.2.1 Target trajectory generation

The targets are born according to a Poisson process which is only non-zero at the edge of the surveillance area. Targets are terminated when they move outside the surveillance area. The direction of the initial movement of each target is defined to be within 45° of the line between where the target was born and the origin. The magnitude of the initial velocity is a randomized percentage of a preset maximum initial velocity parameter. A visualization of this can be seen in Figure 6.2.

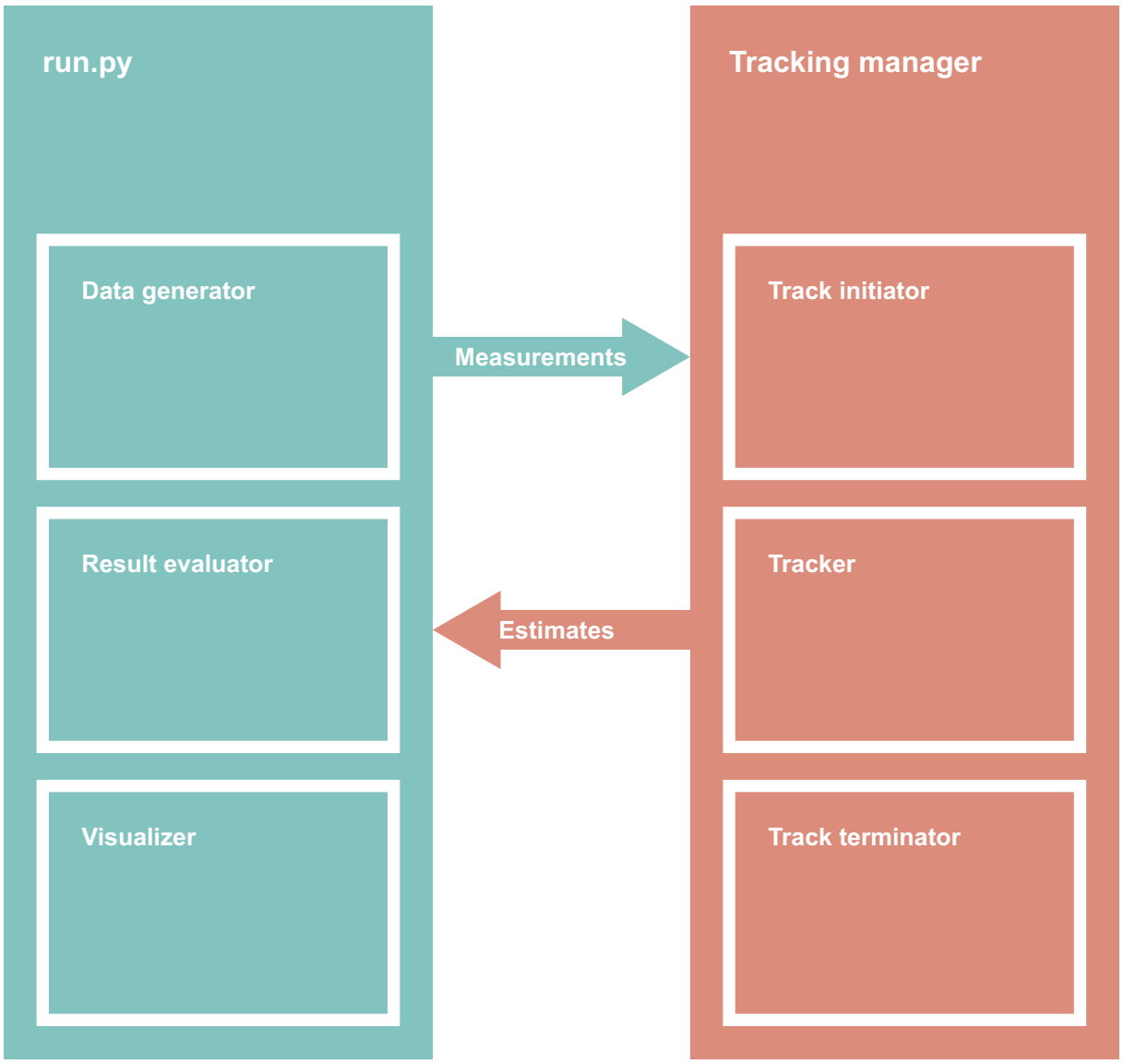

Figure 6.1: Simplified code structure and program flow.

The continuing movement of each target is modeled according to the CV model described in Section 5.3. At each time step the target evolves according to

$$\mathbf{x}_{k|k-1} = \mathbf{F}(\mathbf{x}_{k-1}) + \mathbf{v}_k, \;\; \mathbf{v}_k \sim \mathcal{N}(\mathbf{0}, \mathbf{Q}) \tag{6.1}$$

where $\mathbf{F}$ is the matrix from (5.5), and $\mathbf{Q}$ is the matrix from (5.6). Noise is added to the state vector at each time step. The magnitude of the noise depends on the preset process noise intensity q_a, which determines the covariance of $\mathbf{v}_k$. The times at which the true position of a target is generated depends on the radar sampling rate and times when AIS measurements are generated. The position is generated at the time of each new batch of radar measurements, and at times when a new AIS measurement can arrive. To avoid having to generate the position three times a second the reporting interval for a Class A ship moving at 0-14 knots and changing course, in table Table 2.1, is rounded down to three seconds.

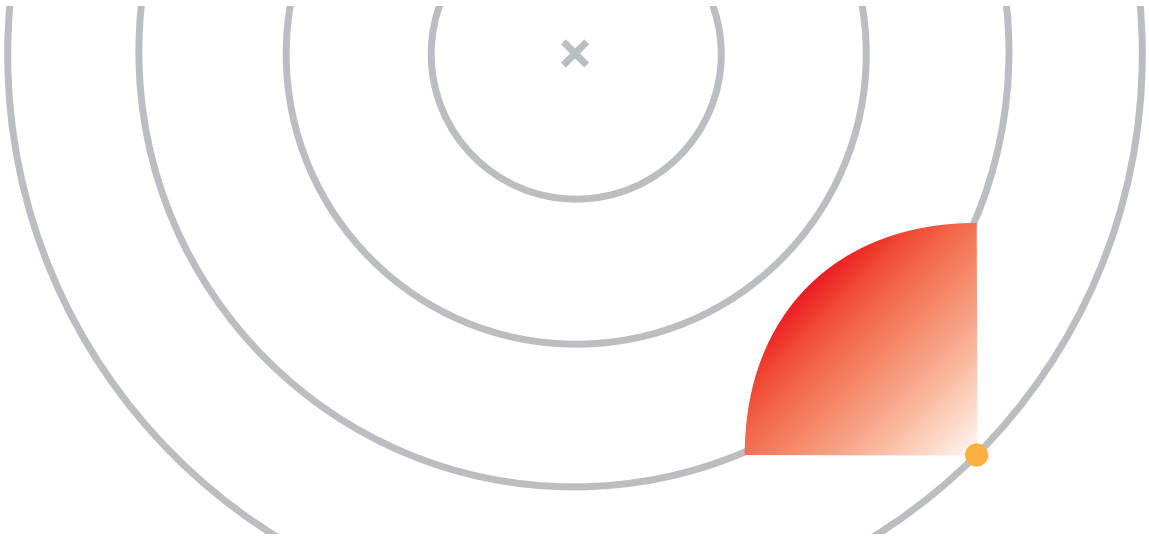

Figure 6.2: Initial velocity for a new generated target.

6.2.2 Radar measurements

When a target trajectory, which represents the true position of the target, has been generated, radar measurements are created for the target at each time step according to the radar model in Section 5.2. That is

$$\mathbf{z}_k = \mathbf{H}_R \mathbf{x}_k + \mathbf{v}_k, \;\; \mathbf{v}_k \sim \mathcal{N}(\mathbf{0}, \mathbf{R}_R) \tag{6.2}$$

Each target has P_D probability of generating a measurement. Only targets that are within the predefined radar range generate radar measurements. After all targets and radar measurements have been created the radar measurements generated on targets that are hidden behind other targets are removed. Clutter measurements are generated according to a Poisson process with a predefined intensity, and the measurements are placed uniformly within the radar surveillance area.

6.2.3 AIS measurements

The first AIS measurements arrive according to Table 2.1 or Table 2.2. The first AIS measurement from each target is created at a random time after target birth, with the maximum time being decided by the aforementioned tables and the velocity of the target. The frequency of the measurements depends on the movement of the simulated target and whether it is a Class A or Class B ship. The probability of a ship having the ability to send AIS messages, denoted as P_{AIS}, can be set, such that only some of the simulated targets transmit messages. The probability of a generated target being of Class A, P_A, or Class B, $1 - P_A$, can also be set.

Measurement noise is added to the true position to create the measurement, according to the AIS measurement model in Section 5.2, i.e.

$$\mathbf{z}_k = \mathbf{H}\mathbf{x}_k + \mathbf{v}_k, \;\; \mathbf{v}_k \sim \mathcal{N}(\mathbf{0}, \mathbf{R}_A) \tag{6.3}$$

An MMSI number is also assigned to each target, and when creating the AIS measurements these MMSI numbers have a predefined probability, P_C, of being corrupted. At each time

step there is also a probability $P_{dropout}$ of the AIS transmitter going offline. This leads to the target not transmitting AIS measurements for some time. The duration of the dropout, in seconds, is determined by a random sampling from a log-normal-distribution with mean $T_{dropout}$.

An example of a complete generated scenario, with the resulting tracks plotted, can be seen in Figure 6.3. The black and gray dots are the radar measurements, and the green dots are the AIS measurements. The measurement colors fade as time passes in the scenario, so the darkest measurements arrived most recently, and the lightest arrived at the start of the scenario. The red lines are the track trajectories output by the tracker, while the orange lines are the true target trajectories. The gray circles represent the distance from the origin where the ownship is situated, and are drawn every 250 meters.

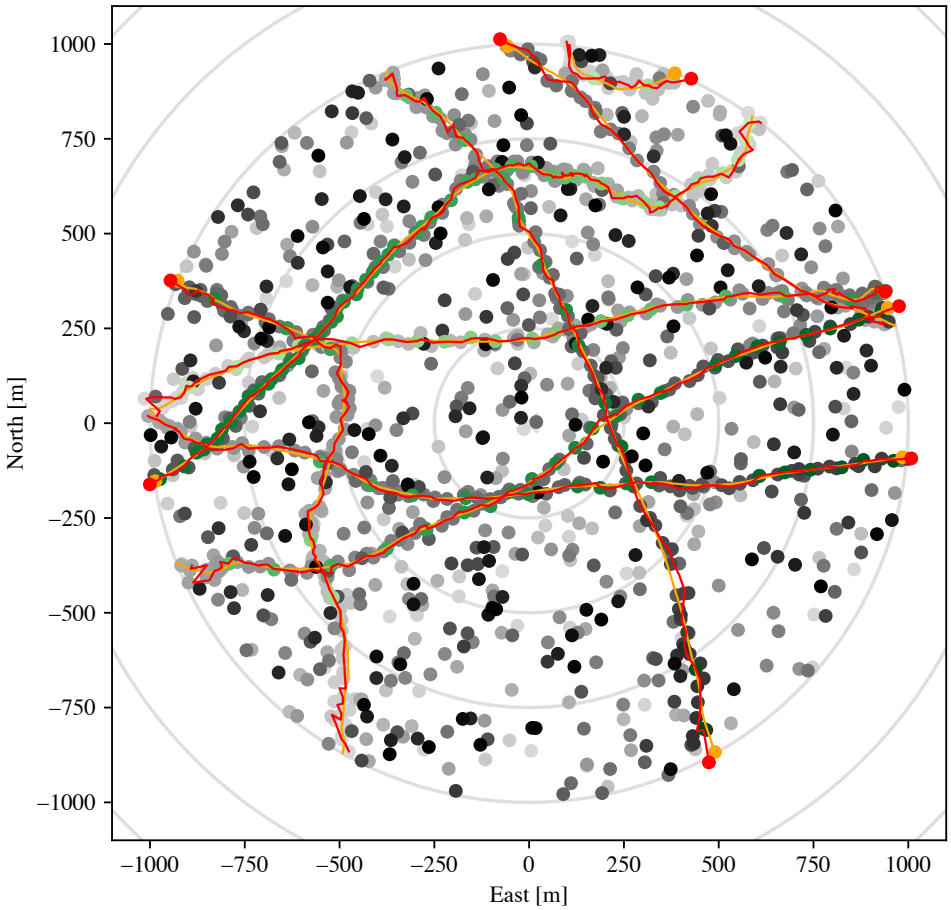

Figure 6.3: Example of a generated scenario.

6.3 Experimental data

The experimental data used for testing were collected during the final demonstration of the Autosea project at NTNU [23]. The experiment took place in the fjord outside of Trondheim. The ownship used during the demonstration was a rigid inflatable boat (RIB) named Telemetron [50], which was equipped with a radar. AIS messages were also collected

from the surrounding ships, which together with the radar measurements constitute the data set. A picture from the demonstration can be seen in Figure 6.4, where Telemetron is the small ship headed towards the camera.

The radar which was used in the demonstration was a Simrad Broadband 4G™ radar [51]. To be convenient for use in a tracker the data was processed through a data extraction process which is described in [47]. It consists of four steps:

1. The detection of objects is handled by the radar. The built-in detection method is optimized for use at sea. The detections are delivered in polar coordinates.
2. The detections are converted to a world fixed reference frame.
3. Detections from land are removed by land masking, which means that the detections in the world fixed frame are compared with a map and removed if they fall within an area marked as land.
4. The detections are clustered to fulfill the assumption of only one measurement being received per target.

Unfortunately, no ground truth is available from the experiment, and the AIS measurements have been interpolated such that they arrive at the same time as the radar measurements. It is nevertheless a relevant real data set for the problem.

Figure 6.4: Drone view of the Autosea final demonstration. Screenshot from [2].

6.4 Evaluation metrics

In the following sections the different evaluation metrics, used to evaluate the performance of the tracker, are presented. These involve well established methods to evaluate the filter consistency, several methods to evaluate different properties of the tracker, and a metric which aims to give an overall view of the performance of a tracker.

6.4.1 Filter consistency

A static estimator is consistent if it converges to the true value of the parameter to be estimated. For state estimators, the consistency has to be decided some other way, as the states change with time. Consistency checks are important, as they tell if a state estimator, or filter, is optimal, and a badly conditioned estimator can also diverge from the true value. As described in [42, p. 233], a filter is consistent within the Gaussian-Linear framework if

$$E[\mathbf{x}_k - \hat{\mathbf{x}}_k] \triangleq E[\bar{\mathbf{x}}_k] = 0 \tag{6.4}$$

and

$$E[[\mathbf{x}_k - \hat{\mathbf{x}}_k][\mathbf{x}_k - \hat{\mathbf{x}}_k]^\top] \triangleq E[\tilde{\mathbf{x}}_k \tilde{\mathbf{x}}_k^\top] = \mathbf{P}_{k|k}. \tag{6.5}$$

These equations leads to three consistency criteria, which checks if a finite set of samples have the same estimation error as their theoretical properties entail. As written in [42] they are:

> The state errors should be acceptable as zero mean and have magnitude commensurate with the state covariance as yielded by the filter.
>
> The innovations should also have the same property.
>
> The innovations should be acceptable as white. [42, p. 234]

The first of the criteria is evaluated by calculating the Normalized estimation error squared (NEES), which is defined as

$$\epsilon_k = \bar{\mathbf{x}}_k^\top \mathbf{P}_{k|k}^{-1} \bar{\mathbf{x}}_k. \tag{6.6}$$

Under Gaussian-Linear assumptions, and assuming that the filter is in fact consistent, the NEES is χ^2-distributed with $n_{\mathbf{x}}$ degrees of freedom. $n_{\mathbf{x}}$ is the dimension of the state $\mathbf{x}$. This means that, for an optimal filter

$$E[\epsilon_k] = n_{\mathbf{x}_k}. \tag{6.7}$$

When considering several samples, the average NEES (ANEES) $\bar{\epsilon}$ can be considered. It is simply the sample mean of the individual NEES values

$$\bar{\epsilon} = \frac{1}{N_k} \sum_{k=1}^{N_k} \epsilon_k \tag{6.8}$$

where N_k is the number of samples. The ANEES is distributed according to a χ^2-distribution with $N_k n_{\mathbf{x}}$ degrees of freedom, which is then used to investigate the filter consistency. The resulting ANEES for the filter is compared to a given confidence interval of the χ^2-distribution, giving an indication of the filter's consistency.

However, the NEES can only be calculated when the true state value is known, and that is only the case for simulations and in some cases monitored experiments. In other cases, the Normalized innovations squared (NIS) can be used to evaluate the filter consistency. It is defined as

$$\epsilon_{\nu,k} = \boldsymbol{\nu}_k^\top \mathbf{S}_k^{-1} \boldsymbol{\nu}_k. \tag{6.9}$$

Similarly to the NEES, the NIS is also χ^2-distributed. However, the χ^2-distribution has $n_{\mathbf{z}}$ degrees of freedom, where $n_{\mathbf{z}}$ is the dimension of the measurement space. As with the ANEES, the average NIS (ANIS) can be calculated as the sample mean of several NIS values. The ANIS has a χ^2-distribution with $Nn_{\mathbf{z}}$ degrees of freedom and is evaluated in the same way as the ANEES.

6.4.2 Evaluating different properties of the tracker

While filter consistency always should be preserved in a tracker, some metrics to evaluate its performance are also needed. One of the more obvious metrics is the *root mean squared error* (RMSE). The RMSE will for a target tracker, when ground truth is available, give the square root of average squared error between the true state and the estimated state. For N_k samples it is defined as

$$\text{RMSE} = \sqrt{\frac{1}{N_k}\sum_{i=1}^{N_k}(\hat{\mathbf{x}}_i - \mathbf{x}_i)^2}. \tag{6.10}$$

The RMSE can be calculated for the whole state, but can also be calculated for just the position or velocity, for example. As the error of the position and velocity can have a different impact and are not always comparable this division can be advantageous.

In [52] some additional metrics for evaluating target trackers are presented. Firstly, some of the terms should be defined:

True tracks: Tracks following an actual target. Whether a track is a true track is determined by the percentage of measurements the track has associated with that actually comes from a target. If this is above 50%, the track is deemed a true track.

False tracks: Tracks not following a target, thus usually originating from clutter. Whether a track is a false track is decided in the same way as for true tracks, i.e. the number of associated measurements that do not come from a target.

Tracks: All created tracks, both true tracks and false tracks.

The first output metric is the *Track probability of detection* (TPD), which is defined as

$$\text{TPD} = \frac{1}{T_{tot}}\sum_{i=1}^{N_{TT}} T_i \tag{6.11}$$

where T_{tot} is the combined duration of the targets in the scenario, N_{TT} is the number of true tracks in the scenario and T_i is the duration of the individual true tracks. The duration of individual tracks is defined as the time between the first and last time the true track associated with a measurement. Any overlaps of true tracks on the same target are removed. This results in the ratio of the sum of the duration of all true tracks and the sum of the duration of all targets.

Furthermore the *Track false alarm rate* (TFAR) is defined as

$$\text{TFAR} = \frac{N_{FT}}{T_{tot}} \tag{6.12}$$

where N_{FT} is the total number of false tracks. This metric gives the number of initialized false tracks divided by the sum of the duration of all targets.

The *Track localization error* (TLE) gives the total average localization error for all true tracks at all time steps. This is done by taking the euclidean norm $\|\cdot\|$ of the difference between the estimated position $\hat{\mathbf{x}}_{pos}$ and the corresponding true position $\mathbf{x}_{pos}$ at each time step

$$\text{TLE} = \frac{1}{N_{TT}} \sum_{t=1}^{N_{TT}} \frac{\|\hat{\mathbf{x}}^t_{pos,1:K_t} - \mathbf{x}^t_{pos,1:K_t}\|}{K_t} \tag{6.13}$$

where K_t is the number of time steps over which track i has been estimated.

The *Track fragmentation rate* (TFR) is defined as

$$\text{TFR} = \frac{N_{TT} - N_T}{T_{tot}} \tag{6.14}$$

where N_T is the number of targets. This shows the number of track fragmentations per second a target is being tracked. A track fragmentation is when a track is terminated prematurely or deviates from the target, and has to be re-initialized on the same target.

While the expressions for calculating these metrics are quite simple, the task of actually evaluating them can be more challenging. In [52] some general issues with tracker-performance evaluation are discussed. Firstly, the times at which to evaluate the tracker has to be considered. When only using radar the obvious choice is to evaluate after each radar update. When including AIS this choice becomes more difficult. One possibility is to only evaluate at the times when a new batch of radar measurements has arrived, as would be done when only using radar. It is also possible to evaluate at all times when either radar measurements or AIS messages have arrived. However, as only one AIS message usually arrives at a time this would create the need to evaluate tracks at times when only a prediction is available for most tracks, and no update based on a measurement. A third option would be to evaluate tracks that have had an AIS measurement update, in addition to evaluating after each radar measurement update. This brings with it some of the problems of the aforementioned case, as in the case where several tracks in a cluster share a single AIS measurement. Due to these potential problems the first method is used, where the tracks are evaluated after each new batch of radar measurements. As the main comparison will be between the tracker with and without AIS measurements this also seems like the most intuitive method.

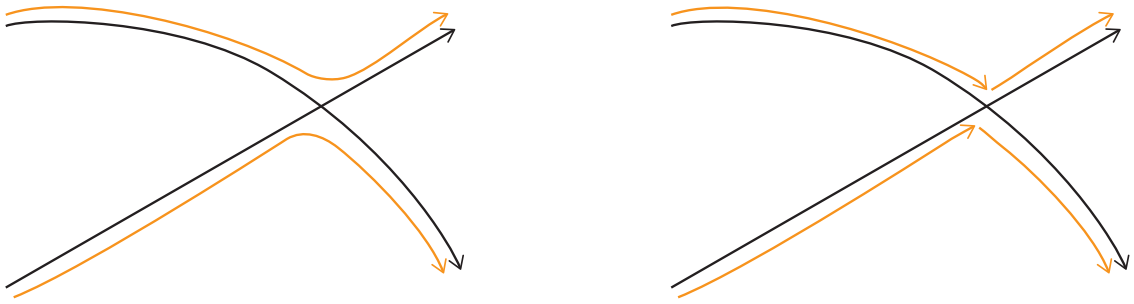

(a) Track switch. **(b)** Splitting of tracks.

Figure 6.5: Estimates (in orange) and the true target they follow (in black).

Another challenge when evaluating a tracker lies in how to assign a track to the ground truth. For example, if a track is assigned to its true target based only on what measurement it was initialized on, a track swap, as pictured in Figure 6.5a, would make the TLE very large. This is a situation that commonly occurs when multiple targets are present and thus needs to be addressed. The chosen solution is to split the tracks when they deviate from the true target, as depicted in Figure 6.5b. This way the effect of a track switch will not impact the TLE to such a large degree, in exchange for a higher TFR. Which true target a track is following at a given time step can be determined by looking at the measurements they have associated with. This scheme does, however, require labeling of the measurements which originate from each target. Thus, such an evaluation becomes difficult when using real data.

6.4.3 Overall performance evaluation

The Optimal subpattern assignment (OSPA) metric was first presented in [53] before it was further expanded upon in [54]. It is a metric that accounts for both spatial errors and cardinality errors, and as such it catches both errors where the estimates are imprecise and errors where a target has not been detected. For a closed and bounded space $W \subset \mathbb{R}^N$ the individual track positions at a given time are elements of W. The track estimates at time k are contained in the finite subset $X_k = \{\mathbf{x}_k^1, \ldots, \mathbf{x}_k^m\} \subset W$, with the true target states in $Y_k = \{\mathbf{y}_k^n, \ldots, \mathbf{y}_k^n\} \subset W$. A metric $d(\mathbf{x}, \mathbf{y})$ on the space $\mathbb{R}^N$ has to fulfill certain criteria:

- $d(\mathbf{x}, \mathbf{y}) \geq 0 \ \forall \ \mathbf{x}, \mathbf{y} \in \mathbb{R}^N$
- $d(\mathbf{x}, \mathbf{y}) = 0 \iff \mathbf{x} = \mathbf{y}$
- $d(\mathbf{x}, \mathbf{y}) = d(\mathbf{y}, \mathbf{x}) \ \forall \ \mathbf{x}, \mathbf{y} \in \mathbb{R}^N$
- $d(\mathbf{x}, \mathbf{y}) \leq d(\mathbf{x}, \mathbf{z}) + d(\mathbf{z}, \mathbf{y}) \ \forall \ \mathbf{x}, \mathbf{y}, \mathbf{z} \in \mathbb{R}^N$

The OSPA metric is defined as

$$\bar{d}_p^{(c)}(X_k, Y_k) = \left(\frac{1}{n} \left(\min_{\pi \in \Pi_n} \sum_{i=1}^{m} d^{(c)}(\mathbf{x}_k^i, \mathbf{y}_k^{\pi(i)})^p + c^p(n-m) \right) \right)^{1/p} \tag{6.15}$$

if $m \leq n$, otherwise $\bar{d}_p^{(c)}(X_k, Y_k) \triangleq \bar{d}_p^{(c)}(Y_k, X_k)$. Here, $d^{(c)}(\mathbf{x}_k^i, \mathbf{y}_k^{\pi(i)}) = \min(c, d(\mathbf{x}_k^i, \mathbf{y}_k^{\pi(i)}))$ where the base distance $d(\mathbf{x}_k^i, \mathbf{y}_k^{\pi(i)})$ is the Euclidean distance between $\mathbf{x}_k^i$ and $\mathbf{y}_k^{\pi(i)}$, and $c > 0$ is a design parameter called the cutoff. The fact that this is a metric is shown in [54]. Π_n is the set of all possible permutations for $\{1, \ldots, n\}$. p is also a design parameter, called the order. The cutoff c can be interpreted as a way to choose how heavily cardinality errors should be punished, while the order p can be interpreted as a way to decide how heavily outliers should be punished.

The OSPA metric as defined in (6.15) only provides an evaluation for a single point in time, and as such is not able to penalize situations such as track switches. For that reason, an OSPA-like metric for tracks, called OSPA$^{(2)}$ was presented in [55]. One would often want to evaluate performance as a function of time throughout the scenario. Then, at each time instant a time window has to be considered. This can be achieved by only considering the tracks for the previous N time steps in a sliding window fashion. It can be summarized as an OSPA metric on an OSPA base distance. The base distance can be defined as

$$\tilde{d}_p^{(c)}(\mathbf{x}_{k:k-N}^i, \mathbf{y}_{k:k-N}^{\pi(i)}) = \begin{cases} \sum_{k' \in \mathcal{D}_x \cup \mathcal{D}_y} \dfrac{\bar{d}^{(c)}(\mathbf{x}_{k'}^i, \mathbf{y}_{k'}^{\pi(i)})}{|\mathcal{D}_x \cup \mathcal{D}_y|} & \text{if } \mathcal{D}_x \cup \mathcal{D}_y \neq \emptyset \\ 0 & \text{if } \mathcal{D}_x \cup \mathcal{D}_y = \emptyset \end{cases} \tag{6.16}$$

where $\mathcal{D}_t$ are the times at which track t exists within the time window. Then, for two sets of tracks $X = \{\mathbf{x}^1, \ldots, \mathbf{x}^m\}$ and $Y = \{\mathbf{y}^1, \ldots, \mathbf{y}^n\}$ an OSPA metric on the sets for $m \leq n$ is

$$\check{d}_p^{(c)}(X_{k|k-N}, Y_{k|k-N}) = \left(\frac{1}{n} \left(\min_{\pi \in \Pi_n} \sum_{i=1}^{m} \tilde{d}^{(c)}(\mathbf{x}_{k|k-N}^i, \mathbf{x}_{k|k-N}^{\pi(i)})^p + c^p(n-m) \right) \right)^{1/p} \tag{6.17}$$

This metric is the OSPA$^{(2)}$. As for the OSPA, if $m > n$ we have that $\check{d}_p^{(c)}(X_{k|k-N}, Y_{k|k-N}) \triangleq \check{d}_p^{(c)}(Y_{k|k-N}, X_{k|k-N})$ It is also defined that $\check{d}_p^{(c)}(\emptyset, X_{k|k-N}) = c$ and $\check{d}_p^{(c)}(\emptyset, \emptyset) = 0$. If $N = 0$ the OSPA$^{(2)}$ metric simplifies to the OSPA metric. To evaluate both (6.15) and (6.17) a 2-D assignment problem has to be solved. This can for example be done with the Auction algorithm [46, p. 137], similarly to what is done for efficient data association, as explained in Section 5.5.

Remark. In addition to the OSPA$^{(2)}$ metric, another version of the regular OSPA metric has been presented, the Generalized optimal subpattern assignment metric (GOSPA) [56]. It is defined as

$$d_p^{(c,\alpha)}(X_k, Y_k) = \left(\min_{\pi \in \Pi_n} \sum_{i=1}^{m} d^{(c)}(\mathbf{x}_k^i, \mathbf{y}_k^{\pi(i)})^p + \frac{c^p}{\alpha}(n-m) \right)^{1/p} \tag{6.18}$$

It has also been extended for use on sets of tracks, and differs from the OSPA metric through the removal of the normalization, and the addition of the α parameter.

CHAPTER 7

Results

In this chapter an evaluation of the tracker described in Chapter 4 and is performed, using an implementation as described in Chapter 5. The performance is evaluated on both simulated data and experimental data, using the metrics presented in Section 6.4.2 and Section 6.4.3. For the simulated data both a general analysis of the tracker and a closer look at specific scenarios which can cause problems were performed. These include scenarios involving corrupted MMSI numbers, track switches, and initialization of close targets. For the experimental data the comparisons are done between tracking using AIS and radar measurements, and tracking using only radar measurements. An analysis of the consistency of the tracker is also performed. The tracker parameters used for all the scenarios can be seen in Table 7.1, which were found after tuning the tracker on the experimental data.

7.1 Simulated data

The simulated data is created mainly in accordance with parts of the scheme detailed in Section 6.2, with some alterations to fit specific scenarios. The parameter values used for creating the targets and measurements were chosen to mirror the tuning parameters in Table 7.1. However, as only the CV model was used for simulating the movement of the generated targets, this was set to a different value. The parameters used to create the simulated data can be seen in Table 7.2.

Parameter	Symbol/Units	Value
Radar sample interval	T [s]	2.5
CV 1 process noise	$q_{a,1}$ [m/s^2]	0.1
CV 2 process noise	$q_{a,2}$ [m/s^2]	1.5
Turn rate process noise	q_ω [1/s^2]	0.05
Cartesian range std. radar	σ_{c_R} [m]	6.6
Cartesian range std. AIS	σ_{c_A} [m]	3
Polar range std.	σ_r [m]	5
Polar bearing std.	σ_θ [deg]	1
Detection probability	P_D [–]	0.92
Survival probability	P_S [–]	0.99
Visibility transition probabilities	w [–]	$\begin{bmatrix} 0.9 & 0.1 \\ 0.52 & 0.48 \end{bmatrix}$
Gate size	g [–]	3
Track fusion hypothesis significance level	α [–]	0.01
Clutter intensity	λ [1/m^2]	2×10^{-7}
Initial new target intensity	b [1/s^2]	1×10^{-8}
Initial velocity std.	σ_{init} [m/s]	15
Initial mode probabilities	μ^0 [–]	$[0.8, 0.1, 0.1]^\top$
Mode transition probabilities	π^{ss} [–]	$[0.99, 0.99, 0.99]$
Existence confirmation threshold	T_c [–]	0.999
TTP initialization threshold	T_{TTP} [–]	0.5
Existence termination threshold	T_d [–]	0.01
MMSI termination threshold	T_τ [–]	1×10^{-15}
Label confidence	P_C [–]	0.99

Table 7.1: Tracker parameters.

Parameter	Symbol/Units	Value
Radar sample interval	T [s]	2.5
CV process noise	q_a [m/s^2]	0.4
Cartesian range std. radar	σ_{c_R} [m]	6.6
Cartesian range std. AIS	σ_{c_A} [m]	3
Polar range std.	σ_r [m]	3
Polar bearing std.	σ_θ [deg]	1
Detection probability	P_D [–]	0.92
Clutter intensity	λ [1/m^2]	2×10^{-7}
Max initial velocity	V_{init} [m/s]	5
Label confidence	P_C [–]	0.99
AIS dropout probability	$P_{dropout}$ [–]	0.01
Mean AIS dropout time	$T_{dropout}$ [s]	30
Class A probability	P_A [s]	0.5

Table 7.2: Simulated data parameters.

7.1.1 Filter consistency

Introducing a different type of sensor, and updating the estimates sequentially, changes the original VIMMJIPDA tracker quite substantially, and it is necessary to examine the consistency of the tracker when using AIS measurements. 2000 Monte Carlo runs were performed and the ANEES was calculated when tracking both with and without using AIS measurements. The scenarios for the consistency evaluation were created according to Table 7.2, with the following specification:

- One target is born at time $T = 0$, and none after.
- The scenario ends at time $T = 1000$.

The resulting ANEES, in addition to the 95% confidence intervals can be seen in Table 7.3.

95% confidence interval	$[3.99, 4.01]$
ANEES without AIS	4.00
ANEES with AIS	4.12

Table 7.3: ANEES values when using only radar measurements, and when using both radar and AIS measurements.

As can be seen, the ANEES when not using AIS measurements is exactly as one would hope, and within the confidence interval. When using the AIS measurements the ANEES is slightly too high, i.e. the tracker is slightly overconfident. This can be due to the lower measurement noise of the AIS measurements, and the certainty the tracker has on the AIS measurements belonging to the target. This lowers the covariance of the estimate whenever they appear, which possibly makes the tracker too confident in the subsequent radar measurements. It can, however, also be due to the tuning. Nevertheless, the ANEES values do not show any particularly large consistency issues.

Furthermore, the consistency of the course estimates were evaluated. To do this, the course estimates from the scenario were extracted, and their standard deviations were calculated by linearizing the covariance matrices. The percentage of estimates with a course error larger than their standard deviation was also calculated. The results can be seen in Table 7.4.

	With AIS	Without AIS
Average course RMSE [deg]	3.20	3.60
Average course std. dev. [deg]	29.19	36.48
Percentage outside 1σ-bounds	27.99	28.36
Percentage outside 2σ-bounds	10.63	11.58

Table 7.4: Comparison of course estimate consistency with and without the use of AIS measurements.

For the course estimates the tracker is more consistent when using AIS, but the differences are small. The course estimates achieved when using the AIS measurements

are more accurate, and also have lower standard deviations. When comparing the number of estimates with a larger course RMSE than their standard deviations, these numbers are lower when using AIS measurements. The same is the case for the number of estimates with a larger course RMSE than twice their standard deviations. This contrasts the results from Table 7.3, where the tracker was more confident when using AIS measurements. Here the opposite seems to be the case. Nevertheless, none of these results hints towards any large consistency issues with the tracker.

7.1.2 Using AIS and radar versus using only radar

For the inclusion of AIS measurements in the VIMMJIPDA to be meaningful it should show some performance improvement upon its regular usage when it only uses radar measurements. To evaluate this, the tracker performance was evaluated on the same data set over a range of probabilities for a given track to generate AIS measurements, P_{AIS}. For each probability 2000 Monte Carlo simulations were performed.

The scenarios were created according to Table 7.2, with the following specification:

- Four targets are born at time $T = 0$, while four targets are born at time $T = 100$.
- The scenario ends at time $T = 400$.

The mean of the OSPA$^{(2)}$-values across all time steps and simulations, for each P_{AIS}, are shown in Figure 7.1. These were calculated with $N = 10$, $c = 100$, and $p = 2$. As $N = 10$, track jumps and track losses are penalized across 10 time steps, while any cardinality errors are penalized with a value of 100. The OSPA$^{(2)}$ decreases linearly as more targets transmit AIS measurements, resulting in a 32% combined decrease. In Figure 7.2 the OSPA$^{(2)}$-values for the scenarios with $P_{AIS} = 0$ and $P_{AIS} = 1$ are shown for different N, with $p = 2$ and $c = 100$. When $N = 1$, track jumps and track losses are not penalized, while for $N = 40$ they are penalized for the last 40 time steps, which amount to a large part of the scenario. Not surprisingly, the OSPA$^{(2)}$ increases as N increases. The difference in performance between when using AIS and not, does however remain nearly constant.

The OSPA$^{(2)}$ values for different orders, p, are shown in Figure 7.3. As mentioned in Section 6.4.3, a high order will penalize outliers more than a lower order. As can be seen, the error increases with increasing p, with the difference between when using AIS and using only radar also increasing slightly. This indicates that the tracker outputs more outliers when not using AIS, but the difference is not large. In Figure 7.4, the OSPA$^{(2)}$ values for different values of the cutoff, c, is shown. The most obvious effect of changing the value of c is that cardinality errors are punished more, or less, severely. It also determines the point where an outlier estimate is discarded in favor of a cardinality error. If $c = 1$, the inherent optimization problem in the OSPA$^{(2)}$ metric will disregard all estimates with a base distance larger than 1 from the ground truth. With $c = 500$, only the most obvious outliers will be discarded. Nevertheless, the errors seem to increase linearly with the increasing c, indicating that only the first effect have much of an impact. That is, the higher value of c results in a higher OSPA$^{(2)}$ value due to more severely punished cardinality errors. Furthermore, the difference between using AIS and not increases with increasing c, indicating that there are fewer cardinality errors when using AIS.

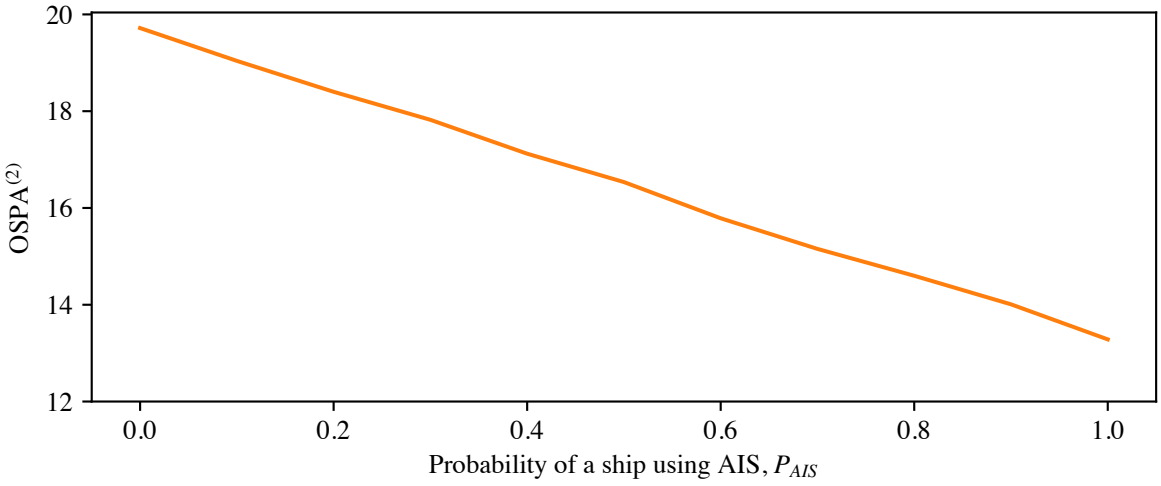

Figure 7.1: OSPA$^{(2)}$ with $N = 10$, $c = 100$, and $p = 2$.

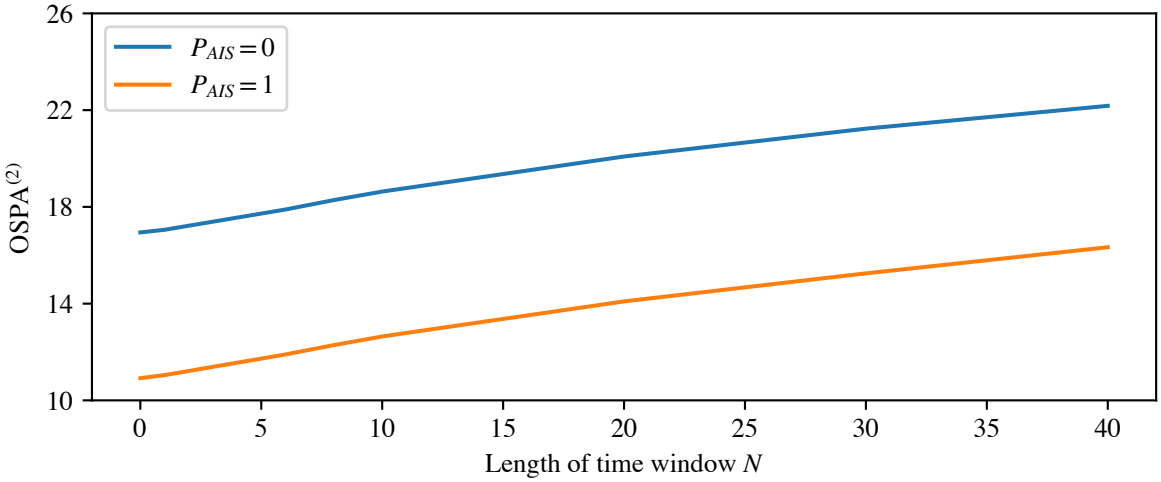

Figure 7.2: OSPA$^{(2)}$ for varying N, $c = 100$, and $p = 2$.

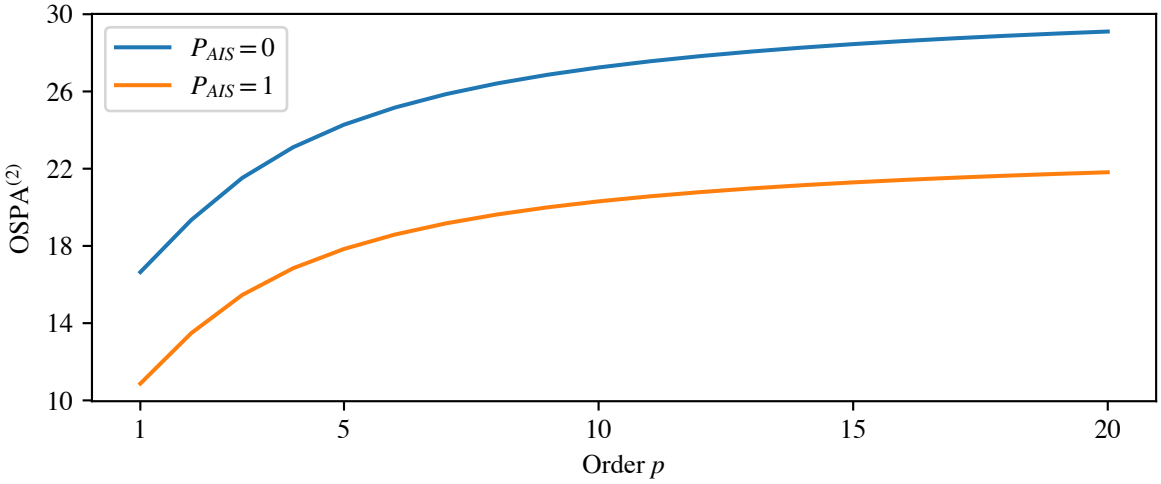

Figure 7.3: OSPA$^{(2)}$ for varying p, $c = 100$, and $N = 10$.

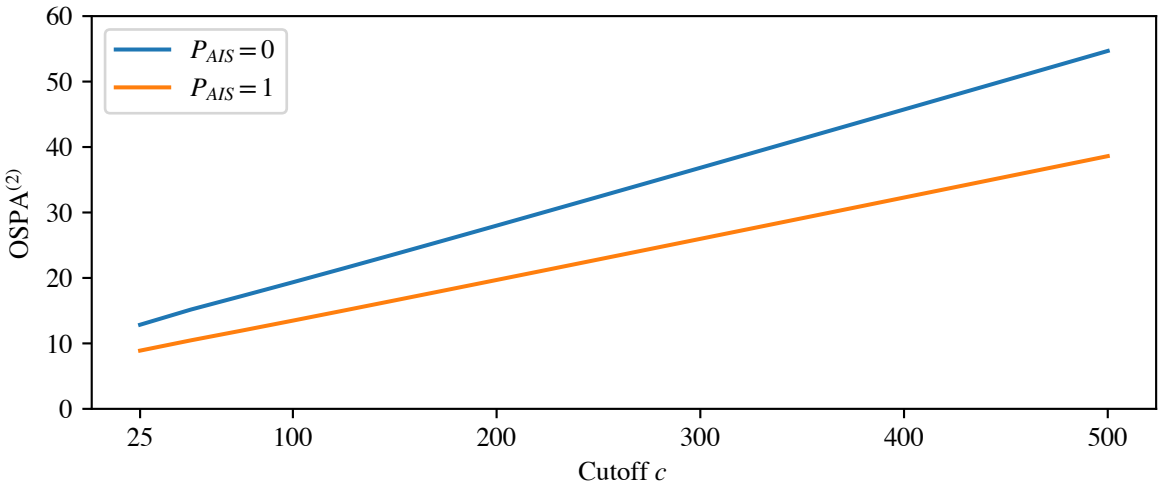

Figure 7.4: OSPA$^{(2)}$ for varying c, $N = 10$, and $p = 2$.

The average TLE values across the time steps and simulations for different P_{AIS} are shown in the uppermost plot in Figure 7.5. As for OSPA$^{(2)}$, the error decreases linearly as P_{AIS} increases. The performance gain is a bit larger than for the OSPA$^{(2)}$, with a total decrease of 35%.

The TPD is shown in the second plot from the top in Figure 7.5. Also here, a clear linear trend can be seen as P_{AIS} increases. The gains are, however quite small, with the TPD increasing by 1.1% between $P_{AIS} = 0$ and $P_{AIS} = 1$.

In the second plot from the bottom in Figure 7.5, the TFR can be seen for the different P_{AIS} values. The value remains almost constant, regardless of the amount of tracks transmitting AIS measurements. The fragmentation rate is already quite low when using only radar, but the addition of AIS measurements seems unable to prevent fragmentation occurring when using radar.

The TFAR is shown in the bottom plot in Figure 7.5, and is also seemingly unaffected by the addition of AIS measurements. This makes sense, by keeping in mind how the false alarms are defined. The false alarms are not associated to any target, and as such they must come as a result of clutter. Then, the addition of AIS measurements shouldn't have any noticeable impact. Nevertheless, the TFAR is generally very low.

By examining these metrics, one can assume that much of the improvement found from the OSPA$^{(2)}$ metric comes from improved individual track estimates. Some of it also comes from faster initialization of tracks, as reflected by the TPD. This is likely why the OSPA$^{(2)}$ increases faster with increasing c when only using radar, as depicted in Figure 7.4. The cardinality errors resulting from track fragmentation and false alarms, do however stay mostly the same regardless of the availability of AIS measurements. This fits nicely with what was discovered when looking at the OSPA$^{(2)}$ values for varying time windows. If the differences in false alarms and track fragmentation were large this would result in a proportionally larger increase for large N when using only radar. The cardinality errors as a result of a worse TPD, however, would occur at the start or end of the life span of the tracks, and will as such not result in a large change with increasing window length.

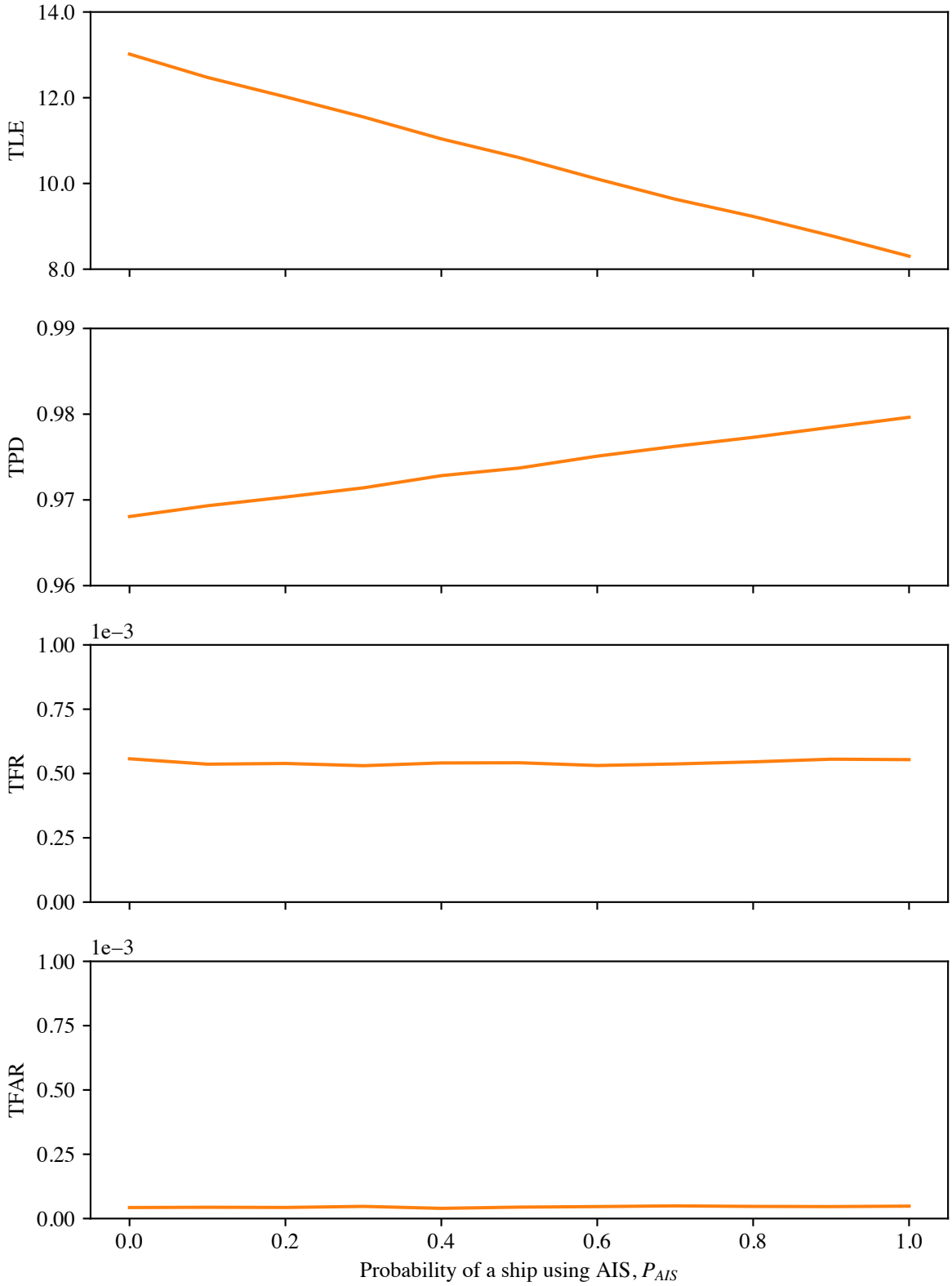

Figure 7.5: Track localization error (TLE), Track probability of detection (TPD), Track fragmentation rate (TFR) and Track false alarm rate (TFAR) for $P_{AIS} \in [0, 1]$.

7.1.3 Dynamics of the Total track probability

As explained in Section 5.6 the regular scheme of initializing tracks only on measurements outside the validation gates of the tracks can cause problems when dealing with AIS measurements. For that reason a new mechanism was added, initializing on all measurements with a previously undetected MMSI number if the Total track probability (TTP) of the new target is large enough. Here the effect of this addition is evaluated.

To examine the dynamics of the TTP parameter a simple test environment was created. This environment calculates the TTP when a measurement with a different MMSI number than what has previously been observed arrives. It consists of a single track, and then evaluates if a new track should be initialized on the new measurement. The test environment is setup as follows:

- The covariance of the track position and the measurement covariance are user-defined parameters. These are needed to create the innovation covariance matrix for the measurement likelihood. A Cartesian measurement model is used, with the same covariance in the x- and y-directions.
- The track uses only one kinematic model to simplify calculations and avoid the consideration of too many parameters.
- The track has three MMSI numbers in its state vector, $-1, 0, 1$. These are the probability of having an unknown MMSI number, no MMSI number and MMSI number 1, respectively. The probabilities of any of these being the correct MMSI number is user-defined.
- The confidence in the MMSI number of the new measurement not being corrupted, P_C, is also user-defined.
- The existence probability of the track, and the birth intensity are also user-defined.
- The new measurement arrives a user-defined number of meters away from the track.

With this setup the impact of the different parameters used to calculate the TTP can be evaluated. The default parameters used can be found in Table 7.5.

Parameter	Value
Existence probability r^t	0.99
MMSI number probabilities ξ^t	$[1 \times 10^{-10}, 1 - 1 \times 10^{-10}]^\top$
Positional covariance $\mathbf{P}_{xy}$	$I_{2\times 2}5^2$
Measurement covariance $\mathbf{R}$	$I_{2\times 2}4^2$
MMSI confidence P_C	0.99
Birth intensity b	1×10^{-8}

Table 7.5: Default TTP parameters.

Figure 7.6 shows the TTP as a function of distance from the estimated position of the target to the measurement, or the innovation. The dotted lines represent the point

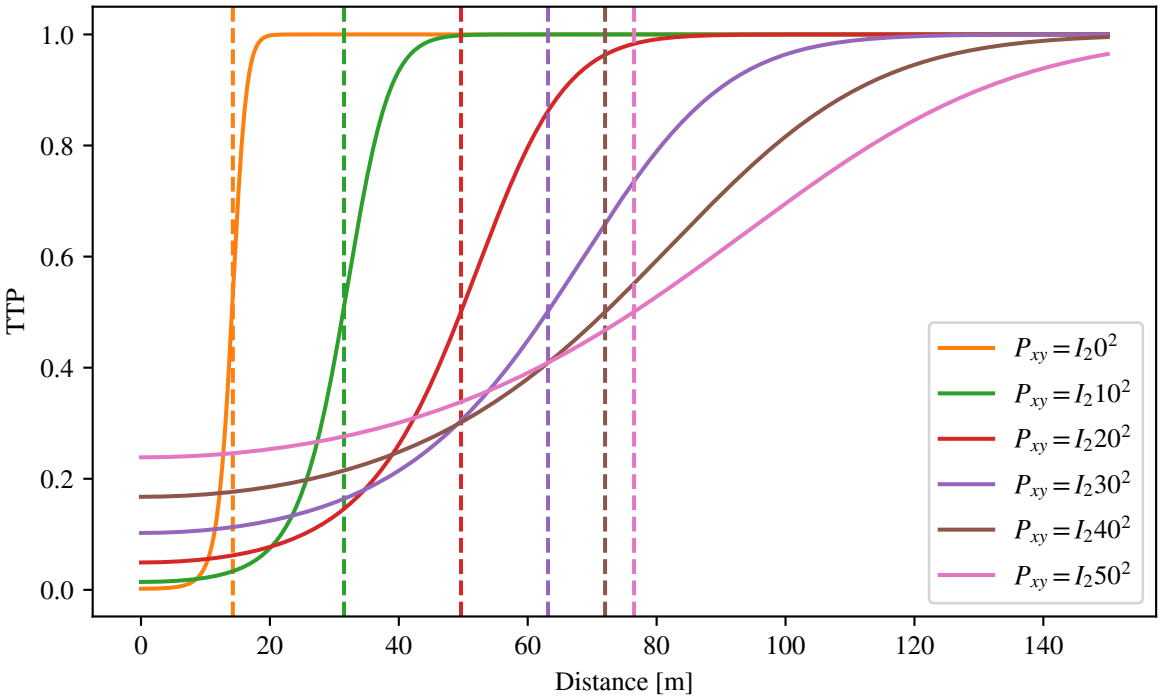

Figure 7.6: TTP value as a function of the distance to a new measurement for different positional standard deviations.

where the TTP is above 0.5, which means that a new target is to be initialized. The TTP increases as the innovation increases, as this makes the measurement less likely to belong to the track. Also, as the uncertainty of the position of the target increases the distance needed before a new target is initialized also increases. This is because this impacts the likelihood of the measurement belonging to the track, and is also the intuitive behavior. If the tracker is uncertain of where a target is located a measurement has to be further away before it is certain that it does not belong to the target. The same dynamic is seen when changing $\mathbf{R}$, which follows from how the $\mathbf{S}$ matrix is computed, see Table 5.1.

The TTP is also impacted by the existence probability and MMSI probabilities of the track. Figure 7.7 shows how far apart the track and the measurement has to be for a track to be initialized on the measurement, as a function of these values. The single MMSI probability which mainly impacts this is the probability of the MMSI being unknown, $\xi^{t\tau-1}$. This is because the new measurement has a previously unencountered MMSI number, with a probability of being correct proportional to $\xi^{t\tau-1}$. The measurement likelihood, and thus also the distance needed for an initialization, increases as $\xi^{t\tau-1}$ increases. Furthermore, the distance needed for an initialization increases with increasing existence probability. If the existence probability of the track is small the weight in (4.26) also becomes small, resulting in a lower TTP. In addition, the existence probability is present in (5.14) itself. This is in line with what is expected, as a target with very low probability of existence should have a smaller probability of being the origin of a new measurement. This should then lead to a new target being initialized. It can also be seen that the needed distance for a new initialization increases quickly as the existence probability increases.

The pre-defined MMSI confidence probability P_C and birth intensity b also impact the TTP. In Figure 7.8 it is shown how far apart the target and the new AIS measurement has to be for an initialization, for different values of b and P_C.

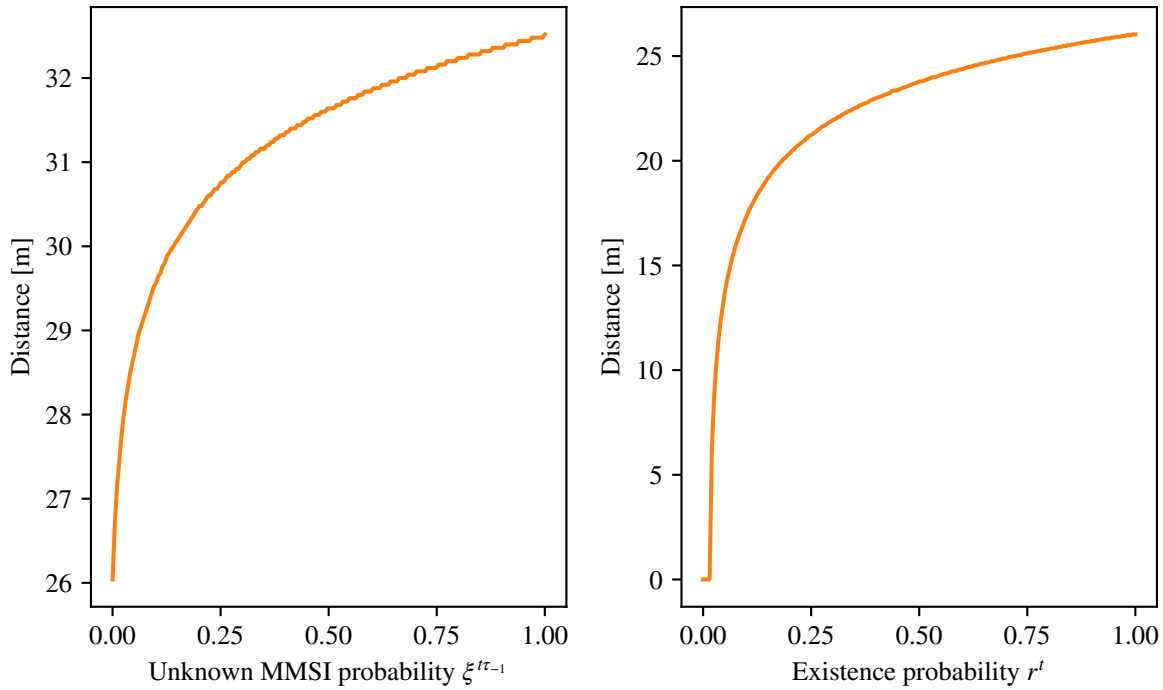

Figure 7.7: The distance between the target and the measurement needed for a new target to be initialized, as a function of the unknown MMSI probability $\xi^{t\tau_{-1}}$, and the existence probability, r^t.

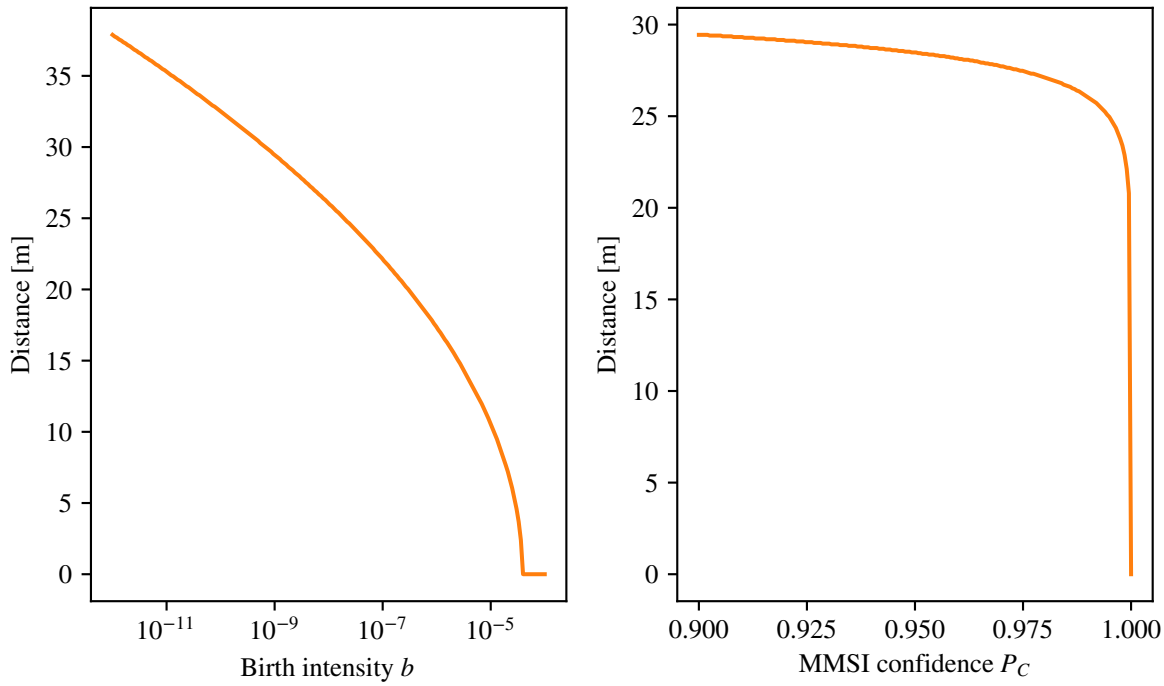

Figure 7.8: The distance between the target and the measurement needed for a new target to be initialized, as a function of the birth intensity b, and the MMSI confidence, P_C.

The birth intensity dictates the weight of the new target hypothesis in (5.14). As can be seen, if the birth intensity is much higher than 10^{-5} a new track is initialized on the AIS measurement no matter what. A high birth intensity would indicate that many of the measurements comes from new targets, which is reflected in the TTP. Furthermore, as the new measurement has a previously unencountered MMSI number the probability of the MMSI number being corrupt has quite a large impact on the TTP. With a large certainty in the MMSI number of the new measurement being correct a new target will be initialized even if the distance between the target and the measurement is small. This is because a high P_C leads to a lower measurement likelihood for the already existing targets.

7.1.4 Initialization on AIS measurements for closely spaced targets

To show how initialization using TTP is used in practice a simple scenario has been constructed. The scenario consists of two targets moving in the same direction with the same velocity. They are born at the same time, but one target starts transmitting AIS messages before the other. Firstly the scenario is considered using only AIS measurements, to provide a clearer explanation of the core problem. In Figure 7.9a the tracking results when using TTP are shown. A single validation gate is shown, as a orange circle. As can be seen, the validation gate encompasses the measurements from both targets. Because track 1 is initialized first, the track on target 2 would be left uninitialized when only initializing on measurements not claimed by any validation gates.

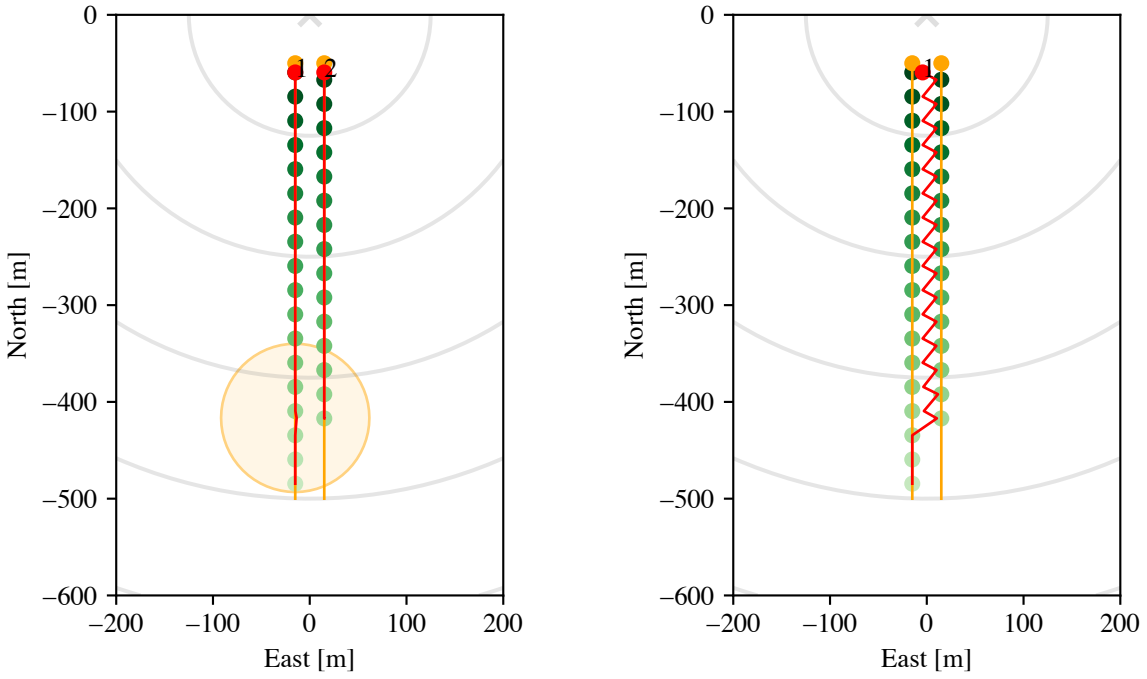

(a) Tracking result when using TTP, with the validation gate of track 1 plotted when the first measurement of target 2 arrives.

(b) Tracking result when not using TTP.

Figure 7.9: Tracking results for two closely spaced targets with and without the use of TTP, when using only AIS measurements.

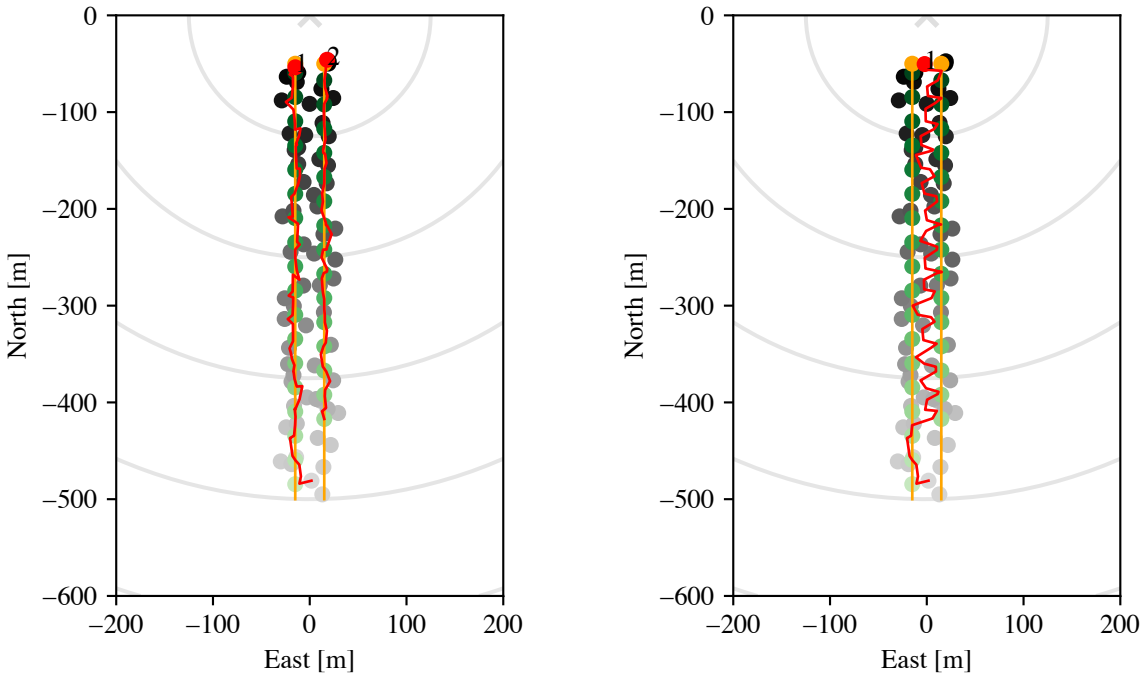

(a) Tracking result when using TTP.

(b) Tracking result when not using TTP.

Figure 7.10: Tracking results for two closely spaced targets with and without the use of TTP, with both radar and AIS measurements present.

However, due to the additional initialization logic both tracks are initialized, in line with the wanted behavior. The results when not using TTP are shown in Figure 7.9b. Here, no new track is initialized on the other target, which leads to the track jumping between the measurements from the two targets. This is similar to the situation sketched in Figure 5.1.

This works well also when considering both radar and AIS measurements. As can be seen in Figure 7.10a a new track is initialized on target 2 as soon as the first AIS measurement from it is received. The track for target 1 is initialized on a radar measurement, and the first radar measurements originating from target 2 then falls within the validation gate of track 1. However, these can be "ignored" by the track, and the tracker is able to follow the correct target either way. However, no new track is initialized until the AIS measurements from target 2 arrives. Then, a new track is created, giving a result similar to the one in Figure 7.9a. In Figure 7.10b the results are again shown when the tracker does not use TTP. The result is similar to when only using the AIS measurements. For the first couple of time steps the tracker is able to stick to a single target, but no initialization is made on the radar measurements from the other target. When the AIS measurements from target 2 starts appearing, the track starts jumping from target to target.

7.1.5 Corrupted MMSI numbers

As mentioned in Section 2.1.2, one cannot completely trust the received AIS measurements. This problem can be mitigated with pre-processing, some methods are mentioned in [19], but one would have to assume that incorrect information can be received by the tracker. The case of corrupted kinematic data would not cause too much of a problem, as this would be analogous to a noisy measurement which any tracker is designed to handle. If the MMSI number is wrong, however, this could cause problems, and how these corrupted

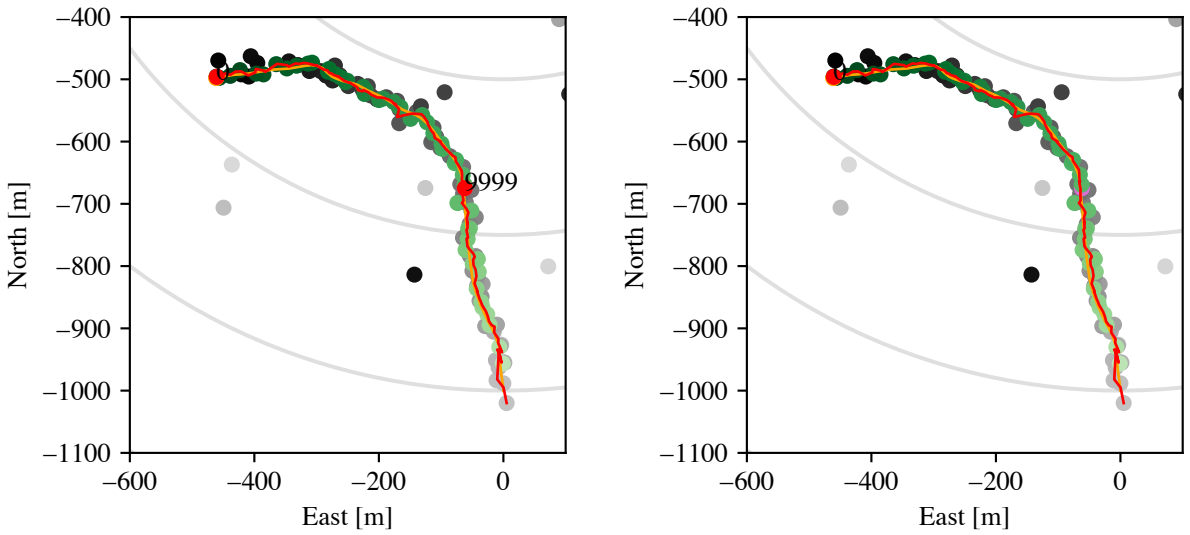

(a) Tracker result when a target is initialized on the corrupt AIS measurement.

(b) Tracker result when a target is not initialized on the corrupt AIS measurement.

Figure 7.11: Impact of a corrupt AIS measurement for a single track.

MMSI numbers impact the tracker should therefore be examined.

Firstly, a situation where an AIS measurement with a corrupted MMSI number appears from a target with an already established track is considered. As there is only one track present there are two possible outcomes: either the AIS measurement is associated to the already existing track or it is deemed to be a new track due to the previously unencountered MMSI number. This will depend on the TTP from (5.14). The two possible outcomes are pictured in Figure 7.11a and Figure 7.11b. The AIS measurement arriving at time $T = 97.48$ has the corrupted MMSI number 9999 while all the others have the correct MMSI number 0. In the first plot the P_C parameter is set to $1 - 10^{-6}$, leading to the initialization of a new track with the corrupted MMSI number 9999. In the other plot, with $P_C = 0.99$, the AIS measurement with corrupted MMSI number is deemed to come from the same target as the previous AIS measurements.

The label probabilities for track 0 for the two scenarios are shown in Figure 7.12a and Figure 7.12b. Notice the logarithmic scale on the y-axis. As can be seen from the graphs the corrupted AIS measurement does not make a large impact. The track is initialized on a radar measurement, and thus has probability equal to one of having MMSI number 0. However, when the AIS measurements starts appearing it quickly acquires a high probability of having MMSI number 1. As mentioned in Section 5.7, the probability of having an unencountered MMSI number cannot go below 1×10^{-10}, as it would otherwise eventually cause numerical underflow. The prior probability a of corrupted MMSI number is small, due to the small probability of the target having a unencountered MMSI number. In the case where a new target is initialized on the corrupted MMSI measurement the probability is even smaller than when a new target is not initialized. This is because the introduction of a new target lowers the association probability between track 0 and the measurement, which then propagates to the label probability, as seen from (4.87). As MMSI number 9999 only appears once, the probability of it being the correct MMSI number plummets quickly. The MMSI number is removed from the hybrid state when the probability falls below T_τ.

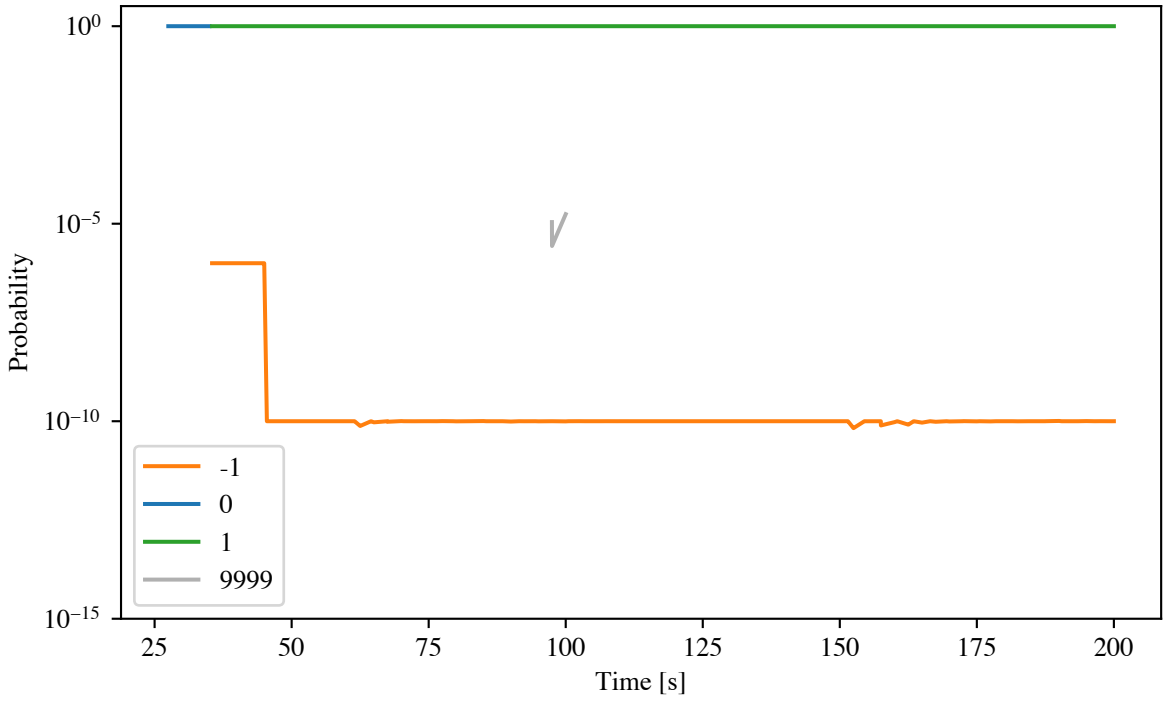

(a) MMSI probabilities when a target is initialized on the corrupt AIS measurement.

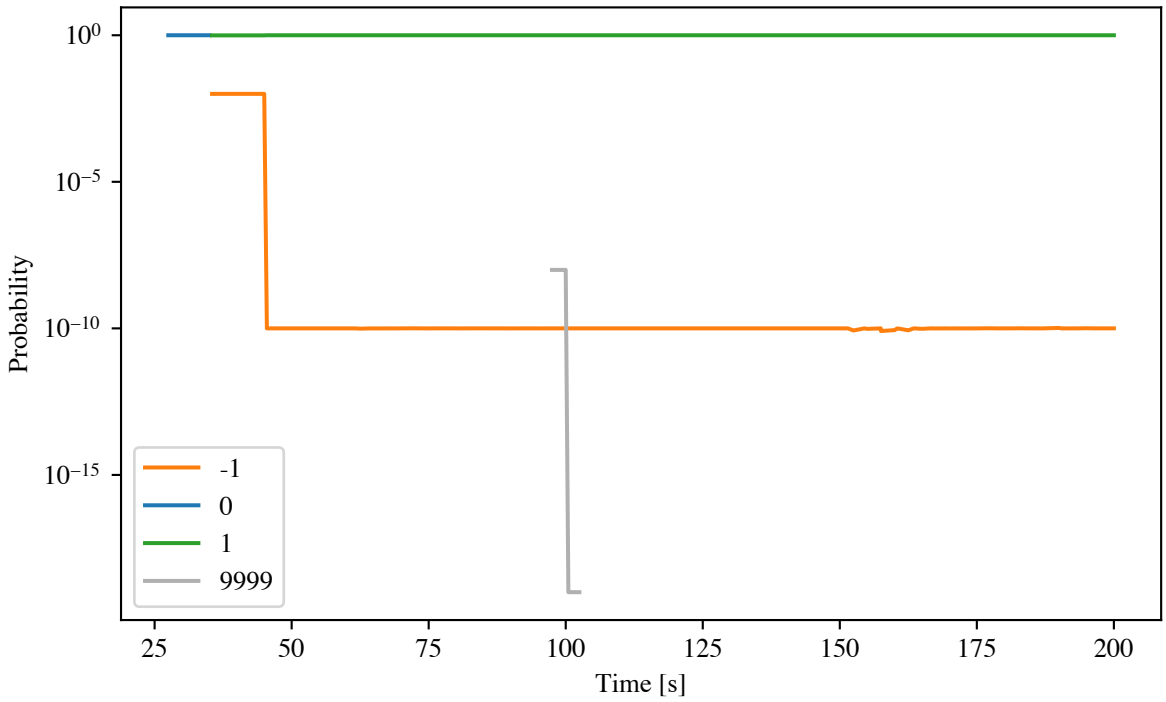

(b) MMSI probabilities when a target is not initialized on the corrupt AIS measurement.

Figure 7.12: Impact of a corrupt AIS measurement on the MMSI probabilities.

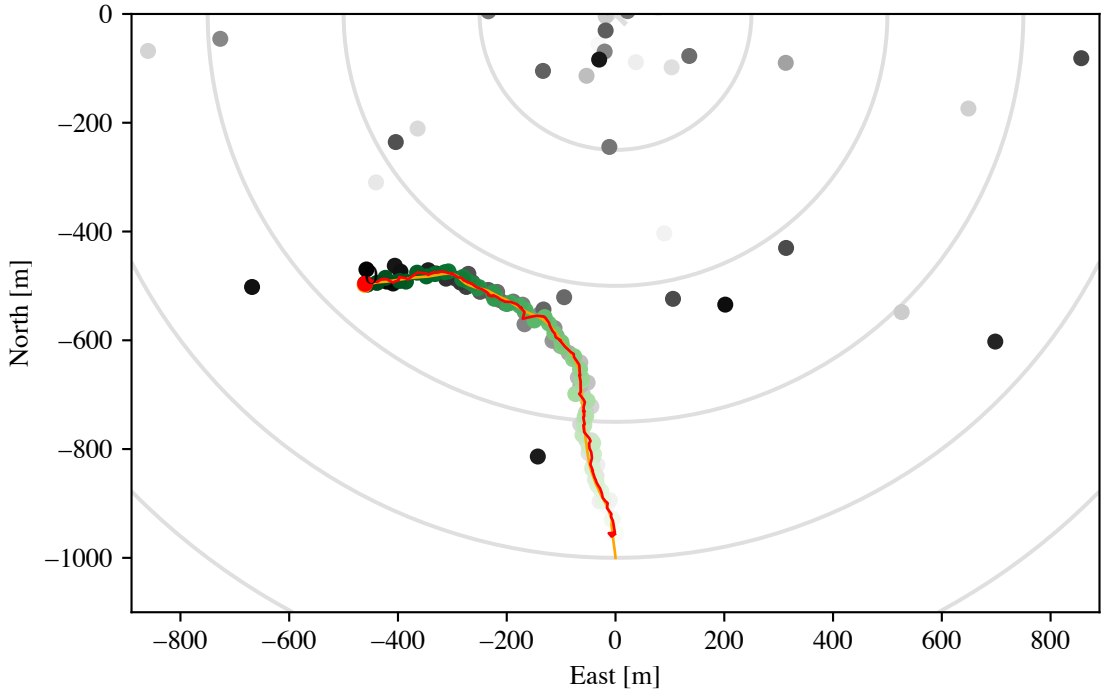

Figure 7.13: Plot when the first measurement of a track is a corrupt AIS measurement.

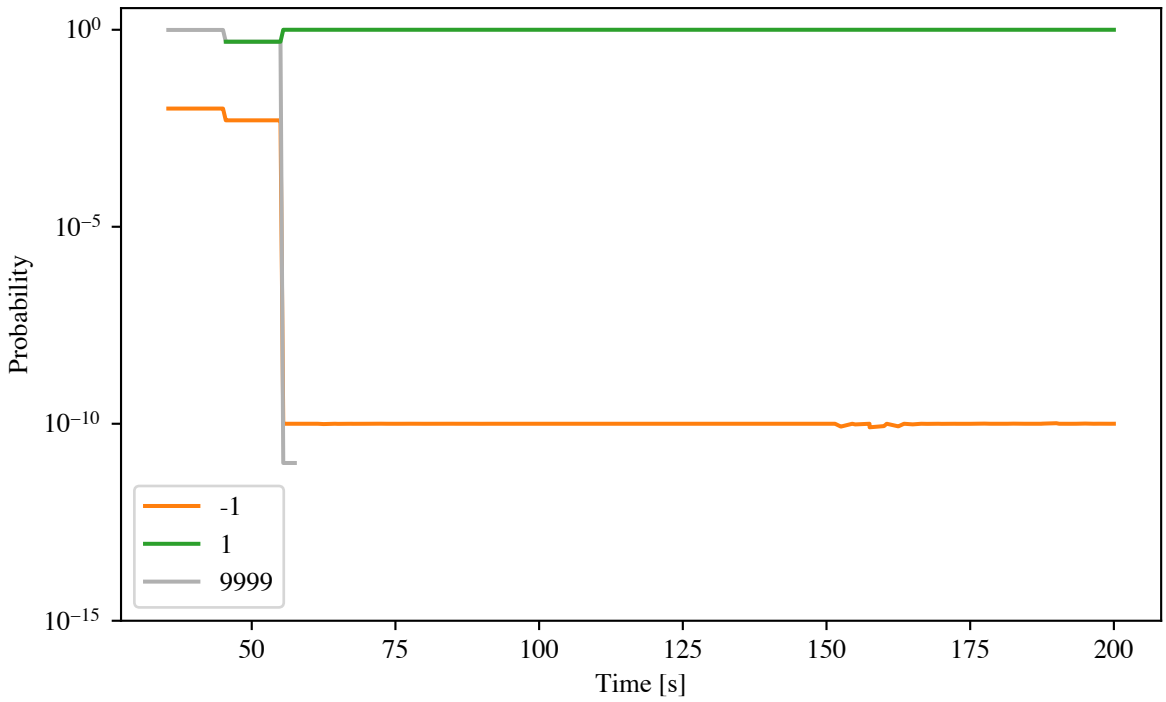

Figure 7.14: MMSI probabilities when the first measurement of a track is a corrupt AIS measurement.

Another scenario that can be suspected to cause problems, is when a new track is initialized on a corrupt AIS measurement. This is examined by using the same scenario as above. To make sure that the track is indeed initialized on an AIS measurement, all radar measurements that appear before the first AIS measurement are removed. The first AIS measurement has the corrupt MMSI number 9999 while the rest has the correct MMSI number 1. Figure 7.13 shows the tracking result, and as can be seen the tracker has no problems following the track without erroneous termination and re-initialization. The label probabilities, shown in Figure 7.14, shows how the track initially has high confidence in 9999 being the correct MMSI number, and it is initialized with with probability P_C of being correct. However, as soon as the AIS measurements with the correct MMSI number start appearing the probability for MMSI number 9999 being correct becomes lower, and the MMSI number is eventually removed from the state vector.

7.1.6 Crossing targets

A situation which could possibly cause problems when corrupted targets appear is the one where two targets cross paths. The scenario in question consists of two targets which both pass the center of the surveillance area, $(0, 0)$, depicted in Figure 7.15. They do not cross at exactly the same time, as that would amount to a collision, but target 2 crosses shortly after target 1. Just as target 1 crosses $(0, 0)$ it transmits an AIS measurement with corrupted MMSI number, which is the only measurement in purple. As can be seen from Figure 7.15 this scenario does not pose any difficulties for the tracker, and both targets are followed correctly.

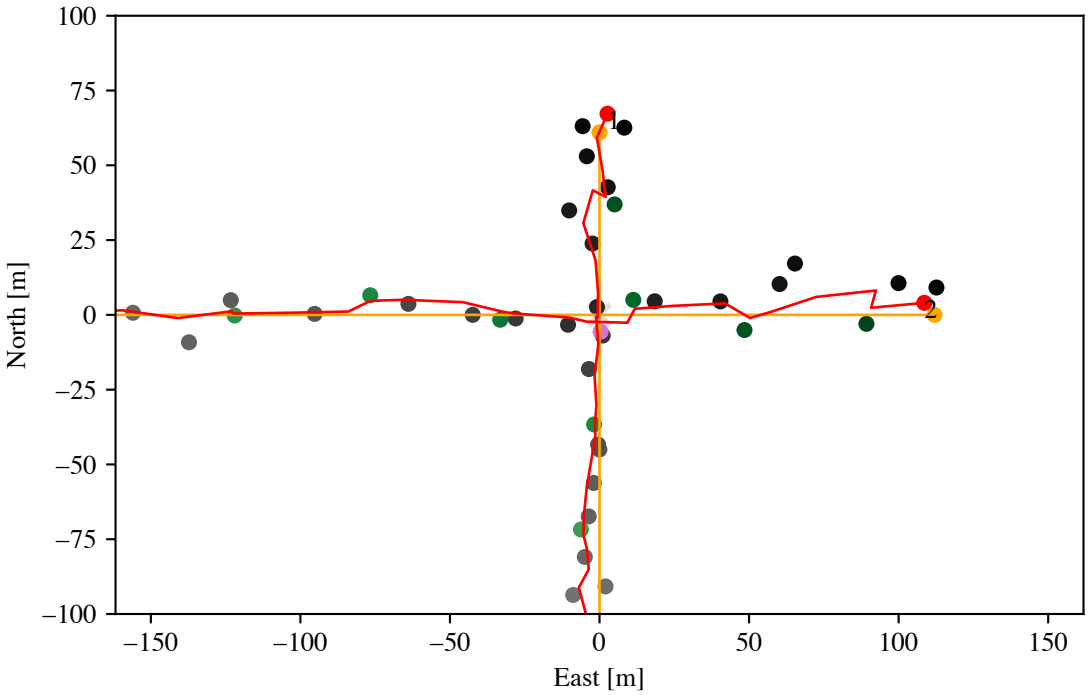

Figure 7.15: Tracking result for two crossing targets encountering a corrupt AIS measurement.

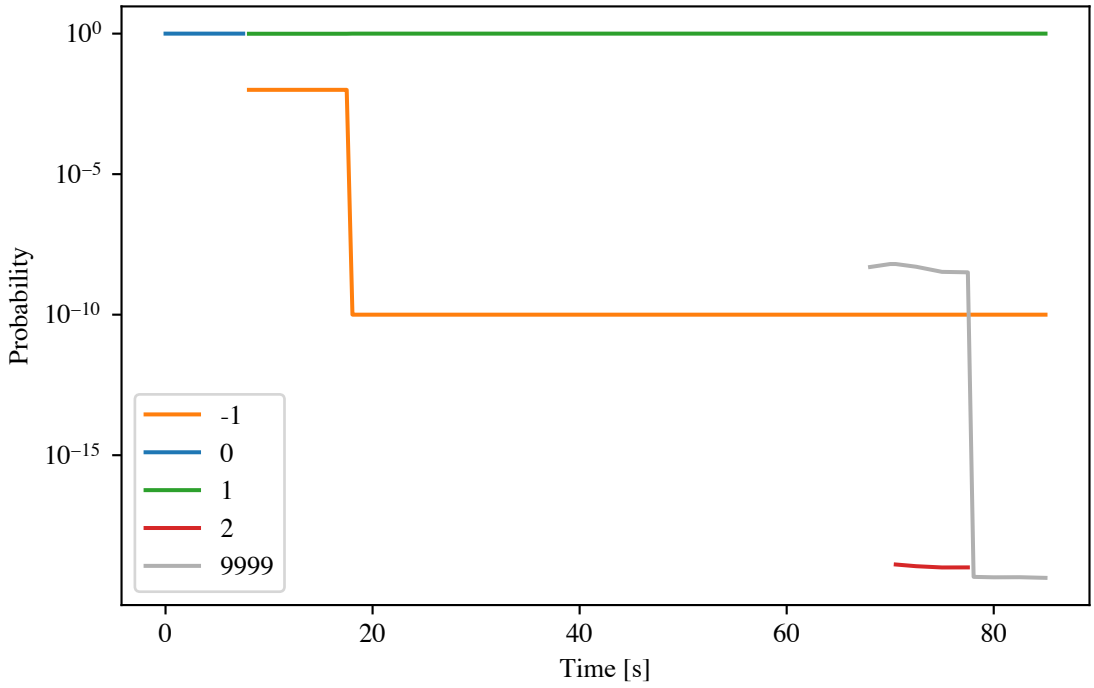

(a) Track 1.

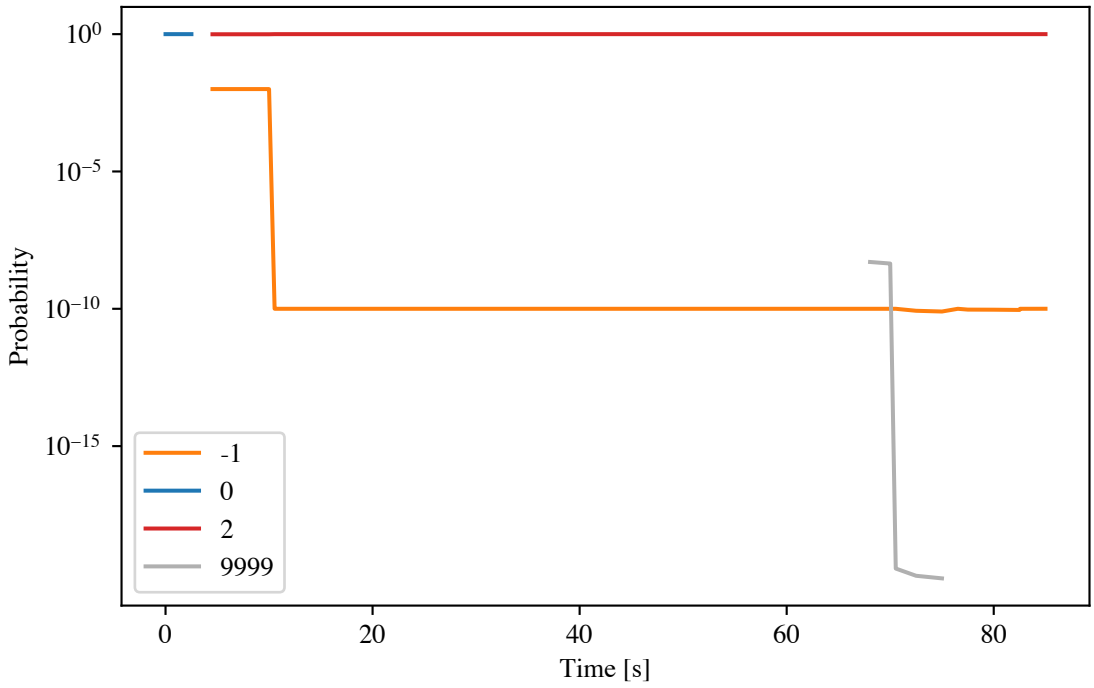

(b) Track 2.

Figure 7.16: MMSI probabilities for two crossing targets encountering a corrupt AIS measurement.

Figure 7.16a and Figure 7.16b shows MMSI probabilities of track 1 and 2. Both tracks are initialized on radar measurements, as can be seen by the fact that the only initial MMSI number is 0. Shortly after, both tracks encounter an AIS measurement, giving a high probability for the MMSI numbers in the measurements, while a smaller probability for all other MMSI numbers. When further AIS measurements arrive, the tracker becomes even more certain in the encountered MMSI numbers being correct. When the corrupted AIS measurement appears (9999), it only attains a low probability for both tracks. The corrupted MMSI number is quickly removed from the state. As can be seen from Figure 7.16a, track 1 also encounters an AIS measurement originating from target 2, but this has little impact. While most of the changes in the MMSI number probabilities occur upon encountering AIS measurements, there are some changes also during radar updates, but these are small.

7.1.7 Track jumps

A more difficult, and perhaps more interesting case is shown in Figure 7.17. Here there are two targets, both headed towards point $(0, 0)$ before they make sharp 90° turns. This confuses the tracker, which believes that the targets behave in the same way as in Figure 7.15. It is no surprise that a track jump occurs here. The AIS measurements arrive with quite a low frequency, and as the targets are quite close when they turn. The radar measurements are too noisy to provide much help. When the next AIS measurements arrive they are outside the validation gates of the tracks which originally tracked the respective targets, and thus the tracker isn't able to recover. Even though a track jump isn't critical in itself, it is important that the MMSI number probabilities are able to adapt in such a situation.

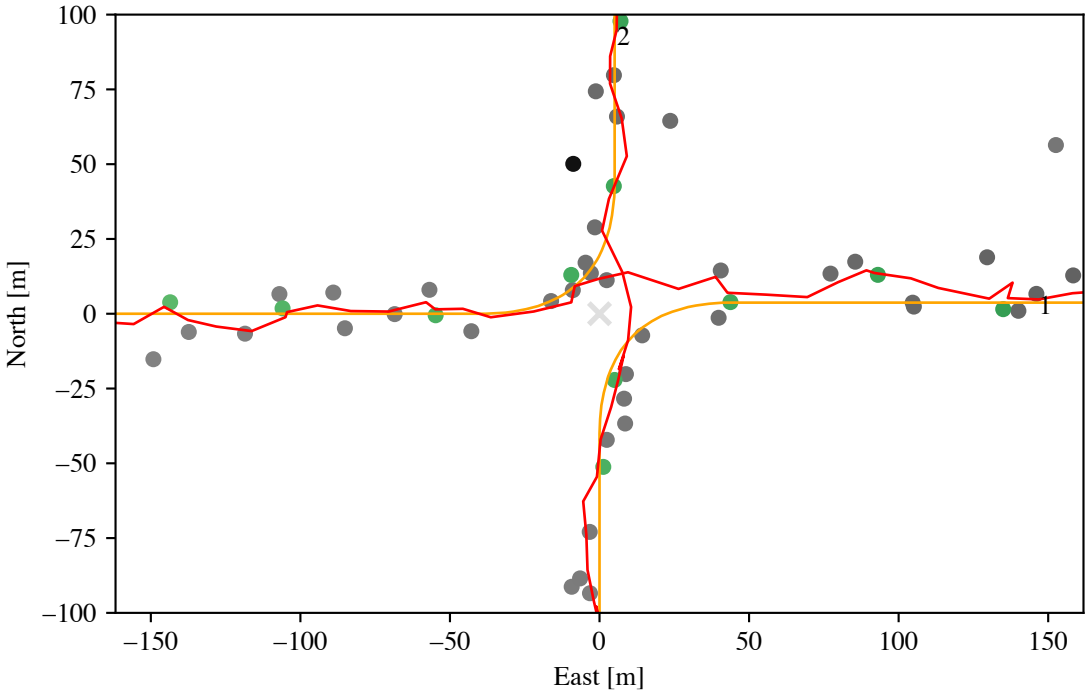

Figure 7.17: Tracking result for two targets making sharp turns.

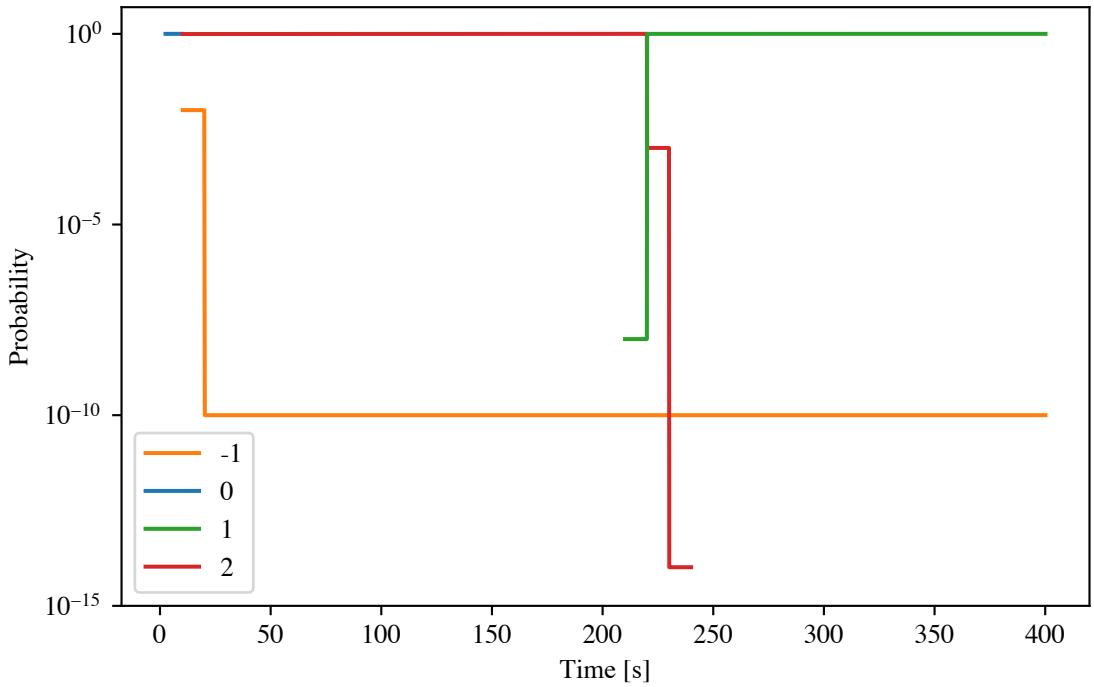

(a) Track 1.

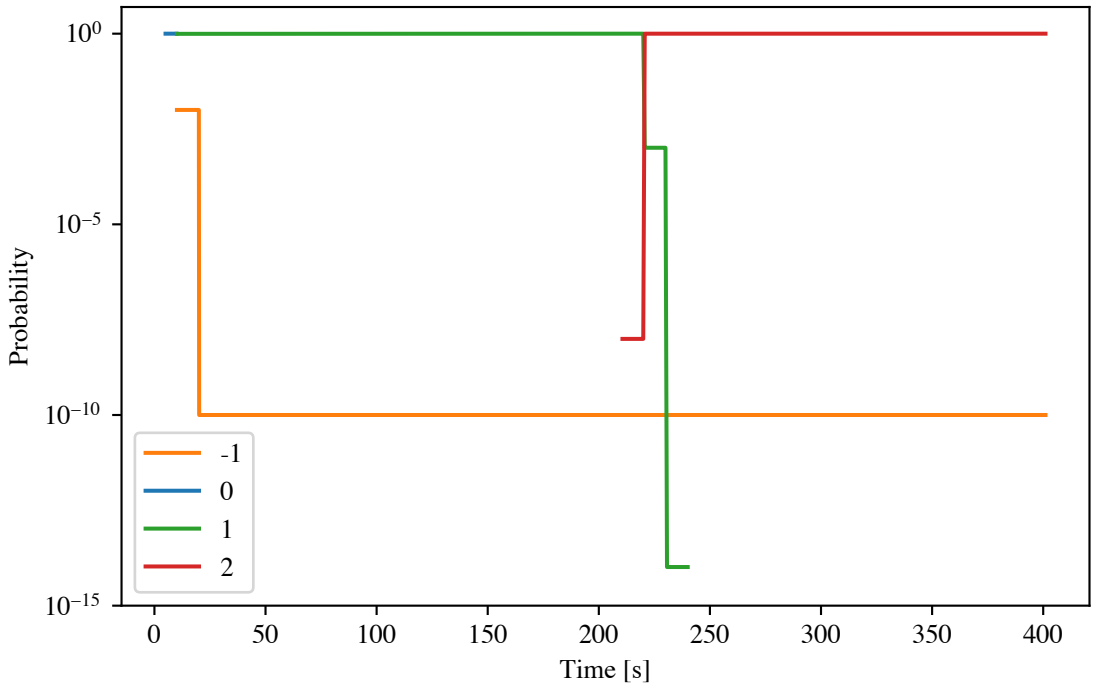

(b) Track 2.

Figure 7.18: MMSI probabilities for two targets making sharp turns.

The MMSI probabilities can be seen in Figure 7.18a and Figure 7.18b, and both tracks are able quickly to adapt to the track switch. Both tracks are initialized on radar measurements, and thus they initially have MMSI number 0. However, they quickly encounter AIS measurements, and as both tracks are in separate clusters with only one AIS measurement each, the AIS measurements are associated to the tracks with absolute certainty. This leads to the MMSI number of the AIS measurements being assigned to the targets with P_C certainty, with the rest of the MMSI numbers, represented by -1, have a combined probability of $1 - P_C$. Both tracks become more certain in their MMSI number, until the track switch occurs. Due to the association to AIS measurements with new MMSI numbers, the probability of the new MMSI numbers are calculated, each with a prior probability determined by the probability of MMSI number -1. After a few time steps, the tracks have changed MMSI number, reflecting the MMSI number of the target they follow.

7.1.8 Computational performance

To evaluate the computational performance of the tracker, a scenario able to accommodate a lot of targets at the same time was created. It was created according to the specification detailed in Section 6.2, except for the following changes:

- The scenario starts at $T = 0$ and ends at $T = 300$.
- All targets are born at a random time between $T = 0$ and $T = 100$. They are uniformly distributed within an area around the origin with radius $r = 2000$.
- The surveillance area has a large radius of $r = 4000$ to avoid that targets move out of the area during the scenario.
- Only Cartesian noise is added to the radar measurements.

The performance was evaluated by timing the tracker both when using the AIS measurements and when only using radar. The timing started when all targets had been born, at $T = 100$, and ended at $T = 300$. This was done for an increasing number of targets, from $N_T = 5$ to $N_T = 50$. For each number of targets 100 Monte Carlo simulations were performed, and the mean time used to track the scenario was found. This value was then divided by the duration of the scenario, giving the time the tracker used to track the targets relative to the time passed in the scenario. The results can be seen in Figure 7.19.

As can be seen, the inclusion of AIS measurements increases the computing time considerably. The time the tracker uses to track the targets for 1 second of the scenario should be below 1 second, so the tracker doesn't lag behind the scenario. This is achieved up to and including when 50 targets are present, but for 50 targets the running time is close the 1 second limit. This large increase is, however, not surprising. As more and more targets are born, the tracker has to perform a prediction for all tracks at more times. All the AIS measurements have different timestamps, and are therefore handled one at a time. If 50 tracks all transmit an AIS measurements between two radar updates, the tracker has to do this 50 times. In addition, more tracks means more MMSI numbers, which lead to more calculations for each update.

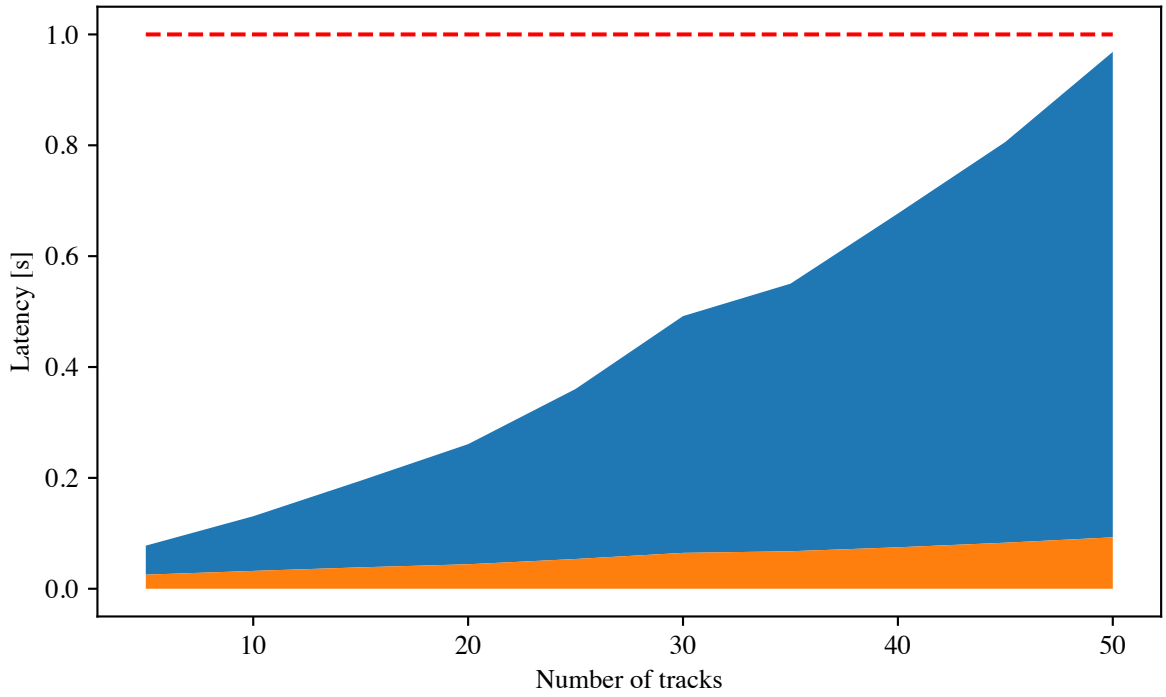

Figure 7.19: Computing time for scenarios with an increasing number of targets.

7.2 Experimental data

The source of the experimental data, as well as the pre-processing used to make the data suitable for the tracker model, is described in Section 6.3. The scenario can be summarized as follows:

- The scenario lasts for 1550 seconds, or 25 minutes and 50 seconds.
- As the scenario starts, a larger ship, Gunnerus, moves northwards. After some time it makes a u-turn and continues southwards until the scenario ends. Gunnerus transmits AIS measurements of good quality.
- Three RIBs appear shortly after the start of the scenario. These move fast, and are quite close to each other. Of these, only one of the boats have an AIS transponder, which transmits a single AIS measurement throughout the scenario duration.
- Approximately halfway in the scenario another larger ship appears, Munkholmen II. This travels eastwards, before making a turn. Munkholmen II also transmits high quality AIS measurements.
- The gray line is Telemetron, the ownship.

To make the plots less cluttered, the first 500 seconds of the scenario, the part involving the RIBs, is displayed in separate figures. The tracking results for the first part, with and without the use of AIS measurements, can be seen in Figure 7.20 and Figure 7.21, while the last part is displayed in Figure 7.22 and Figure 7.23. Firstly the impact the use of AIS measurements has on the tracking of Gunnerus and Munkholmen II is discussed,

and then the impact the AIS measurements have on the three fast-moving RIBs. The tracking parameters are the same as the ones used for the simulated data, and can be seen in Table 7.1.

7.2.1 Gunnerus and Munkholmen II

Both Gunnerus and Munkholmen II provide high quality AIS measurements which help the tracking noticeably. The radar measurements for both boats are often very noisy, which can be seen at the point where the tracking of Gunnerus starts, in the bottom part of Figure 7.20 and Figure 7.21, and where Munkholmen II enters the area on the left in Figure 7.22 and Figure 7.23. Even without ground truth, when considering both the AIS measurements and the nature of the boats, it is reasonable to assume that they move with nearly constant heading when not maneuvering. Thus, the estimates achieved when using AIS measurements are a noticeable improvement when the radar measurements are noisy. While the radar measurements become noisier as the distance between the ownship and detected target increases, this is not the case with the AIS measurements, giving comparatively better estimates for long range targets.

When using the AIS measurements, the tracker is also able to avoid some of the abrupt turns which occur when tracking using only radar. This is most noticeable for the u-turn being undertaken at the top of Figure 7.22 and Figure 7.23. Here, the radar measurements are very noisy, while the AIS measurements are not. When using AIS, the noisy radar measurements lead to the initialization of a new track, while when using radar the track makes a sharp turn.

Course estimates for Gunnerus are shown in Figure 7.24, both when using AIS measurements and when using only radar, for some time before the u-turn, during the u-turn and after the u-turn. Not surprisingly, the tracker is better able to estimate the course when utilizing the AIS measurements. When using only radar, the noisy measurements makes the course estimate fluctuate considerably. At one point during the turn, after approximately 800 seconds, the course estimate changes by over 180° from one time step to the next. This shows one of the main strengths when using AIS measurements; if they are available, and in good quality relative to the radar measurements, they can improve the estimates by a large margin.

7.2.2 The three RIBs

The three RIBs show a different side of tracking with AIS. Of the three, only one transmits AIS measurements, and that is done quite infrequently. In fact, only a single AIS measurement arrives during the span of the scenario, and the tracker thus has to rely mainly on the radar measurements. As can be seen, when comparing Figure 7.20 and Figure 7.21, the three RIBs are tracked almost identically whether the tracker uses the AIS measurements or not. The main difference is that the tracker using AIS is able to identify one of the three RIBs, Crazy Raven. This highlights the importance of a well-performing radar tracker as a basis, while AIS can be thought of as an enhancement to the underlying radar tracker. In some cases, as for Gunnerus and Munkholmen II, the AIS measurements are able to make a large difference, while they have little to no impact in other cases. It also highlights the importance of the AIS capabilities not interfering with the radar tracking performance.

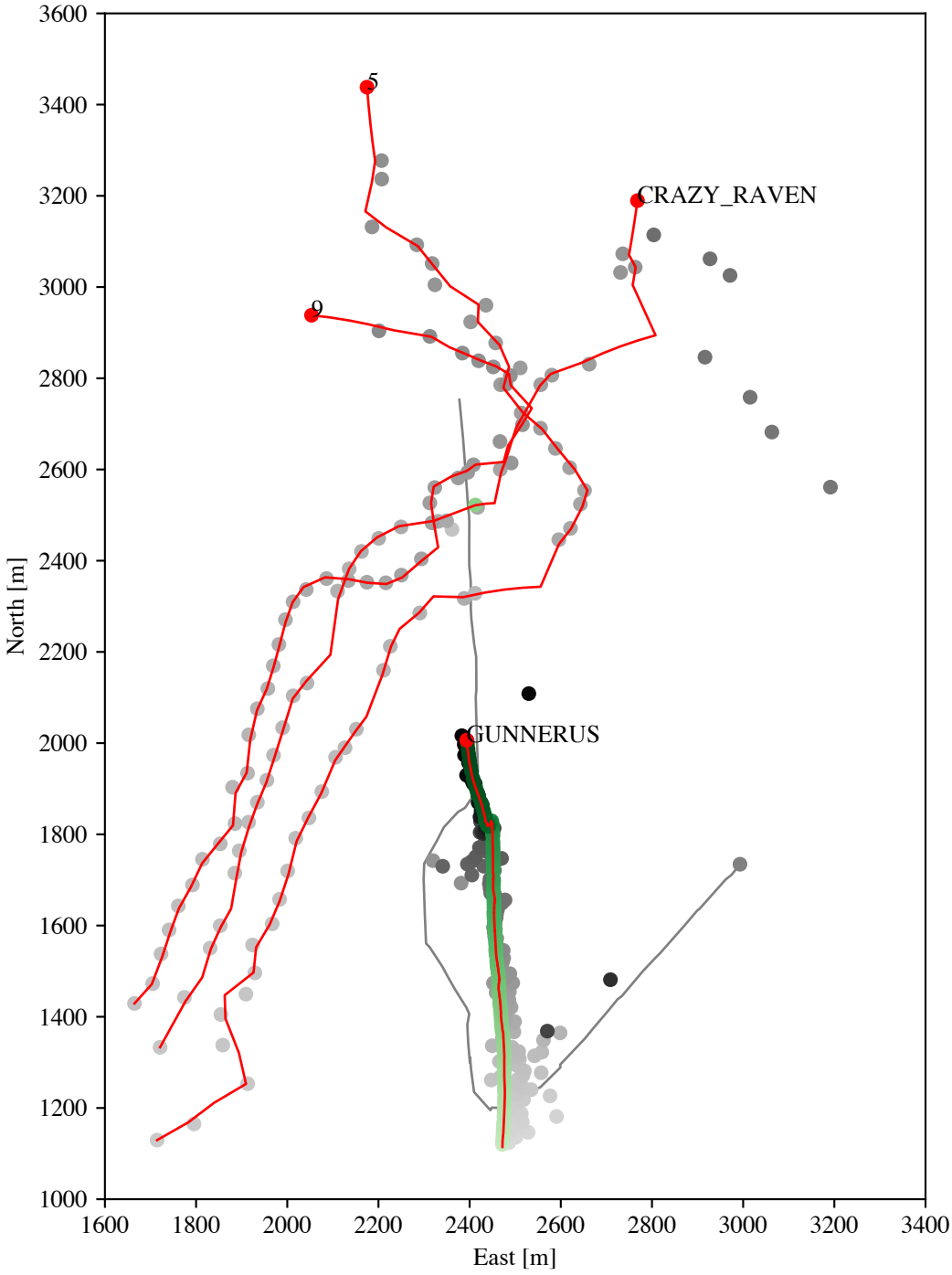

Figure 7.20: Tracking result for the first 500 seconds of the final demonstration data when using the AIS measurements.

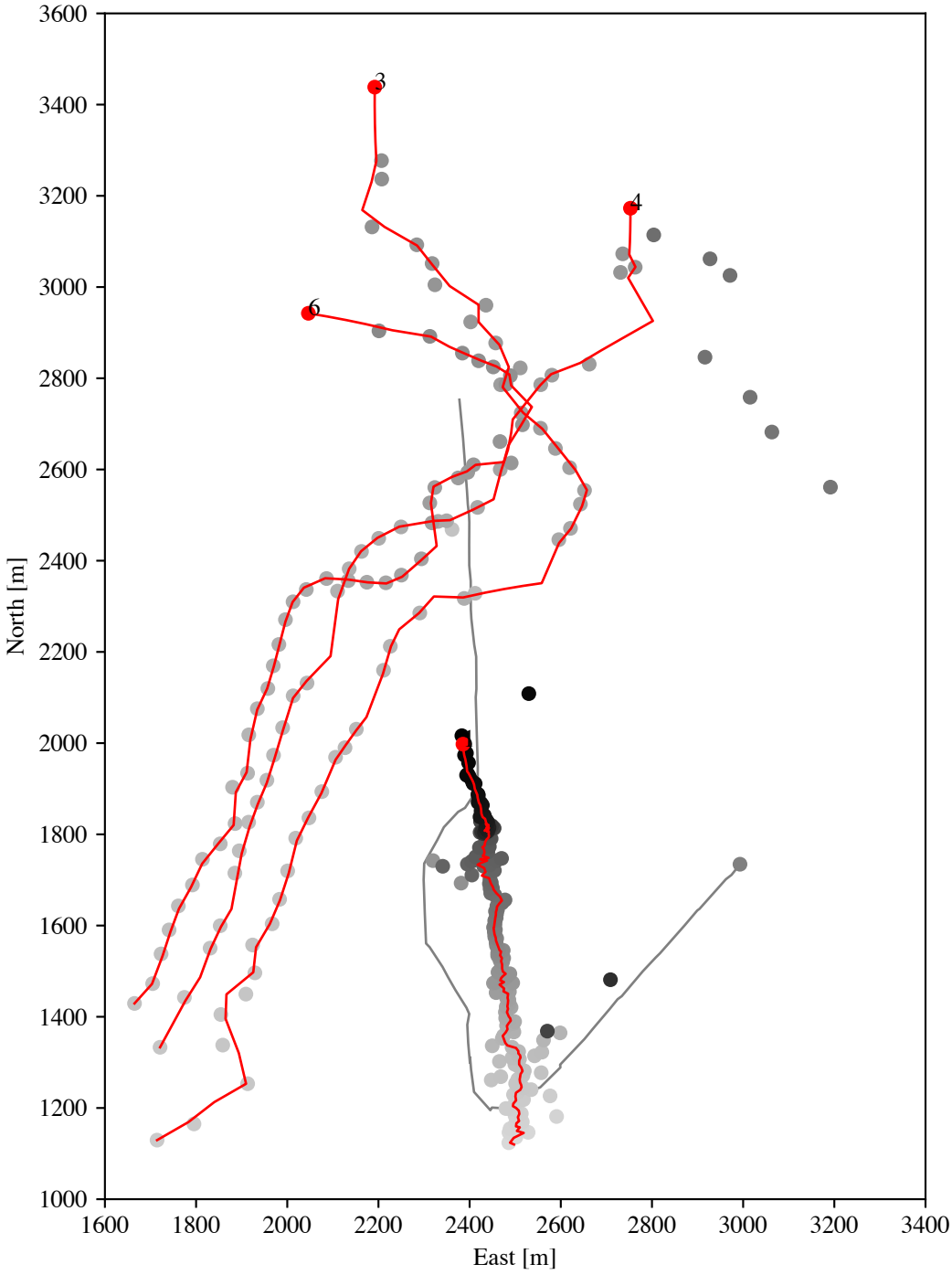

Figure 7.21: Tracking result for the first 500 seconds of the final demonstration data when using only radar.

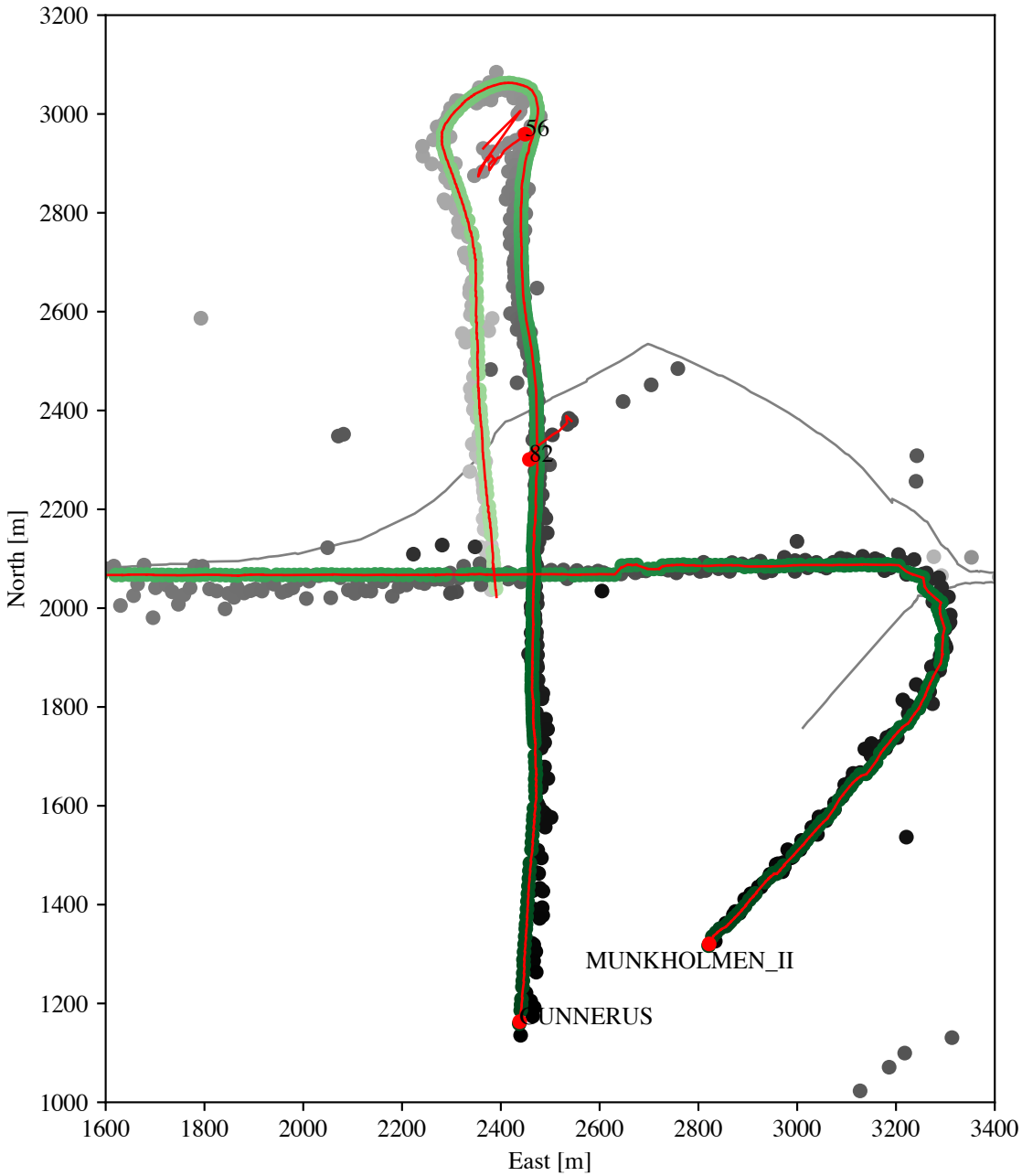

Figure 7.22: Tracking result for the last 1050 seconds of the final demonstration data when using the AIS measurements.

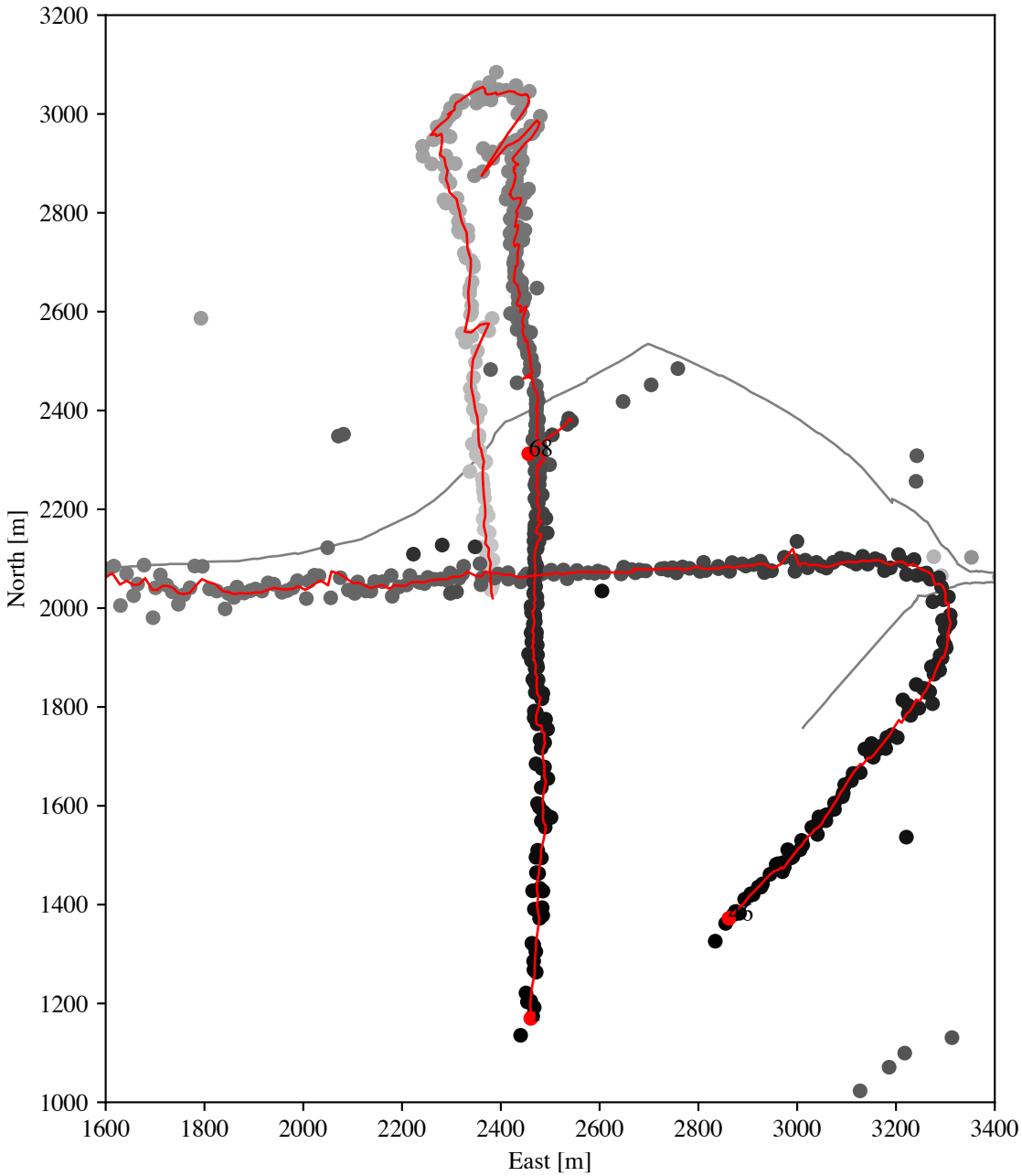

Figure 7.23: Tracking result for the last 1050 seconds of the final demonstration data when using only radar.

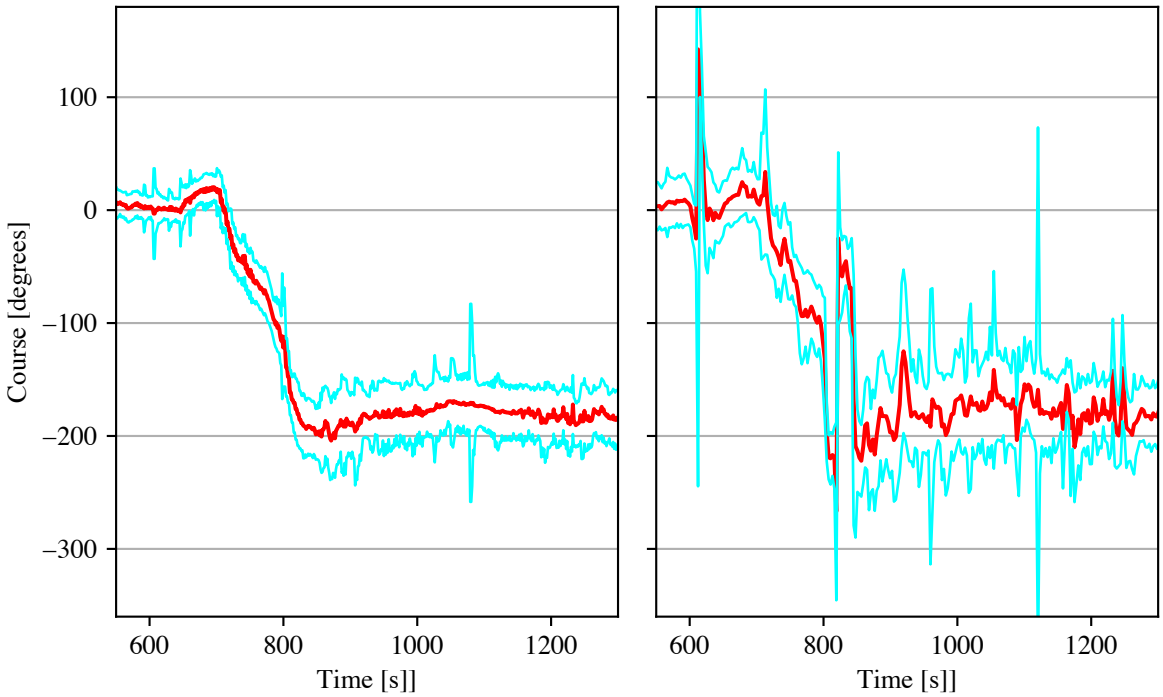

Figure 7.24: Course estimates for Gunnerus, with 1 σ bounds. Tracking results with AIS measurements on the left, without on the right.

CHAPTER 8

Discussion

When creating a target tracker several choices have to be made. Even though one would want to explore all possible ways of solving a problem, that is rarely possible. Throughout the thesis there has been some hints towards other potential methods for solving certain problems, and these are discussed in more detail here. Firstly, however, the tracking results are discussed on a more general level than what was done in Chapter 7.

8.1 Performance gains

When it comes to the tracking performance, using the AIS measurements generally results in better estimates. This is seen both through the Monte Carlo simulations in Section 7.1.2 and the comparison in Section 7.2. The improvement can be large when a target transmits high quality, frequent AIS measurements. There are also no obvious drawbacks with regards to the results, when using AIS.

These performance gains are, however, achieved only through the use of a small part of the AIS measurement. In addition to the position and the MMSI number, the AIS measurements contain information on heading, velocity, ship size and much more. The heading and velocity information can, relatively easily, be used to improve the estimates even further. Information regarding the ship size and ship type, which can either be found from the AIS measurement or by looking up the MMSI number, can be used to improve the kinematic models.

Furthermore, AIS measurements can serve a role in other parts of the software needed in an autonomous ship. Then, it will likely be useful to make a connection between the radar and AIS measurements in the tracker, before the AIS measurements are used in other parts of the system.

8.2 Undesirable behavior

Not much undesirable behavior was observed. The ANEES is slightly too high when using the AIS measurements. This can have several different reasons. It may be a result of the

tuning. It can also be that the tracker becomes too certain of the estimates due to the low measurement noise of the AIS measurements, in combination with a high certainty in the data association. This can reduce the covariance of the estimates too much whenever AIS measurements appear. That would be a difficult problem to solve, as it is a result of the tracking model itself.

Also, in relation to this, the AIS measurement model could be more refined than the one which is used here. In [47], such a model is described, which could improve results for real world data. In addition, some kind of bias compensation could be useful. This is because the clustering methods used for the radar measurements, and the position of the GPS signal resulting in the AIS measurement, have no guarantee of being the same point. Especially for large ships, this may become a problem.

8.3 Computational complexity

The computational complexity is significantly larger when utilizing the AIS measurements, in comparison to when using only radar. However, pruning of MMSI numbers and clustering of tracks keep the complexity to a manageable level. In addition, more efficient implementations are definitely possible. In the current implementation the AIS measurements were handled as they arrived, all with different timestamps. In a real life implementation it would be more convenient to handle all measurements which have arrived since the last run of the tracker. This facilitates a reduction in the time resolution, resulting in fewer steps between radar measurements. This could solve the problem with the computational complexity, at the expense of a small reduction in accuracy. Pruning of MMSI numbers from the hybrid state could also become more aggressive to reduce the number of computations. The computations of probabilities and updates for the different MMSI numbers are also well suited for parallelization, something which has not been utilized here. Furthermore, a more effective implementation should be able to speed up the tracker considerably, as that has not been the focus of the current one.

8.4 MMSI numbers

Much of the increased complexity of this tracker comes as a result of the MMSI numbers. These are introduced as a new state in the hybrid state space, giving both more complex mathematics and the need for more computations. The MMSI numbers introduce a new aspect to the data association, which can, when handled properly, enhance it. In Section 3.2, two methods of incorporating the MMSI numbers in the model are outlined, of which only one is explored. The other method, to give all MMSI numbers a small initial probability, is discarded because it would break the independence assumption for the undetected targets. Questions about how labels relate to the unknown target intensity in a PMBM has been raised in [41], and it seems as though there are possibilities in using such a framework. Solutions to the problem are sketched out, which could perhaps remove the need for the somewhat artificial change in MMSI probabilities upon detection. After all, in the real world the MMSI number of a target is static. Using labeled RFSs, as is done in the GLMB, could also be a possibility.

Furthermore, it is worth to reflect on how these MMSI numbers relate to labels as they are thought of in the GLMB and versions of PMBM. Here, the labels are in many ways a

method of ensuring track continuity, with the labels themselves having no direct connection to the real world. In a JIPDA, track continuity arises from the first measurement each track associated to, so even though labels are normally not used, this first measurement can be seen as the track label. The MMSI numbers, however, arrive as part of the measurements, and have a physical meaning in the same way the coordinates in the measurements have. They can be thought of as labels describing the targets, instead of labels describing the tracks, which one can argue is the case for how they are used in the aforementioned methods. As such, a track can change MMSI number if a track jump occurs, which would not be the case for a track label. There is nevertheless a question of whether the labels, as they are used in e.g. GLMB, can be "translated" to work with MMSI numbers, and measurements with IDs in general.

8.5 Choice of tracking method

The discussion regarding the handling of the MMSI numbers hints toward the use of different target tracking methods than a JIPDA. The JIPDA has several advantages; it is well-known, and it is fairly simple to implement with a feasible computational complexity. This is often not the case for other methods, where a range of approximation techniques need to be used to avoid the naturally exponential complexity of the problem. However, other methods based on the RFS framework are quickly becoming more established, and these may fit the problem better. In the remark regarding missed detections in Section 4.3.1, it was explained how the mixture reduction in a JIPDA is not flexible enough to be able to avoid the concept of missed detections for AIS measurements. This could, however, be solved by use of a different tracking method. A measurement-oriented tracker such as the HO-MHT could work, as could a PMBM. The slight consistency discrepancies between when using AIS measurements and when not, may also be caused by the way the JIPDA performs mixture reduction. Even though the JIPDA works well for the problem, the increased flexibility of e.g. a PMBM may be even better suited.

8.6 Initialization method

The Total track probability (TTP) is presented in Section 5.6, and is used for AIS measurements with MMSI numbers which have not previously been encountered by the target. Otherwise, new tracks are initialized on all measurements outside any tracks' validation gates. However, as also mentioned in Section 5.6, it could be beneficial to extend the use of TTP to all measurements. As it must be used for AIS measurements to avoid undesired behavior, to extend the use to all measurements seems natural. This would necessitate some approximation method for calculating the TTP. However, this is not done in this thesis to make the AIS an extension of the VIMMJIPDA without changing the underlying radar tracker. When having a familiar and well-tested tracker as a basis it is easier to evaluate the effects of the AIS measurements, and changing the initialization scheme of the underlying tracker would add a new dimension to the evaluation.

8.7 Security concerns

Something that has not been touched upon in previous chapters, but which nevertheless hold some relevance, is how AIS measurements can introduce security concerns in an autonomous system.

The current AIS protocol is simple, and has no method for authentication of the source, or checking the integrity of the transmitted information. In addition to the problems this causes with regards to the core algorithm, through e.g. the transmitting of corrupted MMSI numbers, it can also be exploited for the benefit of malicious actors. A system believing in all AIS measurements could be fooled by "false" targets created to cause harm, for example if a large number of targets are placed around the autonomous ship. This suggests that tracks created based on the AIS measurements received by the ownship should have some dependence on radar measurements confirming the existence of the target. Changes to the AIS protocol would also solve many of the potential problems. An extension of the AIS protocol, the VHF Data Exchange System (VDES), is already on it's way to becoming a new international standard [57].

CHAPTER 9

Conclusions and further work

9.1 Conclusion

In Chapter 1, three points were proposed, which this thesis was to consider. These were

- The construction of a tracker that handles AIS measurements as they arrive.
- The performance of such a method as opposed to using only radar.
- Whether the increase in computational complexity makes such an approach infeasible.

The first point is thoroughly covered in Chapter 3, Chapter 4, and Chapter 5, where it is shown how such a tracker can be designed. The tracker is an extension of the VIMMJIPDA [1], which again is an extension of the JIPDA. The JIPDA is well-known, and used for many different applications. This is one of the advantages of such an approach, especially since the VIMMJIPDA can be reduced to a regular JIPDA by choosing parameters a specific way (e.g. by using a single kinematic model, and only allowing the target to be in a visible state). With that in mind, the methods described in this thesis are possible to apply to a regular JIPDA as well. Similarly, when not using AIS measurements the tracker described in this thesis is simply a VIMMJIPDA. The addition of AIS measurements is no substitute for good radar tracking performance, and this ensures that the AIS functionality can be built around an already tested radar-tracker without interfering with its performance.

The second point considers the performance gain in using the AIS measurements. The performance gain is noticeable, and most prominent for targets with frequent AIS measurements. Course estimates, especially, are drastically improved when frequent AIS measurements are available. The help of the AIS measurements is also prominent when the radar measurements are of low quality, which often happens when the target is far away from the ownship. Furthermore, the synergy effects the AIS measurements can have with other parts of the tracker are many. They can provide the opportunity for tailoring the kinematic modeling to each target, and the data association performed in the tracker can be used in other parts of the system which uses AIS information.

The third point raises the question of computational complexity, and whether the tracker will be practical to use in real-time applications. Even though the addition of AIS measurements increases the computing time considerably, it is manageable, and can be further reduced if needed.

Furthermore, the methods described in this thesis do not only apply to AIS measurements. Even though AIS measurements are the most immediate use-case, the measurements can be any type of measurement being transmitted from surrounding targets. As such, when the next iteration of the AIS protocol arrives no major changes have to be made. The exact type of measurement will only become relevant when other parts of the measurement is used, in any potential extensions. As the current AIS protocol is somewhat lacking in integrity and security, it is good that a new framework for communication at sea is on the way. A better protocol also hints to a more important role for AIS, or similar, in tracking at sea. Then it is important to have methods for these measurements to be utilized.

9.2 Further work

Even though a functioning tracker for AIS and radar fusion is presented here, much work is needed both for the specific problem, and related problems. Some of this is to be conducted as part of the author's PhD project.

Firstly, the method described in [14], and the similar method implemented by the author in an earlier assignment, should be benchmarked against the method described here. This is already planned as part of an article. Testing on more real data would also be valuable, in addition to field tests, as performance in the real world is an important aspect of a robust and secure system.

Furthermore, other tracking methods should be investigated in relation to inclusion of AIS measurements, or similar measurements. The mixture reduction in the JIPDA can be a fundamental obstacle when including measurements transmitted from surrounding vessels, and other methods, e.g. PMBM, could be a better option. In addition, using labeled RFSs to model the problem could also be an interesting opportunity, considering the nature of the MMSI numbers.

The additional information contained in the AIS measurements should also be considered. While this thesis doesn't delve into the filtering aspect of the algorithm, there is definitely potential in using the velocity, heading, and ship type to achieve better estimates.

Initialization of new targets with the use of TTP is also an untapped opportunity. This can avoid the use of validation gates, and will bring the tracker described here conceptually even closer to a PMBM. Other initialization methods can also be investigated, as it is evident that using only validation gating is not sufficient for the problem. After all, a method such as TTP has to be used for AIS measurements either way.

The security of a system using AIS measurements is worthy of further investigation, and should be considered in tandem with the new protocols which are currently being developed. To directly use an algorithm such as the one described here in a safety-critical system would be unwise, considering how easy it is to manipulate and transmit false AIS measurements.

Lastly, the visibility state in the hybrid state, and how it relates to the other states is still a topic of further research. The possibility of using a more advanced scheme, similar to the one used in [7], is also a possibility.

Bibliography

[1] E. Brekke, A. G. Hem, and L.-C. N. Tokle, "The VIMMJIPDA: Hybrid state formulation and verification on maritime radar benchmark data," in *Global OCEANS 2020 Online Proceedings*, 2020.

[2] Maritime Robotics AS, "*Autosea final demonstrations, June 2019*," 2019, URL: https://www.youtube.com/watch?v=XqZ_lbwwspo [Accessed: 2020-12-09].

[3] L. Kretschmann, H.-C. Burmeister, and C. Jahn, "Analyzing the economic benefit of unmanned autonomous ships: An exploratory cost-comparison between an autonomous and a conventional bulk carrier," *Research in transportation business & management*, vol. 25, pp. 76–86, 2017.

[4] M. Blanke, M. Henriques, and J. Bang, "A pre-analysis on autonomous ships," *Danish Maritime Authority report*, 2017.

[5] SFI Autoship, "*SFI Autoship*," 2020, URL: https://www.ntnu.edu/sfi-autoship [Accessed: 2020-11-27].

[6] D. Musicki and R. Evans, "Joint Integrated Probabilistic Data Association: JIPDA," *Aerospace and Electronic Systems, IEEE Transactions on*, vol. 40, pp. 1093 – 1099, 2004.

[7] E. Wilthil, Y. Bar-Shalom, P. Willett, and E. Brekke, "Estimation of Target Detectability for Maritime Target Tracking in the PDA Framework," *2019 22th International Conference on Information Fusion (FUSION)*, pp. 1–8, 2019.

[8] T. E. Fortmann, Y. Bar-Shalom, and M. Scheffe, "Multi-target tracking using joint probabilistic data association," in *1980 19th IEEE Conference on Decision and Control including the Symposium on Adaptive Processes*, 1980, pp. 807–812.

[9] Y. Bar-Shalom and E. Tse, "Tracking in a cluttered environment with probabilistic data association," *Automatica*, vol. 11, no. 5, pp. 451 – 460, 1975.

[10] M. Schuster, M. Blaich, and J. Reuter, "Collision avoidance for vessels using a low-cost radar sensor," *IFAC Proceedings Volumes*, vol. 47, no. 3, pp. 9673 – 9678, 2014, 19th IFAC World Congress.

[11] J. Dezert and Y. Bar-Shalom, "Joint probabilistic data association for autonomous navigation," *IEEE Transactions on Aerospace and Electronic Systems*, vol. 29, no. 4, pp. 1275–1286, 1993.

[12] H. A. P. Blom and Y. Bar-Shalom, "The interacting multiple model algorithm for systems with markovian switching coefficients," *IEEE Transactions on Automatic Control*, vol. 33, no. 8, pp. 780–783, 1988.

[13] D. Musicki and S. Suvorova, "Tracking in clutter using imm-ipda-based algorithms," *IEEE Transactions on Aerospace and Electronic Systems*, vol. 44, no. 1, pp. 111–126, 2008.

[14] D. Gaglione, P. Braca, and G. Soldi, "Belief Propagation Based AIS/Radar Data Fusion for Multi - Target Tracking," in *2018 21st International Conference on Information Fusion (FUSION)*, 2018, pp. 2143–2150.

[15] A. Bole and W. Dineley, "1 - basic radar principles," in *Radar and ARPA Manual*, A. Bole and W. Dineley, Eds. Newnes, 1990, pp. 1 – 25.

[16] ——, "2 - the radar system — operational principles," in *Radar and ARPA Manual*, A. Bole and W. Dineley, Eds. Newnes, 1990, pp. 26 – 125.

[17] ——, "10 - extracts from official publications," in *Radar and ARPA Manual*, A. Bole and W. Dineley, Eds. Newnes, 1990, pp. 384 – 408.

[18] U.S. Department of Homeland Security: The Navigation Center of Excellence, "*AIS Messages* ," 2019, URL: https://www.navcen.uscg.gov/?pageName=AISMessages [Accessed: 2021-01-05].

[19] C. Iphar, A. Napoli, C. Ray, E. Alincourt, and D. Brosset, "Risk Analysis of falsified Automatic Identification System for the improvement of maritime traffic safety," in *ESREL 2016*, 2016, pp. 606–613.

[20] R. E. Kalman, "A New Approach to Linear Filtering and Prediction Problems," *Transactions of the ASME–Journal of Basic Engineering*, vol. 82, no. Series D, pp. 35–45, 1960.

[21] R. G. Sea, "An efficient suboptimal decision procedure for associating sensor data with stored tracks in real-time surveillance systems," in *1971 IEEE Conference on Decision and Control*, 1971, pp. 33–37.

[22] D. Musicki, R. Evans, and S. Stankovic, "Integrated probabilistic data association," *IEEE Transactions on Automatic Control*, vol. 39, no. 6, pp. 1237–1241, 1994.

[23] E. F. Brekke, E. F. Wilthil, B.-O. H. Eriksen, D. K. M. Kufoalor, Ø. K. Helgesen, I. B. Hagen, M. Breivik, and T. A. Johansen, "The Autosea project: Developing closed-loop target tracking and collision avoidance systems," *Journal of Physics: Conference Series*, vol. 1357, p. 012020, 2019.

[24] R. J. Fitzgerald, "Track biases and coalescence with probabilistic data association," *IEEE Transactions on Aerospace and Electronic Systems*, vol. AES-21, no. 6, pp. 822–825, 1985.

[25] T. Fortmann, Y. Bar-Shalom, and M. Scheffe, "Sonar tracking of multiple targets using joint probabilistic data association," *IEEE Journal of Oceanic Engineering*, vol. 8, no. 3, pp. 173–184, 1983.

[26] K. G. Murty, "An Algorithm for Ranking all the Assignments in Order of Increasing Cost," *Operations Research*, vol. 16, no. 3, pp. 682–687, 1968.

[27] D. Reid, "An algorithm for tracking multiple targets," *IEEE Transactions on Automatic Control*, vol. 24, no. 6, pp. 843–854, 1979.

[28] S. S. Blackman, "Multiple hypothesis tracking for multiple target tracking," *IEEE Aerospace and Electronic Systems Magazine*, vol. 19, no. 1, pp. 5–18, 2004.

[29] I. R. Goodman, R. P. Mahler, and H. T. Nguyen, *Mathematics of Data Fusion*. USA: Kluwer Academic Publishers, 1997.

[30] J. L. Williams, "Marginal multi-bernoulli filters: RFS derivation of MHT, JIPDA, and association-based member," *IEEE Transactions on Aerospace and Electronic Systems*, vol. 51, no. 3, pp. 1664–1687, 2015.

[31] E. F. Brekke and M. Chitre, "The multiple hypothesis tracker derived from finite set statistics," in *2017 20th International Conference on Information Fusion (Fusion)*, 2017, pp. 1–8.

[32] R. P. S. Mahler, "Multitarget Bayes filtering via first-order multitarget moments," *IEEE Transactions on Aerospace and Electronic Systems*, vol. 39, no. 4, pp. 1152–1178, 2003.

[33] R. Mahler, "PHD filters of higher order in target number," *IEEE Transactions on Aerospace and Electronic Systems*, vol. 43, no. 4, pp. 1523–1543, 2007.

[34] K. Granström, L. Svensson, Y. Xia, J. Williams, and Ángel F. García-Fernández, "Poisson Multi-Bernoulli Mixtures for Sets of Trajectories," *ArXiv*, vol. abs/1912.08718, 2019.

[35] B. Vo and B. Vo, "Labeled Random Finite Sets and Multi-Object Conjugate Priors," *IEEE Transactions on Signal Processing*, vol. 61, no. 13, pp. 3460–3475, 2013.

[36] F. Papi, B. Vo, B. Vo, C. Fantacci, and M. Beard, "Generalized Labeled Multi-Bernoulli Approximation of Multi-Object Densities," *IEEE Transactions on Signal Processing*, vol. 63, no. 20, pp. 5487–5497, 2015.

[37] A. F. Garcia-Fernandez, J. L. Williams, K. Granstrom, and L. Svensson, "Poisson multi-bernoulli mixture filter: Direct derivation and implementation," *IEEE Transactions on Aerospace and Electronic Systems*, vol. 54, no. 4, p. 1883–1901, 2018.

[38] M. K. Kalandros, L. Trailovic, L. Y. Pao, and Y. Bar-Shalom, "Tutorial on multisensor management and fusion algorithms for target tracking," in *Proceedings of the 2004 American Control Conference*, vol. 5, 2004, pp. 4734–4748 vol.5.

[39] K. Granström, L. Svensson, Y. Xia, J. Williams, and A. F. García-Femández, "Poisson Multi-Bernoulli Mixture Trackers: Continuity Through Random Finite Sets of Trajectories," in *2018 21st International Conference on Information Fusion (FUSION)*, 2018, pp. 1–5.

[40] K. Panta, B.-N. Vo, S. Singh, and A. Doucet, "Probability hypothesis density filter versus multiple hypothesis tracking," *Proceedings of SPIE - The International Society for Optical Engineering*, vol. 5429, pp. 284–295, 2004.

[41] R. Mahler, "Exact Closed-Form Multitarget Bayes Filters," *Sensors*, vol. 19, no. 12, p. 2818, 2019.

[42] Y. Bar-Shalom, X. Li, and T. Kirubarajan, *Estimation with Applications to Tracking and Navigation: Theory, Algorithms and Software*. John Wiley & Sons, 2004.

[43] L.-C. N. Tokle, "Multi target tracking - Using random finite sets with a hybrid state space and approximations," Master's thesis, Norwegian University of Science and Technology, 2018.

[44] D. Mušicki and R. Evans, "Integrated probabilistic data association-finite resolution," *Automatica*, vol. 31, no. 4, pp. 559 – 570, 1995.

[45] G. Grimmett and D. Stirzaker, *Probability and Random Processes*. OUP Oxford, 2001.

[46] E. Brekke, *Fundamentals of Sensor Fusion: Target tracking, navigation and SLAM*. NTNU, 2019.

[47] E. F. Wilthil, A. L. Flåten, and E. F. Brekke, "A Target Tracking System for ASV Collision Avoidance Based on the PDAF," in *Sensing and Control for Autonomous Vehicles: Applications to Land, Water and Air Vehicles*, T. I. Fossen, K. Y. Pettersen, and H. Nijmeijer, Eds. Cham: Springer International Publishing, 2017, pp. 269–288.

[48] H. W. Kuhn, "The Hungarian Method for the Assignment Problem," *Naval Research Logistics Quarterly*, vol. 2, no. 1–2, pp. 83–97, 1955.

[49] Y. Bar-Shalom and X. Rong-Li, *Multitarget-Multisensor Tracking: Principles and Techniques*. Yaakov Bar-Shalom, 1995.

[50] Maritime Robotics AS, "*Field Demos of Autonomous Collision Avoidance*," 2019, URL: https://www.maritimerobotics.com/post/field-demos-of-autonomous-collision-avoidance [Accessed: 2020-10-30].

[51] Navico AS, *Broadband 3GTM Radar and Broadband 4GTM Radar, Installation Guide*, 2011.

[52] S. Coraluppi, D. Grimmett, and P. de Theije, "Benchmark evaluation of multistatic trackers," in *2006 9th International Conference on Information Fusion*, 2006, pp. 1–7.

[53] D. Schuhmacher and A. Xia, "A new metric between distributions of point processes," *Advances in Applied Probability*, vol. 40, pp. 651–672, 2008.

[54] D. Schuhmacher, B. Vo, and B. Vo, "A consistent metric for performance evaluation of multi-object filters," *IEEE Transactions on Signal Processing*, vol. 56, no. 8, pp. 3447–3457, 2008.

[55] M. Beard, B. T. Vo, and B. Vo, "A solution for large-scale multi-object tracking," *IEEE Transactions on Signal Processing*, vol. 68, pp. 2754–2769, 2020.

[56] A. S. Rahmathullah, A. F. García-Fernández, and L. Svensson, "Generalized optimal sub-pattern assignment metric," in *2017 20th International Conference on Information Fusion (Fusion)*, 2017, pp. 1–8.

[57] F. Lázaro, R. Raulefs, W. Wang, F. Clazzer, and S. Plass, "VHF Data Exchange System (VDES): an enabling technology for maritime communications," *CEAS space Journal*, vol. 11, no. 1, pp. 55–63, 2019.

Audun Gullikstad Hem

Maritime multi-target tracking with radar and asynchronous transponder measurements

NTNU
Norwegian University of
Science and Technology